İZMİR KÂTİP ÇELEBİ UNIVERSITY
GRADUATE SCHOOL OF NATURAL AND APPLIED
SCIENCES

GROWTH OF ZINC OXIDE NANOSTRUCTURES ON CARBON FIBERS: PRODUCTION, CHARACTERIZATION AND PHOTOCATALYTIC PROPERTIES

PhD THESIS

Irmak DOĞAN TUNÇ

Department of Materials Science and Engineering

Thesis Advisor: Associate Professor Fethullah GÜNEŞ

Co-advisor: Associate Professor Mustafa EROL

JULY 2020

İZMİR KÂTİP ÇELEBİ UNIVERSITY

GRADUATE SCHOOL OF NATURAL AND APPLIED SCIENCES

GROWTH OF ZINC OXIDE NANOSTRUCTURES ON CARBON FIBERS: PRODUCTION, CHARACTERIZATION AND PHOTOCATALYTIC PROPERTIES

PhD THESIS

Irmak DOĞAN TUNÇ

(D150111003)

ORCID NO: 0000-0002-3141-8923

Department of Materials Science and Engineering

Thesis Advisor: Associate Professor Fethullah GÜNEŞ

Co-advisor: Associate Professor Mustafa EROL

JULY 2020

İZMİR KÂTİP ÇELEBİ ÜNİVERSİTESİ

FEN BİLİMLERİ ENSTİTÜSÜ

ÇİNKO OKSİT NANOYAPILARIN KARBON FİBER ÜZERİNDE BÜYÜTÜLMESİ: ÜRETİMİ, KARAKTERİZASYONU VE FOTOKATALİTİK ÖZELLİKLERİ

DOKTORA TEZİ

Irmak DOĞAN TUNÇ

(D150111003)

ORCID NO: 0000-0002-3141-8923

Malzeme Bilimi ve Mühendisliği Ana Bilim Dalı

Tez Danışmanı: Doç. Dr. Fethullah GÜNEŞ

Yardımcı Danışmanı: Doç. Dr. Mustafa EROL

TEMMUZ 2020

Irmak DOĞAN TUNÇ, a PhD student of IKCU Graduate School Of Natural And Applied Sciences, successfully defended the thesis entitled GROWTH OF ZINC OXIDE NANOSTRUCTURES ON CARBON FIBERS: PRODUCTION, CHARACTERIZATION AND PHOTOCATALYTIC PROPERTIES", which she prepared after fulfilling the requirements specified in the associated legislations, before the jury whose signatures are below.

Thesis Advisor :   **Assoc. Prof. Fethullah GÜNEŞ**
İzmir Kâtip Çelebi University

Jury Members :   **Prof. Dr. Kadriye ERTEKİN**
Dokuz Eylül University

Assoc. Prof. Aylin ZİYLAN
Dokuz Eylül University

Assoc. Prof. Mücahit SÜTÇÜ
İzmir Kâtip Çelebi University

Dr. Ahmet AYKAÇ
İzmir Kâtip Çelebi University

Date of Defense : 10.07.2020

To my family

FOREWORD

First and foremost, I would like to express my gratitude and appreciations to my advisor, Assoc. Prof. Fethullah GÜNEŞ and co-advisor Assoc. Prof. Mustafa EROL for their supervision and support throughout my thesis study and for giving me the opportunity to work with them.

I wish to express my gratitude to other members of thesis committee for their valuable recommendations and excellent suggestions.

I wolud like to thank to MSc. İslam CANSEVER and MSc. Evren ÇULCULAR for their help in performing SEM-EDX analyses and Dr. Tuğbanur ÖZEN BALABAN for her help in performing XRD analyses at Center Research Laboratory. Also, I wolud like to thank Dr. Hakan BİLGİLİ for performing spectrophotometric analyses at Center Research Laboratory.

I am also very pleased to Dr. Siber OĞUZLAR and MSc. Salih Alper AKALIN technical assistances at Dokuz Eylül University, Center for Fabrication and Application of Electronic Materials for their kind help in performing Spectrophotometric and XRD analyses.

Also I would like to thank Izmir Katip Celebi University, Coordination Office of Scientific Research Projects for supporting my thesis.

I would also thank to MSc. Merve KARAMAN and other colleagues in Izmir Katip Çelebi University for their invaluable supports.

Finally, I wish to express my gratitude to my family especially to my mother Fatma DOĞAN for their endless encouragement and loving, support during my whole life.

July 2020   Irmak DOĞAN TUNÇ

vi

TABLE OF CONTENTS

LIST OF TABLES

LIST OF FIGURES

ABBREVIATIONS

CFs	: Carbon Fibers
NWs	: Nanowires
HT	: Hydrothermal
SEM	: Scanning Electron Microscopy
EDX	: Energy Dispersive X-Ray Spectroscopy
XRD	: X-Ray Difraction
DRS	: Diffuse Reflectance Spectroscopy
DOE	: Design of Experiment
RSM	: Response Surface Methodology
CCD	: Central Composite Design
MB	: Methylene Blue
DE	: Degradation Efficiency

GROWTH OF ZINC OXIDE NANOSTRUCTURES ON CARBON FIBERS: PRODUCTION, CHARACTERIZATION AND PHOTOCATALYTIC PROPERTIES

ABSTRACT

Over the last decades, zinc oxide nanostructures on flexible carbon fibers have been extensively studied due to their superior structural, electrical and optical properties. ZnO is a wide band gap (~3.37 eV) metal oxide semiconductor photocatalyst activating under ultraviolet light. However, as ZnO nanowires are grown on carbon based substrates, due to synergistic effect, narrower band gap structures could be obtained and catalysts become active under visible light irradiation. Owing to this motivation, ZnO nanowires were grown successfully on carbon fibers by hydrothermal method. To obtain most effective photocatalyst, the effects of hydrothermal synthesis parameters, temperature, concentration and growth time, on dimensions of zinc oxide nanowire structures on carbon fibers were evaluated via response surface methodology and central composite design. Morphological, structural, photocatalytic properties of fabricated structures were analyzed by scanning electron microscopy, X-ray diffraction, and UV-Visible spectrophotometer. ZnO nanowires were successfully grown on carbon fibers with zincite hexagonal structure. The length and thickness values of ZnO nanowires vary from 492 nm to 1429 nm and 23 nm to 111 nm, respectively. Photocatalytic activity of structures was tested in the degradation of methylene blue. Results showed that concentration is the significant parameter on dimensions and the photocatalytic properties of ZnO nanowires. Samples produced at 30 mM showed the best photocatalytic activity. The sample produced at 120 °C, 30 mM $Zn(NO_3)_2.6H_2O$ and 4 hours hydrothermal synthesis parameters exhibited the highest photocatalytic activity with *DE%* and k_{app} of 99.86% and 1.2707 h^{-1}, respectively.

Furthermore, ZnO nanowires grown on carbon fibers were substituted by potassium and aluminum to enhance the photocatalytic activity. To determine the effects of incorporation; structural, morphological, optical and photocatalytic properties of the samples were evaluated. The potassium and aluminum concentration values of 0.5%, 1%, 5% and 10% of zinc concentration were tested. Potassium and aluminum substituted ZnO nanowires have hexagonal zincite crystal structure. Optical band gap values determined by diffuse reflectance spectroscopy. 0.5% Potassium and Aluminum substitution reduced the band gap of ZnO by 0.1 and 0.05 eV, respectively. Substitution also improved the photocatalytic activity of ZnO nanowires.

Keywords: Zinc Oxide Nanowires; Carbon Fiber; Photocatalysis; Response Surface Method; Central Composite Design; Potassium; Aluminium.

ÇİNKO OKSİT NANOYAPILARIN KARBON FİBER ÜZERİNDE BÜYÜTÜLMESİ: ÜRETİMİ, KARAKTERİZASYONU VE FOTOKATALİTİK ÖZELLİKLERİ

ÖZET

Son yıllarda, karbon fiber üzerine büyütülmüş çinko oksit nano yapıları, üstün yapısal, elektriksel ve optik özellikle dolayısı ile yoğun olarak çalışılmaktadır. ZnO, geniş band aralığı (3.37 eV) nedeniyle morötesi ışık altında aktive olabilen bir yarı iletken fotokatalizördür. Ancak, çinko oksidin karbon temelli malzemeler üzerinde büyütülmesi veya yapısına metallerin katkılanması ile yasak band aralığının daraltılması ve görünür bölge ışığı altında aktive edilmesi sağlanabilir. Bu bilgiler ışığında, yapılacak çalışmada, çinko oksit nanotellerin, karbon fiber üzerinde hidrotermal yöntem ile büyütülmesi amaçlanmıştır. Fotokatalizör olarak en etkin yapıyı elde etmek için, hidrotermal yöntem koşulları olan sıcaklık, konsantrasyon ve süre optimize edilmiştir. Hidrothermal sentez parametlerinin, ZnO nanotellerin boyutları üzerine etkileri yanıt yüzey yöntemi ve merkezi kompozit yöntemi ile incelenmiştir. Hidrotermal yöntem parametrelerinin, üretilen yapılar üzerindeki etkilerinin anlaşılabilmesi için, yapısal, morfolojik, optik ve fotokatalitik özellikleri detaylı bir şekilde analiz edildi.

ZnO nanoteller karbon fiber zerinde başarıyla büyütüldü. Çinko oksit nanotellerin boy ve kalınlık değerleri sırayla, 492 nm'den 1429 nm'ye and 23 nm'den to 111 nm'ye değişiklik göstermektedir. Yapıların, metilen mavisinin parçalanması üzerindeki fotokatalitik etkinlikleri test edildi. Sonuçlar, konsantrasyonun, ZnO nanotellerin boyutları üzerindeki etken parametre olduğu göstermektedir. 30 mM çözelti konsantrasyonu ile üretilen örneklerin fotokatalitik etkinliklerinin daha yüksek olduğu görüldü. 120 °C, 30 mM $Zn(NO_3)_2.6H_2O$ ve 4 saat hidrotermal sentez koşullarında üretilen örneğin, % 99.86 *% DE* ve 1.2707 h^{-1} k_{app} değerleri ile daha yüksek fotokatalitik etkinlik gösterdi.

Ayrıca karbon fiber üzerine büyütülmüş çinko oksit nanotellere, fotokatalitik özelliklerini geliştirmek amacı ile potasyum ve alüminyum katkı yapıldı. Katkılama işleminin, örneklerin morfolojik, yapısal, optik ve fotokatalitik özelliklerine etkisi incelendi. Çinko konsantrasyonun % 0.5, % 1, % 5 ve % 10'u konsantrasyonu değerleri test edildi. Potasyum ve alüminyum katkılanmış ZnO nanoteller altıgen zinkit kristal yapısına sahiptir. Optik bant aralığı değerleri dağınık reflektans spectroskopi yöntemi ile tespit edildi. % 0.5 Potasyum ve alüminyum katkılama ile bant aralığında sırasıyla, 0.1 eV ve 0.05 eV'lik düşüş görüldü. Katkılama işlemi, ile ZnO'in fotokatalitik etkinlikliğinde artış sağladı.

Anahtar kelimeler: Çinko Oksit Nanotel; Karbon Fiber; Fotokataliz; Yanıt Yüzey Yöntemi; Merkezi Kompozit Tasarımı; Potasyum; Alüminyum.

CHAPTER 1

INTRODUCTION

1.1.   Background

Zinc Oxide (ZnO) is a semiconducting material that has a hexagonal crystal structure. The structure of ZnO can simply be described as follows: countless closely packing O^{2-} and Zn^{2+} layers alternately stacked in the direction of the c axis, with the adjacent layers of O^{2-} and Zn^{2+} forming a tetrahedral structure [1]. ZnO has received a broad attention because of its semiconductivity, large exciton binding energy (60 meV), superior electrochemical stability, non-toxicity, suitability for doping, and low cost. Due to its electrical and optical properties it is also intensively used for photonics, solar cells, piezoelectric devices, nano-generators, photovoltaic devices, strain sensors, biosensors, chemical sensing devices and photocatalysts [2]. ZnO have been produced in various structures such as nanotubes, nanodisks, nanowires [3], nanorods [4, 5] and flower-like nano particles and nano films [6]. Synthesis of ZnO on different substrates can be performed by electrodeposition, hydrothermal method, sol–gel method, laser ablation technique or chemical vapor deposition, electrospinning [2, 7, 8] etc.

Under irradiation, ZnO can only absorb ultraviolet (UV) light to produce holes and photoelectrons owing to its wide band gap (3.37 eV). In order to extend the spectral response range to the visible light range (to decrease the band gap) and to provide more efficient charge separation in ZnO structures, utilization of carbon-based materials as substrates, introduction of surface photo-sensitization and incorporation of several elemental metals have been frequently studied [3]. To provide efficient charge separation and to decrease the band gap by the formation of ZnO-carbon junction, carbon fiber is a promising substrate due to its chemical stability, high electrical conductivity, high specific surface area and suitable porosity. As well as, photocatalyst nanoparticles cannot be separated easily from treated wastewater.

Agglomeration of nanoparticles is another problem in photocatalytic application of nanoparticles. Using carbon as a substrate also can be solution to these problems [9]. Another approach to decrease the band gap is the incorporation of some metals into ZnO structure by doping and/or substitution [2]. Interaction of such metals with ZnO lead to a change in acceptor or donor energy levels, narrowing the band gap and increasing the optical response to the visible range.

1.2. ZnO Nanostructures and Applications

Among other methods for the production of ZnO nanostructures on carbon fiber, hydrothermal synthesis has been considered as one of the promising methods for growing textured and aligned ZnO structures [10]. In this part, few studies on the production and characterization of ZnO nanostructures will be discussed. In the study of Chen et al. ZnO NWs have successfully grown on CFs by hydrothermal method at low temperatures as shown in Figure 1.1. Figure 1.1 shows the SEM images of ZnO NWs on CFs that synthesized hydrothermal method by Chen et al. Figure 1.1(a) presents the SEM image of the CFs having ~ 8 µm thickness. Figure 1.1(b) presents the ZnO NWs-coated CFs with the ZnO NWs deposited by HT for 4 hour. This Figure shows that ZnO NWs are homogenously distributed on CFs. A high resolution SEM in Figure 1.1(b) indicates that the dimension of ZnO NWs is about 100–150 nm. ZnO NWs stand almost vertical to the CFs. Figure 1.1(b) shows that the average length of ZnO NWs is about 3 µm. When reaction duration increases to 8 h, both the dimension and length of ZnO NWs increase, as shown in Figure 1.1(d). The dimension has a wide distribution ranging from 150 to 500 nm and the average length increases to about 5 µm (Figure 1.1(d)). These results indicates that well aligned ZnO NWs could be deposited on CFs by hydrothermal method at low temperature.
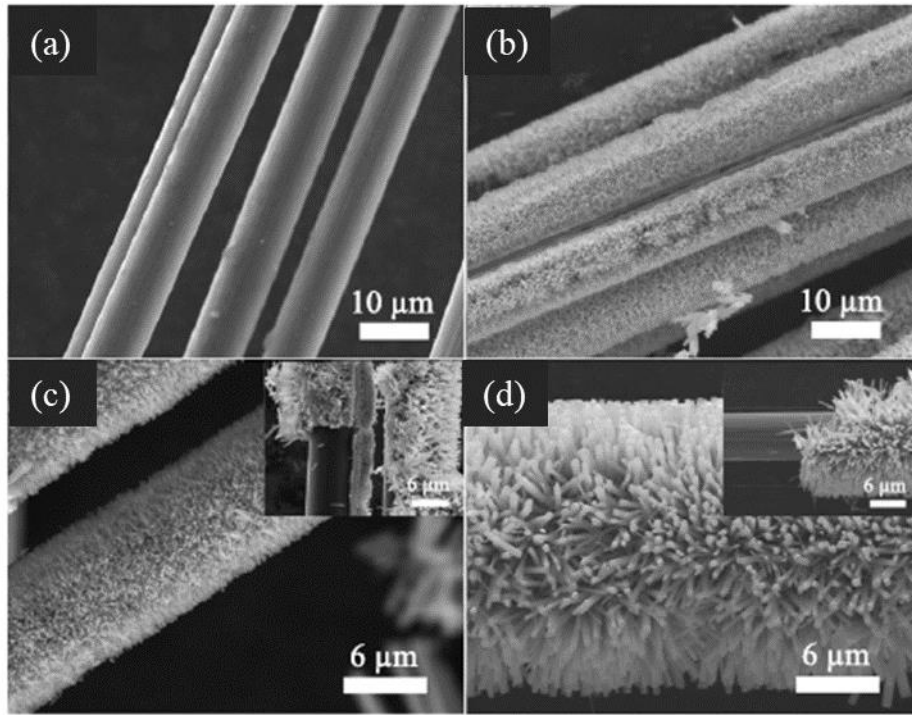
Figure 1.1 SEM images of CFs (a), ZnO NW-coated CFs with the ZnO NWs (b) and (c) deposited by HT for 4 hour, and ZnO NW-coated CFs with the ZnO NWs (d) deposited by HT for 8 hour [11].

In Figure 1.2(a) TEM image of single-crystal structure of ZnO NWs is given. The Figure indicates that the dimension of ZnO NWs is about 100 nm. In Figure 1.2(b), a high-resolution TEM (HRTEM) image taken from the edge of ZnO NWs is given. It is demonstrated that ZnO NWs grow along the [002] direction. Crystalline structure of ZnO NWs was characterized by XRD as illustrated in Figure 1.3. XRD results confims the similar rasults.
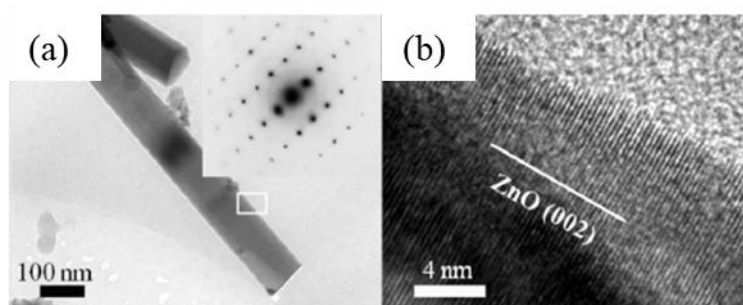
Figure 1.2 (a) TEM and (b) HRTEM images of ZnO nanowires [11].
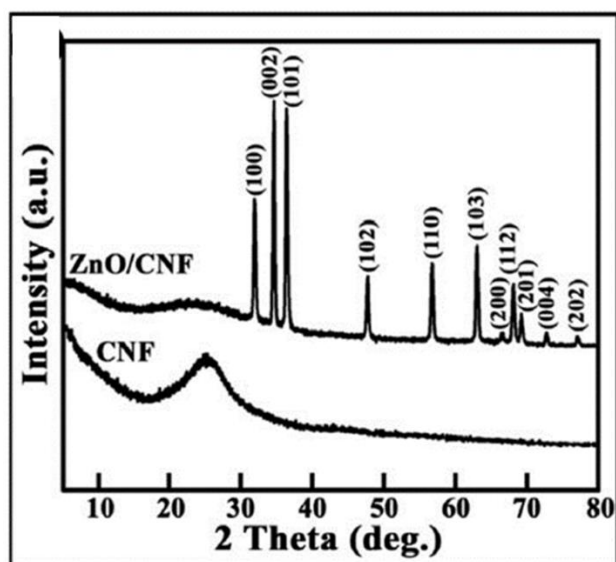
Figure 1.3 XRD pattern of the ZnO nanowires grown on carbon fibers [3].

Pant et al, synthesized pristine and Ag substituted ZnO on carbon fibers and analysed the optical properties of structures by UV–vis absorption spectroscopy (Figure 1.4). A red shift of the absorption edge is seen in Ag substituted ZnO NWs/CFs, which causes decrease in the band gap and improves the photocatalytic activity of structure. This might be result of interfacial electronic coupling between the zinc oxide and Ag.
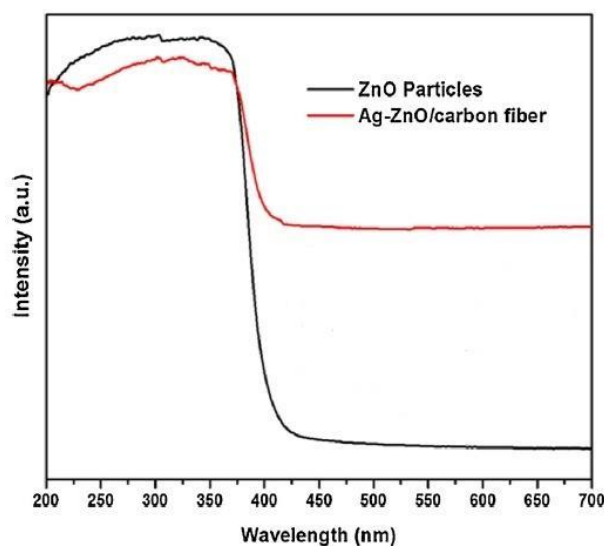
Figure 1.4 UV–vis spectra of the pristine and Ag substituted ZnO nano-structures on carbon fibers [9].

ZnO has also been extensively studied with carbon based materials and other metal oxides. Its applications as energy storage device, power generator, solar cell, sensor,

biosensor and photocatalytic applications were studied. Some studies in literature based on ZnO nanostructure grown on carbon based materials are listed in Table 1.1.

Table 1.1 Some studies in literature ZnO nanostructure grown on carbon based materials.

Structure	Application	Reference
ZnO nanowires on carbon fiber	Nano generator	[12, 13]
ZnO-ZnSe bilayer structure wire on carbon fiber	Piezoelectric nanogenerator	[14]
Ni-Co layered double hydroxide anchored ZnO NWs on CF	Energy storage device	[15]
ZnO nanowires on aramid fiber	Power generator	[16]
Branched ZnO nanotrees on fiber	Piezoelectric energy harvesting system	[17]
ZnO nanocable on carbon fiber	Ascorbic acid sensing	[18]
ZnO nanofiber on Carbon Nanotube	Malaria biomarker sensing	[19]
ZnO core-shell hybrids on carbon fiber	Ascorbic acid/uric acid sensing	[20]
CF/ZnO nanorods as electrode	Dopamine sensing	[21]
Ag NPs/ZnO nano wedge	Detection of H_2O_2	[22]
ZnO on carbon fiber	Strain sensor	[23]
ZnO on carbon fiber	Gas sensor	[24]
CF-ZnO-CdS Double shell microwire	Photon detector	[25]
Ag NPs on ZnO nanosheets on CF	SERS based detection of organic pollutants	[26]
TiO_2/ZnO core–sheath nanofibers film	Photoanode of dye-sensitized solar cells	[27]
ZnO thin films on carbon fibres	Photo anodes for DSSC	[28]
TiO2/ ZnO core-sheet nanofibers	Solar cell	[8]
CF/ZnO-CdS double shell microwire	Enhanced visible/UV photodetector	[25]
ZnO/CF	Biosensor	[29]

CF/ZnO/CdS	Solar cell	[11]
ZnO/CF	Photocatalytic	[30]
Horn-like ZnO structures on carbon films	Photocatalysts on solar hydrogen production	[31]
Ag-ZnO photocatalyst ancored on CNFs	Photocatalytic effect	[9]
Flowerlike ZnO microstructure on CF	Photocatalytic activity	[32]
ZnO film on CF	Photodegradation of acrolein	[33]
Sn doped ZnO microspheres on CF	Photocatalytic on methylene blue	[34]
CuS NPs/ZnO nanorods arrays on CF	Photocatalytic properties on methylene blue degradation	[10]
Ag/ZnO (3D) on CF	Photocatalytic degradation of pollutants	[7]
ZnO nanorod arrays on CF	CO_2 photocatalytic reduction catalysts	[35]
ZnO Nanowire on graphene foam	Biomarker Detection of Parkinson's Disease	[36]
Carbon nanofibers wrapped with zinc oxide nano-flakes	Electrode material for supercapacitors	[37]
ZnO nanoparticles onto CF	Filaments for infrared heaters	[38]
In_2O_3 nanoparticles on ZnO hollow nanotubes using CF	Gas sensor	[39]
ZnO nanowires on CF via HT	Paper-based friction materials	[40]
ZnO rod-activated CF	Tetracycline removal	[41]
Synthesis of carbon-ZnO nanocomposite	Photocatalytic performance	[42]

1.3.   Photocatalytic Applications

Photocatalytic degradation and complete mineralization of toxic organic compounds in water, soil and air in the presence of semiconductor materials have received a great attention over the few decades. Electronic structure of a semiconductor is

6

characterized by its filled valence band and empty conduction band. When a semiconductor is irradiated with light of sufficient energy corresponding to or exceeding its band gap, an electron is promoted into the conduction band leaving a hole in the valence band. The electrons and holes are good reductants and powerful oxidants, respectively, and they can initiate redox reactions on the semiconductor surface (Figure 1.5) [27].

There are two mechanisms proposed for the degradation of methylene blue by zinc oxide nanostructures grown on carbon based materials under visible light, as follows: 1-Electronic transfer in dye, acting as a light sensitizer, occurs by the excitation of dye electrons into carbon fiber and to conduction band of Zinc Oxide as the light irradiates. 2-Reduction in ZnO occurs by the promotion of an electron into the conduction band of ZnO leaving a hole in the valance band, as the light irradiates, where carbon fiber acts as a step for electron transfer. As a result, an oxidative surface occurs on CFs and organic compound MB is oxidized. Energy diagrams of ZnO, carbon fiber and methylene blue is shown in Figure 1.5.
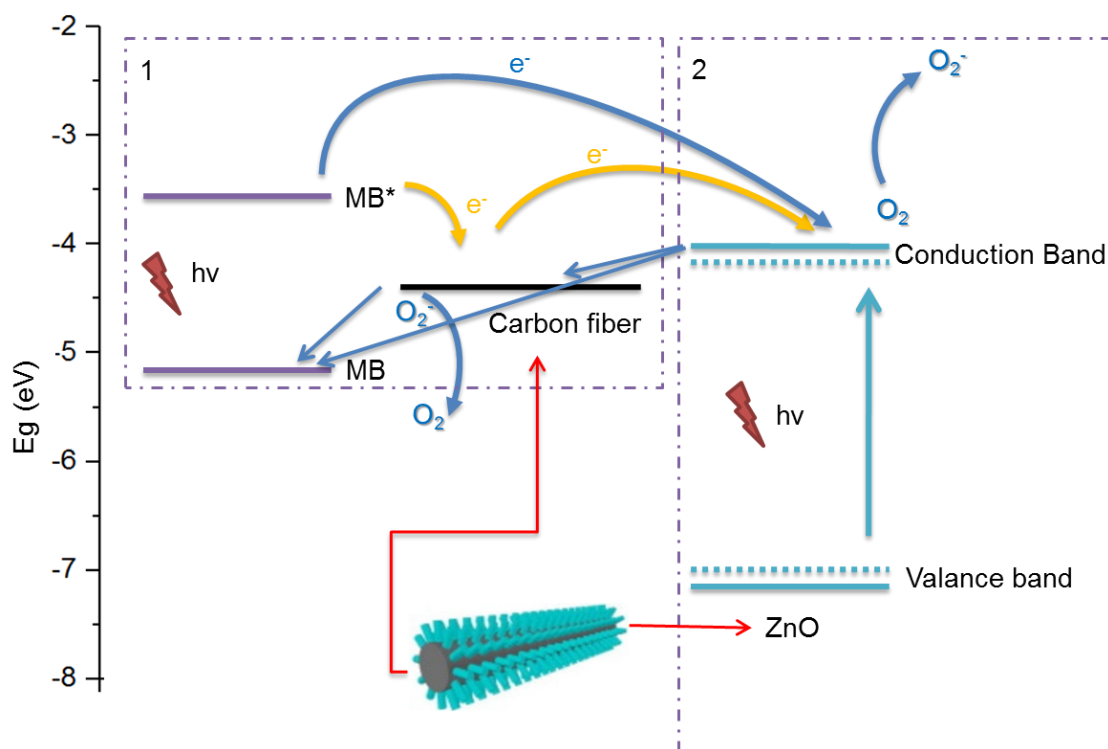
Figure 1.5 Proposed mechanism for the photodegradation of methylene blue (MB) by ZnO nano structures on carbon fiber under visible-light irradiation.

1.4.   Objectives

The aim of this study is to synthesize ZnO nanostructures on a conductive carbon fiber by hydrothermal synthesis method and to determine the effect of the synthesis parameters in order to obtain optimum photocatalytic properties. The composites resulting from the synthesis were characterized by scanning electron microscopy (SEM), energy dispersive x-ray spectroscopy (EDX), x-ray diffraction (XRD) and UV-Visible spectrophotometer. The effects of temperature, concentration of solution and hydrothermal process duration on the formation of ZnO nanostructures on carbon fiber were evaluated by means of morphological, structural and optical analyses. As well as, response surface methodology (RSM) and central composite design (CCD) were applied to optimize the hydrothermal synthesis parameters.

Moreover, aluminum and potassium were incorporated into ZnO nanowires to improve the photocatalytic properties of the structure. The resulting composites from the synthesis were characterized by scanning electron microscopy (SEM), energy dispersive x-ray spectroscopy (EDX), x-ray diffraction (XRD) and diffuse reflectance spectroscopy (DRS). Also, the effect of aluminum and potassium on photocatalytic properties of structures were analysed by UV-Visible spectrophotometer.

1.5.   Dissertation Outline

In Chapter 2, the effect of zinc nitrate concentration on dimensions of ZnO NWs grown on carbon fibers are reported. Fabricated samples were characterized to determine their morphological, structural and photocatalytic properties using different analysis methods.

In Chapter 3, optimization of the hydrothermal process parameters, temperature, concentration and time, using response surface methodology (RSM) and central composite design (CCD) is reported. Morphological, structural and photocatalytic properties were analysed by scanning electron microscopy (SEM), X-ray diffraction (XRD) and UV–Visible spectrophotometer.

Results of the study on incorporation of potassium at different ratios into zinc oxide nanowires are discussed in chapter 4. The effect of potassium on morphological, structural, optical and photocatalytical properties of zinc oxide nanowires were

evaluated through scanning electron microscopy (SEM), X-ray diffraction (XRD), diffuse reflectance spectroscopy (DRS) and UV–Visible spectrophotometer.

Incorporation of aluminum at different molar ratios into zinc oxide nanowires structure is reported in chapter 5. The effect of aluminum concentration on morphological, structural, optical and photocatalytic properties of ZnO NWs were characterized by scanning electron microscopy (SEM), X-ray diffraction (XRD), diffuse reflectance spectroscopy (DRS) and UV–Visible spectrophotometer.

Finally, in chapter 7, it was concluded that zinc oxide nanowires on carbon fibers are successfully synthesized, the effect of hydrothermal process parameters on dimensions, and photocatalytic properties of zinc oxide nanowires grown on carbon fibers were evaluated. Ppotassium and aluminum substitution into zinc oxide is accomplished and optical and photocatalytic properties are enhanced with potassium and aluminum incorporation.

CHAPTER 2

The Effect of Growth Solution Concentration on Dimensions and Photocatalytic Activity of ZnO Nanowires Grown on Carbon Fiber

Abstract

ZnO nanowires were successfully fabricated on carbon fibers by hydrothermal method. The effect of $Zn(NO_3)_2.6H_2O$ concentration on dimensions of ZnO nanowires and photocatalytic activity on methylene blue under visible light were investigated. The X-Ray diffraction analysis revealed that the ZnO nanowires exhibits hexagonal zincite phase. The morphology of the ZnO nanowires were analyzed by SEM. Dimensions of nanowires increases and aspect ratio of zinc oxide nanowires decreases with increasing $Zn(NO_3)_2.6H_2O$ concentration. Photocatalytic degradation rate of methylene blue also increased with $Zn(NO_3)_2.6H_2O$ concentration. However, further increase of aspect ratio cause to decrease in photocatalytic degradation rate. It is seen that, most effective structure produced at 30 mM $Zn(NO_3)_2.6H_2O$.

Keywords: Zinc Oxide Nanowires; Carbon Fiber; Hydrothermal Synthesis; Photocatalysis.

2.1. Introduction

Semiconductor photocatalysts has been given great attention as a solution for environmental problems. Zinc oxide is an excellent photocatalyst due to its high quantum efficiency, redox potential, non-toxicity, high chemical and physical stability. ZnO is a wide band gap (~3.37 eV) semiconductor photocatalyst. Therefore it can only be activated under ultraviolet light. In order to, obtain narrower band gap structure, ZnO can be grown on carbon based substrates resulting in expansion of activation energy of the composite into the visible range. So that obtained composite structure becomes active under visible light irradiation. In addition, zinc oxide can be produced with variety of methods such as electrodeposition, hydrothermal synthesis, sol–gel method, laser ablation technique, chemical vapor deposition and

electrospinning [2, 44-46]. In this study ZnO nanowires were grown on carbon fibers (CFs) by hydrothermal method. The effect of hydrothermal process concentration on the dimensions of zinc oxide nanowires (ZnO NWs) and photocatalytic activity of ZnO nanowires grown on carbon fiber (ZnO NWs/CFs) were investigated. Structural, morphological and photocatalytic properties of the samples were evaluated in details.

2.2. Experimental Study

The synthesis method was presented in our previous work [43] (Tunç et al 2020). ZnO nanowires on carbon fiber photocatalysts were synthesized via hydrothermal synthesis. The carbon fibers (Aksaca, 12K A-42) were washed with nitric acid (30%), water and ethanol and dried at 60 °C in air. To grow ZnO on carbon fiber, a seeding layer coated on CFs using zinc acetate dihydrate solution by dip coating method at room temperature. ZnO seed solution prepared by dissolving 25 mg zinc acetate dihydrate ($Zn(CH_3COO)_2$) and 10 mg sodium hydroxide in 100 mL ethanol and obtained solution was stirred for 1.5 hour. Carbon fibers were then dipped into prepared ZnO seed solution for 10 min. and annealed at 150 °C for 10 min. The process repeated for four times. After that, ZnO seed-coated carbon fibers were immersed in zinc nitrate hexahydrate ($Zn(NO_3)_2 \cdot 6H_2O$) and hexamethylenetetramine (HMTA) solution in teflon-lined stainless steel autoclave. Hydrothermal synthesis performed at 90 °C for 2 hours. Then ZnO NWs coated CFs were washed with distilled water and dried at 60 °C in air. Heat treatment (250 °C, 120 minutes, in the air) was followed by this process, which transforms the amorphous structure into crystalline zincite phase. To investigate the effect of concentration on dimensions of ZnO nanowires and photocatalytic activity of ZnO NWs/CFs structure 10, 20, 30, 40, 50 mM $Zn(NO_3)_2 \cdot 6H_2O$ concentrations were tested in the presence of of equimolar HMTA.

Crystal structure of ZnO NWs were analyzed using X-ray diffractometer (Panalytical Empyrean XRD, Empreyan Package T-T). The X-ray diffraction data were recorded using Cu Kα radiation (1.5406 A°). The intensity data were recorded over a 2Ө range of 15° to 90°. The morphology of the samples were analysed with scanning electron microscopy (SEM) (Carl Zeiss 300VP SEM). The photocatalytic degradation kinetics were observed by the spectrophotometric measurements (Shimadzu UV-1240). Photocatalytic properties of structure were investigated by

monitoring photodegradation of methylene blue (MB) (10^{-5} M) aqueous solutions. Samples were irradiated with UV-visible light source (Osram, UltraVitalux E27, 300W). The average irradiation intensity of the used light source was 18 W/m^2 for the visible bandwidth, 3.2 W/m^2 for UV-A, 0.004 W/m^2 for UV-B and 0.004 W/m^2 for UV-C [47]. The distance between the light source and the MB aqueous solution was 25 cm. The characteristic absorbance decrease of MB at 664 nm recorded over irradiation time intervals, 0-240 minutes. A blank sample and bare CFs were prepared individually so as to show photocatalyst-free degradation of MB, and adsorbance capacities of ZnO NWs and bare CFs. To report self-degradation in dark and adsorption characteristics, MB aqueous solutions with samples were kept in dark for 24 hours. All chemicals and solvents were purchased from Sigma Aldrich and used without any further purification.

2.3.   Results and Discussion

2.3.1. Material Characterisation

Morphological structure was analysed by scanning electron microscopy. It was seen that from images ZnO nanowires were fabricated on carbon fibers by hydrothermal method, successfully. In general, ZnO nanowires stand almost vertical to the carbon fiber surface. SEM images of samples produced at 90 ^{o}C and 2 hours HT process time at different concentrations as shown in Figure 2.1.
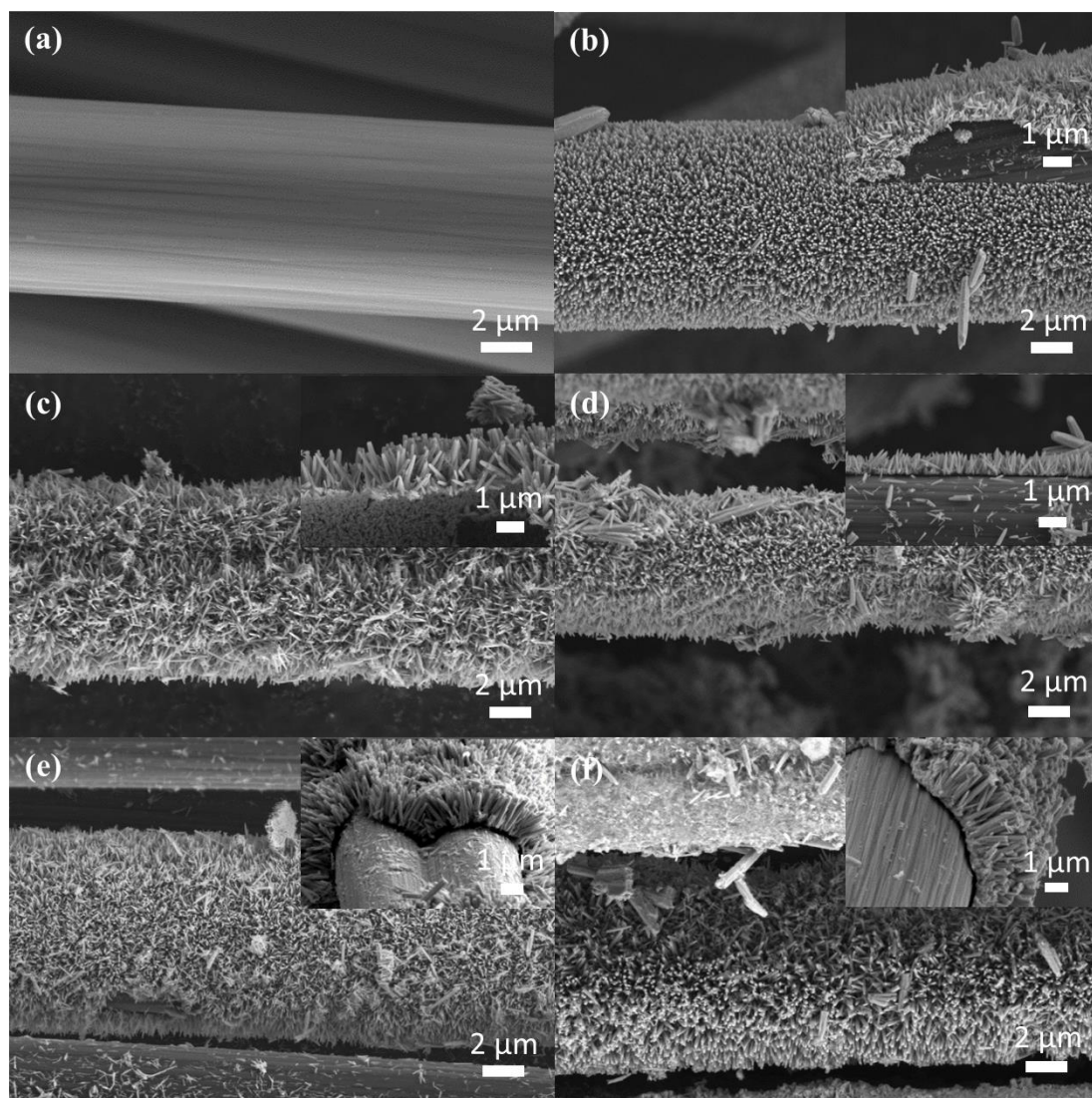
Figure 2.1 SEM images of seed layer coated carbon fiber (a), ZnO nanowires grown on carbon fibers produced at 10 mM (b), 20 mM (c), 30 mM (d), 40 mM (e), and 50 mM $Zn(NO_3)_2 \cdot 6H_2O$ (f).

The length and thickness of ZnO nanowires was measured by using Image J software from SEM images. According to these measurements, when HT process concentration increases from 10 mM to 50 mM, both the diameter and length of ZnO NWs increases. Average length of ZnO nanowires varies from 558±127 nm to 1932±222 nm with increase in concentration from 10 mM to 50 mM. Average thickness values varies from 38±10 nm to 317±95 nm with increase in concentration from 10 mM to 50 mM, as well as, standard deviations increase with increase in concentration. At low concentration more homogeneous size distribution is observed. On the other hand, aspect ratio (length/thickness) value decreases with increase in concentration. At low concentration, higher aspect ratio values are obtained. Average length/thickness values are given in Table 2.1. Dimension values versus

concentration are illustrated as column bar graph in Figure 2.2. Similar results have also been reported by Liu [3]. Its reported that the length and thickness of the produced ZnO nanowires were 1.2 µm and 40 nm, respectively (90 ^{o}C, 10 mM, 30 minute in bath kettle). Zhang also was investigated the effect of $Zn(NO_3)_2$ concentration on growth of zinc oxide nanowires at 90 °C for 4 hour and reported that thickness of zinc oxide nanowires increase as the concentration of growth solution increases [10].

Table 2.1 The length and thickness of ZnO nanowires grown on carbon fibers at different concentration.

C/mM	Length/nm		Thickness/nm		Aspect ratio
	Average	Max-Min	Average	Max-Min	
10	558±127	820-317	38±10	62-17	14.7
20	1376±402	2318-526	123±60	314-31	11.2
30	822±215	1227-437	91±26	135-44	9.0
40	1292±296	1749-625	151±50	236-85	8.6
50	1932±222	2210-1454	317±95	433-171	6
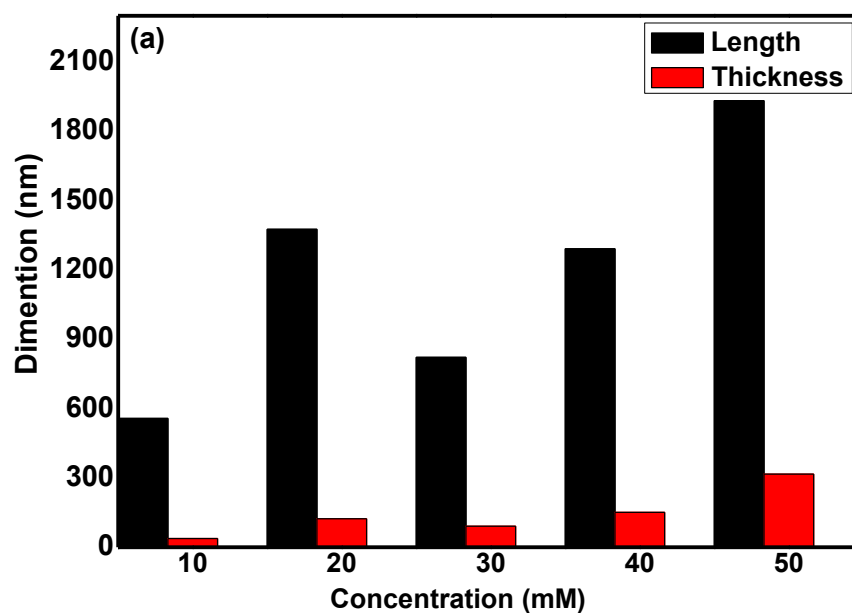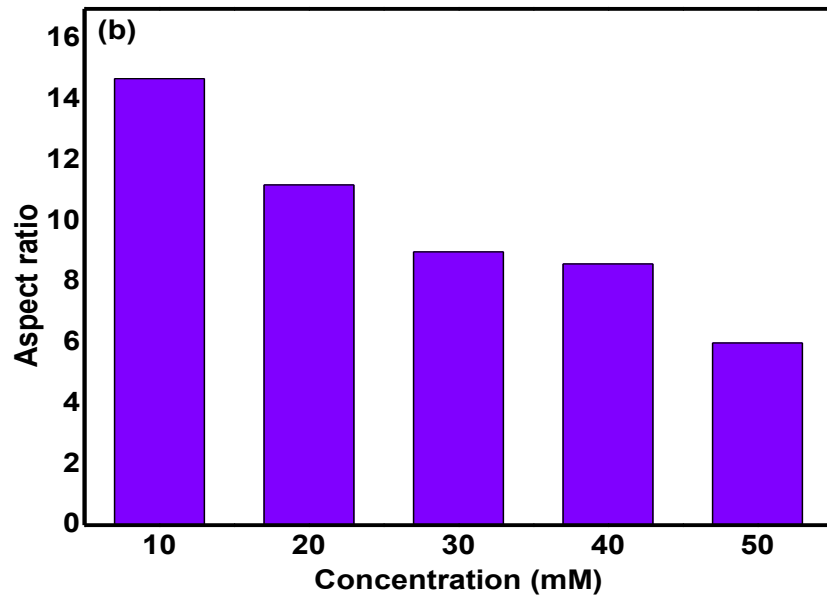
Figure 2.2 (a) The length and thickness and (b) the aspect ratio values of zinc oxide versus hydrothermal process concentration.

In order to reveal the crystallographic structure of the ZnO NWs/CFs structures, XRD analyses was performed (Figure 2.3). XRD results patterns shows samples have similar structure. Search-match process demonstrates that structure composed of Graphite-2H phase (indicated with 1) has hexagonal crystal structure of carbon (common name: cliftonine) (JCPDS number: 00-041-1487) and zincite phase (indicated with 2) has hexagonal crystal structure of ZnO (common name: Chinese white) (JCPDS number: 00-036-1451). The obtained XRD patterns are similar with patterns from Liu's study [48]. With increase in concentration peak intensities and peak widths increases.
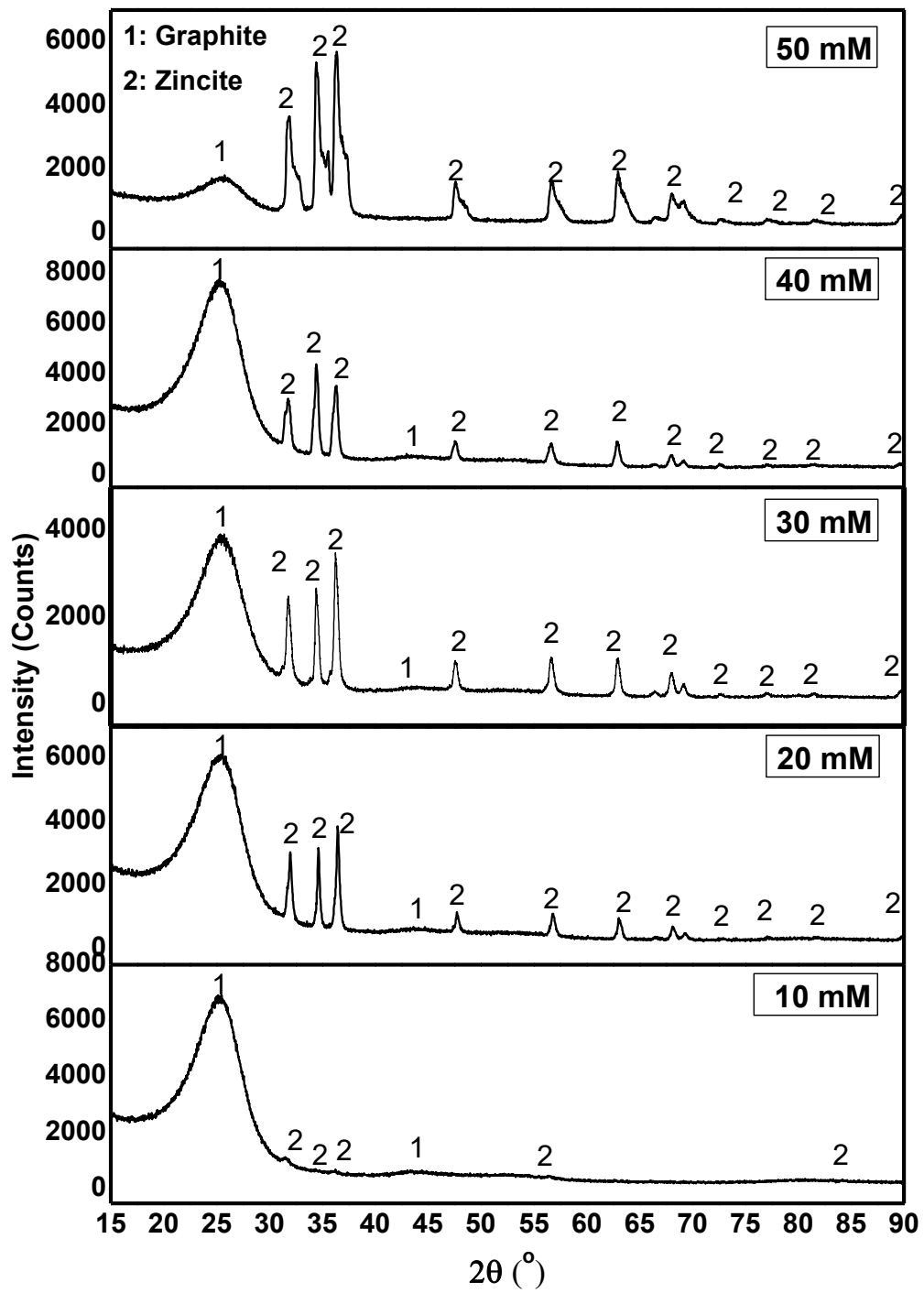
Figure 2.3 XRD patterns of ZnO nanowires grown on carbon fibers structures.

2.3.2. Photocatalytic Activity Test

The photocatalytic activity of ZnO NWs/CFs structures were tested on MB under solar light. The photocatalytic degradation kinetics of ZnO NWs/CFs structures were analysed by the spectrophotometric measurements under various irradiation time intervals. Photocatalytic degradation kinetics, degradation efficiency and percent degradation of ZnO NWs/CFs were analysed (Figure 2.4 and Table 2.2). It is observed that samples displayed Langmuir–Hinshelwood (L-H) kinetics model, which is a widely used kinetic model to explain the kinetics of the heterogeneous catalytic systems (Eq. 3.1).

$$\text{Ln } (C_o/C) = k_{app} \cdot t \tag{3.1}$$

where C_0 is the initial dye concentration, C is the instant dye concentration, k_{app} is the apparent reaction rate constant and t is time. In this model the linear relation is seen between $Ln(C_0/C)$ and t having a slope of $kapp$ [49].

The degradation efficiency values of samples (DE%) was calculated by Eq. 3.2:

$$DE\% = (C_0 - C_t)/ C_0 \times 100 \tag{3.2}$$

where t is the irradiation time, C_0 is the concentration of MB at time 0, and C_t are the concentration of MB at time t, respectively.

Photocatalytic kinetics, degradation ratios and percent degradation of the MB solutions are given in Figure 2.4(a), 2.4(b) and 2.4(c), respectively. The calculated $DE\%$ and k_{app} values are given in Table 2.2 for the all samples. The sample exhibiting the highest degradation rate as 1.5491 h^{-1} and the highest degradation rate as 99.86 % was the sample produced at 30 mM growth solution. The photocatalytic kinetics pointed out that increasing $Zn(NO_3)_2 \cdot 6H_2O$ concentration led to a higher degradation reaction rates. However, samples with higher aspect ratios (with increased catalyst surface area) displayed lower photocatalytic performance. This can be due to the discontinuity in macro level along the carbon fiber during the growth process at low concentrations. Similar results were reported in a study in which ZnO was deposited by sol-gel dip coating method. According to the study, the continuous films produced at the solutions with higher concentration, led to a higher degradation rates [6]. To reveal adsorption abilities of the samples and to show self-degradation of MB, samples were tested at dark for 24 hours. A slight decrease is observed from

self degradation test. Similar behavior is reported in the study by Chen et al [32]. Highest adsorption was observed on sample produced at 10 mM growth solution due to the enlarged surface area of ZnO nanowires. Sample produced at 30 mM growth solution displayed the highest percent degradation as 99.86%.
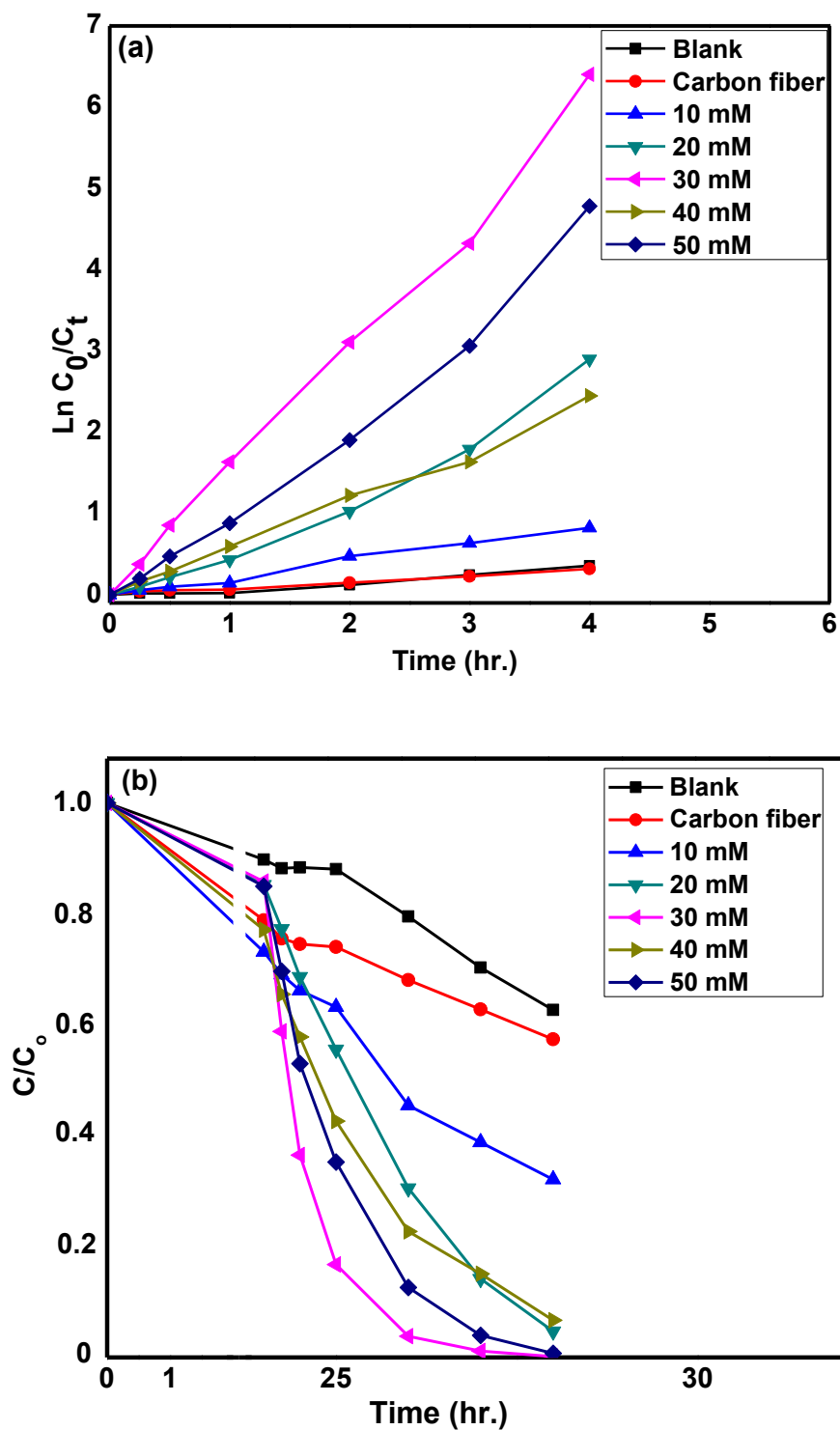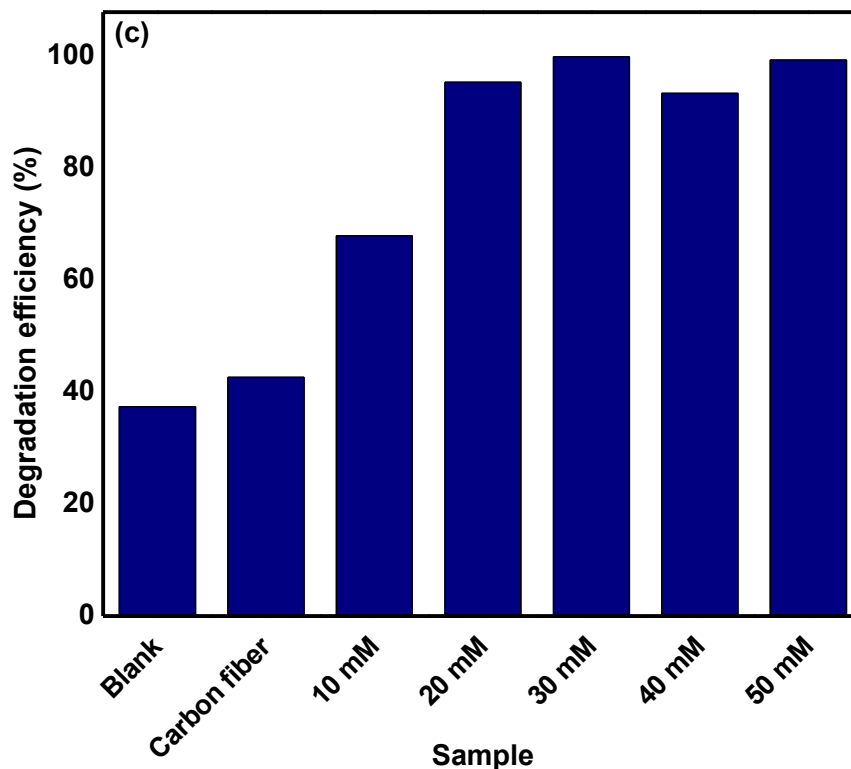
Figure 2.4 (a) Photocatalytic degradation kinetics (b) degradation rate and (c) barchart illustration of percent degradation.

Table 2.2 Photocatalytic degradation kinetic data.

Sample	Degradation efficiency (%)	$k_{app}(h^{-1})$	R^2
Blank	37.36	0.0807	0.9374
Carbon fiber	42.61	0.0775	0.9854
10 mM	67.90	0.2098	0.988
20 mM	95.31	0.6463	0.9633
30 mM	99.86	1.5491	0.9633
40 mM	93.32	0.5909	0.9942
50 mM	99.29	1.0984	0.9812

2.4. Conclusion

In this work, ZnO nanowires were synthesized on carbon fibers by hydrothermal method. SEM images of structures show that well aligned ZnO NWs were successfully grown on CFs. XRD patterns shows that ZnO NWs has zincite phase. The effects of growth solution concentration on dimensions and photocatalytic activity of ZnO nanowires were investigated. Results shows that, increase of concentration from 10 to 50 mM $Zn(NO_3)_2$. $6H_2O$ led to an increase in both, length and thickness and a decrease in aspect ratio. Sample with highest aspect ratio

19

displayed lowest photocatalytic activity. This can be due to the discontinuity of ZnO structure on carbon fiber surface. Sample produced at 30 mM growth solution shows the highest percent degradation as 99.86%.

CHAPTER 3

Optimization of Processing Parameters through Response Surface Methodology /Central Composite Design

Abstract

In this work, effects of hydrothermal (HT) synthesis method parameters, temperature, concentration and growth time, on the formation of zinc oxide nanowire structures on carbon fibers (ZnO NWs/CFs) were evaluated. Morphological, structural, photocatalytic properties were determined through scanning electron microscopy (SEM), X-ray diffraction (XRD), and UV-Visible spectrophotometer. In addition, response surface methodology (RSM) and central composite design (CCD) were applied to optimize the hydrothermal synthesis parameters. The results pointed out that, the change in hydrothermal solution concentration from 3.2 up to 37 mM $ZnNO_3.6H_2O$ and process time from 2.6 up to 9.2 hour led to the increase in thickness and decrease in aspect ratio of zinc oxide nanowires. Whereas, the temperature increases from 80 to 130 °C had a minute effect on the structure. ZnO nanowires with zincite structure were obtained for all processing conditions. Finally, photocatalytic activity of ZnO NWs/CFs on the degradation of aqueous methylene blue solution (MB) were recorded comparatively. ZnO NWs/CFs structure exhibited photocatalytic activity in the degradation of methylene blue (MB). The most effective structure was obtained at 120 °C, 30 mM $Zn(NO_3)_2.6H_2O$ and 4 hours HT synthesis parameters.

Keywords: Zinc Oxide Nanowires; Carbon fiber; Hydrothermal synthesis; Photocatalysis; Central composite design; Response surface methodology.

3.1. Introduction

Pristine ZnO absorbs ultraviolet (UV) light to produce holes and photoelectrons which easily recombine owing to its wide band gap (3.37 eV). To extend the spectral response into the visible light range and to decrease the band gap of ZnO structures, several approaches have been studied previously, such as utilization of carbon

materials as a substrate, surface treatment of photo-sensitization by some molecules with the ability of absorbing light and transferring the energy to the desired reactants and incorporation of different elements into the structure [34, 48, 50].

To produce ZnO nanostructures on carbon fibers, hydrothermal synthesis has been considered as one of the most practical method for growing controlled, textured and well aligned ZnO structures [10, 11]. In literature, researchers have produced and characterized ZnO nanowires on CFs through hydrothermal synthesis method. For example, Chen et al. investigated the effect of processing time [11], Liu investigated the effect of various growth durations [35] and Zhang et al. handled the duration and solution concentration [10]. Although such aforementioned studies dealing with the parametric study of the process parameters on the formation of ZnO NWs/CFs are available in the literature, to the best of our knowledge, we could not report any study evaluating these effects through a statistical design of experiment method. With this motivation, in this study, it is aimed to synthesize ZnO nanostructures on a conductive carbon fiber by hydrothermal synthesis method and evaluate the effect of temperature, concentration and time on structure, morphology and photocatalytic activity of ZnO nanowires on carbon fibers by central composite design providing optimum photocatalytic properties.

3.2.   Experimental Studies

3.2.1. Materials and Method

ZnO nanowires were successfully grown on commercial carbon fibers (CFs) via hydrothermal synthesis. Initially the fibers (Aksaca, 12K A-42) were washed with nitric acid (30%), water and ethanol and it was dried at 60 °C in air. Then, CFs were coated with ZnO seed layer. To prepare ZnO seed solution, 25 mg zinc acetate dihydrate ($Zn(CH_3COO)_2$) 10 mg sodium hydroxide was dissolved in 100 mL ethanol. The solution was stirred for 1.5 hour without heating. CFs was dipped into ZnO seed solution for 10 minutes to obtain ZnO seed layer to be coated on the surface of CFs. Then CFs annealed at 150 °C for 10 min. The process was repeated for four times. For the growth of ZnO nanowires, ZnO seed-coated CFs were immersed in zinc nitrate hexahydrate ($Zn(NO_3)_2 \cdot 6H_2O$) and hexamethylenetetramine (HMTA) solution in Teflon-lined stainless autoclave. ZnO NWs coated CFs were, then rinsed with distilled water and dried at 60 °C. Heat treatment (250 °C, 120 min,

in air) was followed this process which led the transformation of amorphous structure into crystalline zincite phase. The evaluated temperatures, $Zn(NO_3)_2.6H_2O$ concentrations and time are given in Table 3.1.

Crystal structures were analyzed using X-ray diffractometer (Panalytical Empyrean XRD, Empreyan Package T-T). The X-ray diffraction data were recorded by using Cu Kα radiation (1.5406 A°). The intensity data were collected over a 2Ө range of 15° to 90°. The morphology of the samples was investigated with Scanning electron microscope (SEM) (Carl Zeiss 300VP SEM).

The photocatalytic degradation kinetics were monitored by the spectrophotometric measurements (Shimadzu UV-1240). Photocatalytic activity of ZnO NWs/CFs were examined by photodegradation of 10^{-5} M methylene blue (MB) aqueous solutions under UV light source (Osram, UltraVitalux E27, 300W). In addition to ZnO NWs/CFs samples, a blank sample and bare CFs were prepared individually so as to show photocatalyst-free degradation of MB aqueous solutions. Initially, the samples in MB aqueous solutions were kept in dark for 24 hours to report self-degradation and adsorption characteristics. The distance between the MB aqueous solution and the light source was 25 cm. The average irradiation intensity of the employed light source was 18 W/m^2 for the visible bandwidth, 3.2 W/m^2 for UV-A, 0.004 W/m^2 for UV-B and 0.004 W/m^2 for UV-C [47]. The irradiation time intervals, 0-240 minutes, were recorded by means of the characteristic absorbance decrease of MB at 664 nm to obtain photocatalytic kinetics of ZnO NWs/CFs. All chemicals and solvents were purchased from Sigma Aldrich and used without any further purification.

3.2.2. Design of Experiment

As frequently stated in previous photocatalytic studies, the specific surface area of the catalyst is crucial in activity and performance [51-53]. Therefore, the ZnO NWs length, thickness and the aspect ratio were evaluated as critical responses of the study. In order to analyze the effects of these factors and produce the most favorable structure, design of experiments (DOE) is employed [54, 55].

Experimental design is a good strategy to decrease the number of tests and to reduce the time and consumption rate of material resources. By applying the design of experiments, possible interactions among the studied factors and among their probable effect on the response of the process can be analyzed [56]. Response surface methodology (RSM) is a common technique in design of experiments. The

RSM is a set of statistical and mathematical model, which is used to optimize many different processes. Central composite design (CCD) is a kind of RSM method that have high predictability of response [57]. Each factor is varied over three levels: the high level (+1), the low level (-1), axial points (coded as ±α) and the center points (coded as level 0). In the CCD arrays, the levels of the factors are on the edges, center and circumscribed at the center of sides (Figure 3.1) [58].
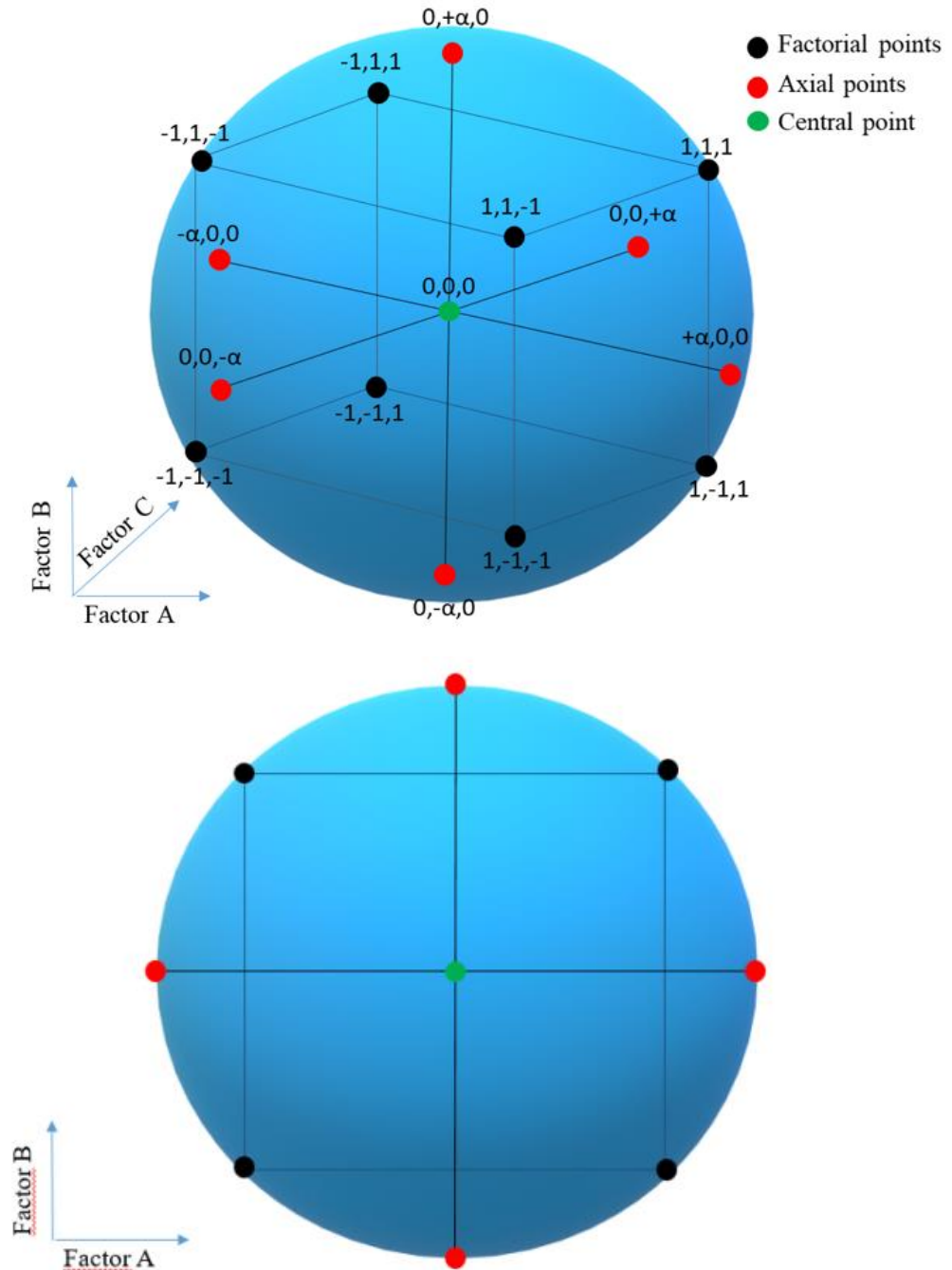
Figure 3.1 Levels of the central composite design.

The relationship between the response and the three variables can be described by an empirical second-order polynomial equation (Eq 4.1):

$$Y(\%) = \alpha_0 + \sum_{i=1}^{n} \alpha_i X_i + \sum_{i=1}^{n} \alpha_{ii} X_i^2 + \sum_{i=1}^{n-1} \sum_{j=2}^{n} \alpha_{ij} X_i X_j + \varepsilon \qquad (4.1)$$

In this model, Y is the predicted answer, $\alpha_\circ$ a constant coefficient, α_i the linear effects, α_{ii} the square effects, α_{ij} the interactive effects, ε the error of the prediction equation and X_i and X_j are encoded independent variables [56]. Each of the variables was examined at five different levels ($-\alpha$, -1, 0, 1, $+\alpha$). The ranges and levels of the process parameters are given in Table 3.1. Experimental runs and variables are given in Table 3.2. In our study, the measured response variables were length and diameter of ZnO NWs. Nanostructures of the samples were analyzed using scanning electron microscope (SEM) and the thickness and length measurements were performed via Image J software.

Table 3.1 Actual and coded values of independent variables used for experimental design.

Variables	Ranges and actual values of coded levels				
	-α	-1	0	+1	+α
Temperature/°C	80	90	105	120	130
Concentration/mM	3.2	10	20	30	37
Duration/hour	2.6	4	6	8	9.6

α = 1.682 (axial point for CCD)

Table 3.2 Experimental runs for experimental design.

Experimental Runs	Factors		
	A	B	C
1	-1	-1	-1
2	1	-1	-1
3	-1	1	-1
4	1	1	-1
5	-1	-1	1
6	1	-1	1
7	-1	1	1
8	1	1	1
9	0	0	0
10	0	0	0
11	0	0	0
12	-α	0	0
13	+α	0	0
14	0	-α	0
15	0	+α	0
16	0	0	-α
17	0	0	+α
18	0	0	0
19	0	0	0
20	0	0	0

α = 1.682 (axial point for CCD)

The Minitab 19 software was used to make regression for regression analysis of experimental data. The main, interaction and quadratic effects were evaluated in this design. 20 different experiments were performed and then the results were reported. So as to evade the systematic errors, the experiments were done in random order. The response of the design experiment was the length and the thickness of ZnO nanowires grown on carbon fiber. The analysis of variance (ANOVA) compares the response variable means at the different factor levels and evaluates the importance of one or more factors. In order to assess the main interaction and quadratic effects in the promoted design, ANOVA was applied.

3.3. Results and Discussion

3.3.1. Materials Characterization

The comparative SEM images of ZnO nanowires on carbon fiber obtained from different temperature, concentration and time via hydrothermal process are given in Figures 3.2-3.4. It is seen that ZnO nanowires were successfully produced. Almost in all structures, ZnO NWs stand vertically to the CFs. The average length, thickness and aspect ratio values of ZnO nanowires are given in Table 3.4. According to these results, the length, thickness and aspect ratio of the ZnO NWs/CFs are varied from 492 nm to 1429 nm, 23 nm to 111 nm and 9.4 to 39.4, respectively. When the hydrothermal process time was increased, thickness of ZnO NWs also increased. Generally, with the increase in concentration, the thickness of ZnO nanowires increases and the aspect ratio decreases. The obtained results are in a good agreement with the results in the literature [10, 11]. In contrast to the effects of concentration and time, temperature is found to be a non-significant parameter on the dimensions of ZnO nanowires.
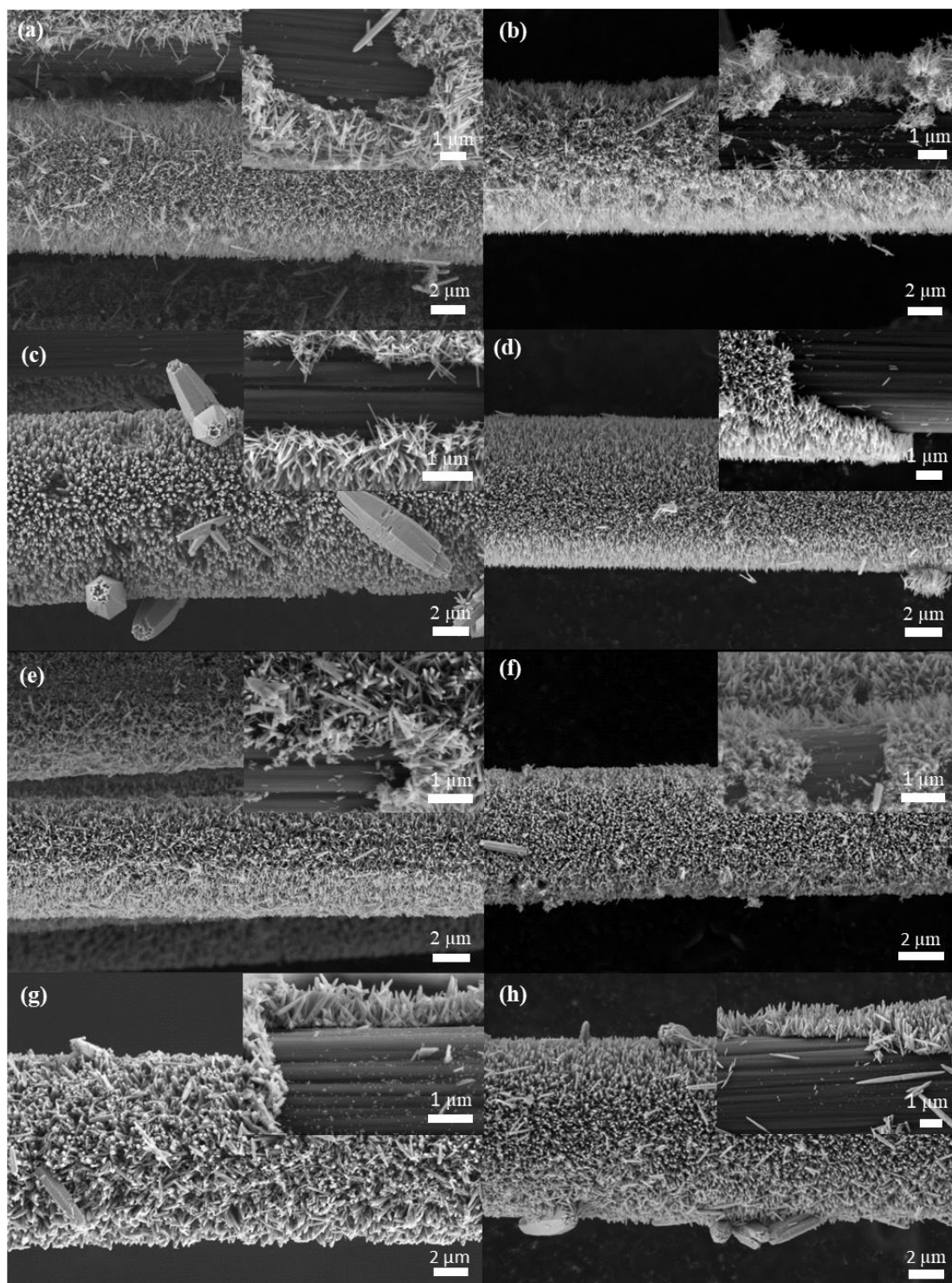
Figure 3.2 SEM images of 90°C 10 mM 4 hour (Run 1) (a), 90°C 10 mM 8 hour (Run 5) (b), 90°C 30 mM 4 hour (Run 3) (c), 90°C 30 mM 8 hour (Run7) (d), 120°C 10 mM 4 hour (Run 2) (e), 120°C 10 mM 8 hour (Run 6) (f), 120°C 30 mM 4 hour (Run 4) (g), 120°C 30 mM 8 hour (Run 8) (h) samples.
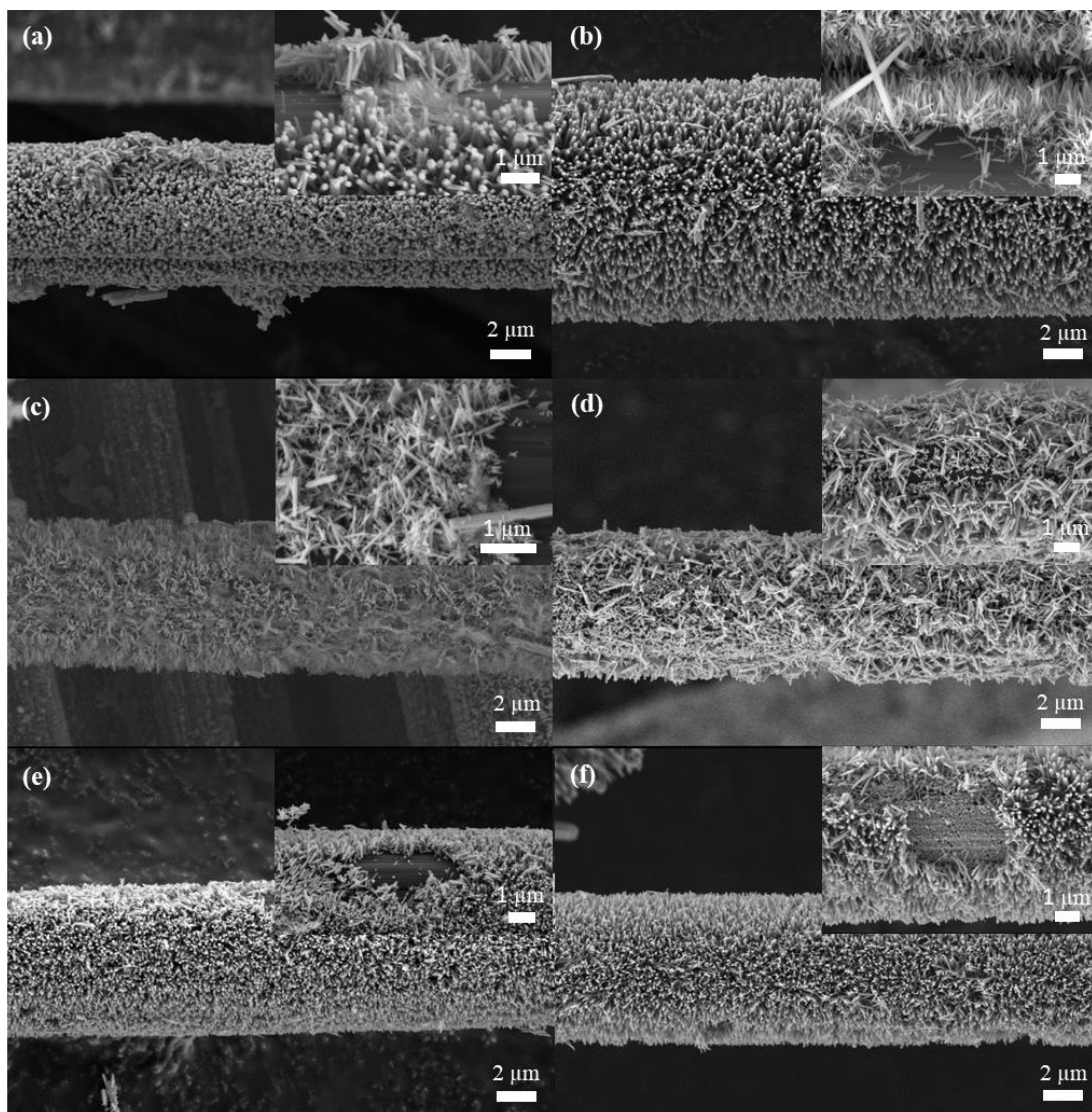
Figure 3.3 SEM images of ZnO NWs/CF structures produced at axial point levels 80 °C (Run 18) (a), 130 °C (Run 10) (b), 3.2 mM (Run 16) (c), 37 mM (Run 17) (d), 2.6 hour (Run 1) (e) and 9.6 hour (Run 13) (f).
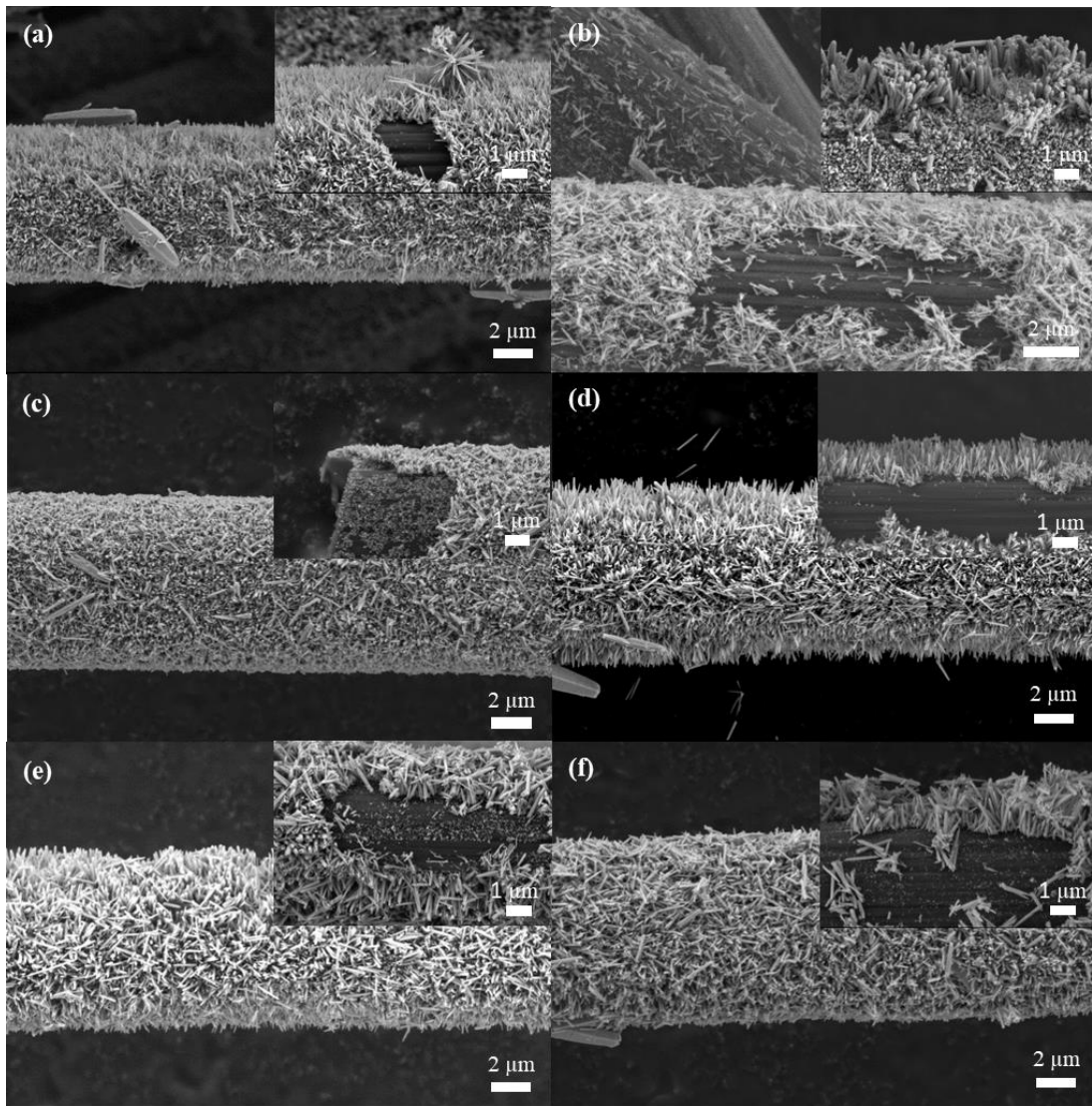
Figure 3.4 SEM images of ZnO NWs/CF structures produced at 105 °C, 20 mM and 6 hour (center point). C1 (Run 4) (a), C2 (Run 11) (b), C3 (Run18) (c), C4 (Run 22) (d), C5 (Run 19) (e) and C6 (Run 20) (f).

In order to reveal the crystallographic structure of the ZnO NWs/CFs, XRD analysis were performed and given in Figure 3.5, 3.6, and 3.7. Patterns demonstrate that the structure is composed of Graphite (indicated with 1) phase from CFs (JCPDS number: 00-041-1487) and zincite phase (indicated with 2) from nanowires (JCPDS number: 00-036-1451). In summary, increasing the $Zn(NO_3)_2 \cdot 6H_2O$ concentration led to increase in ZnO crystallinity and vice versa. The obtained XRD patterns are similar with the patterns from the study of Lui et al. [48].
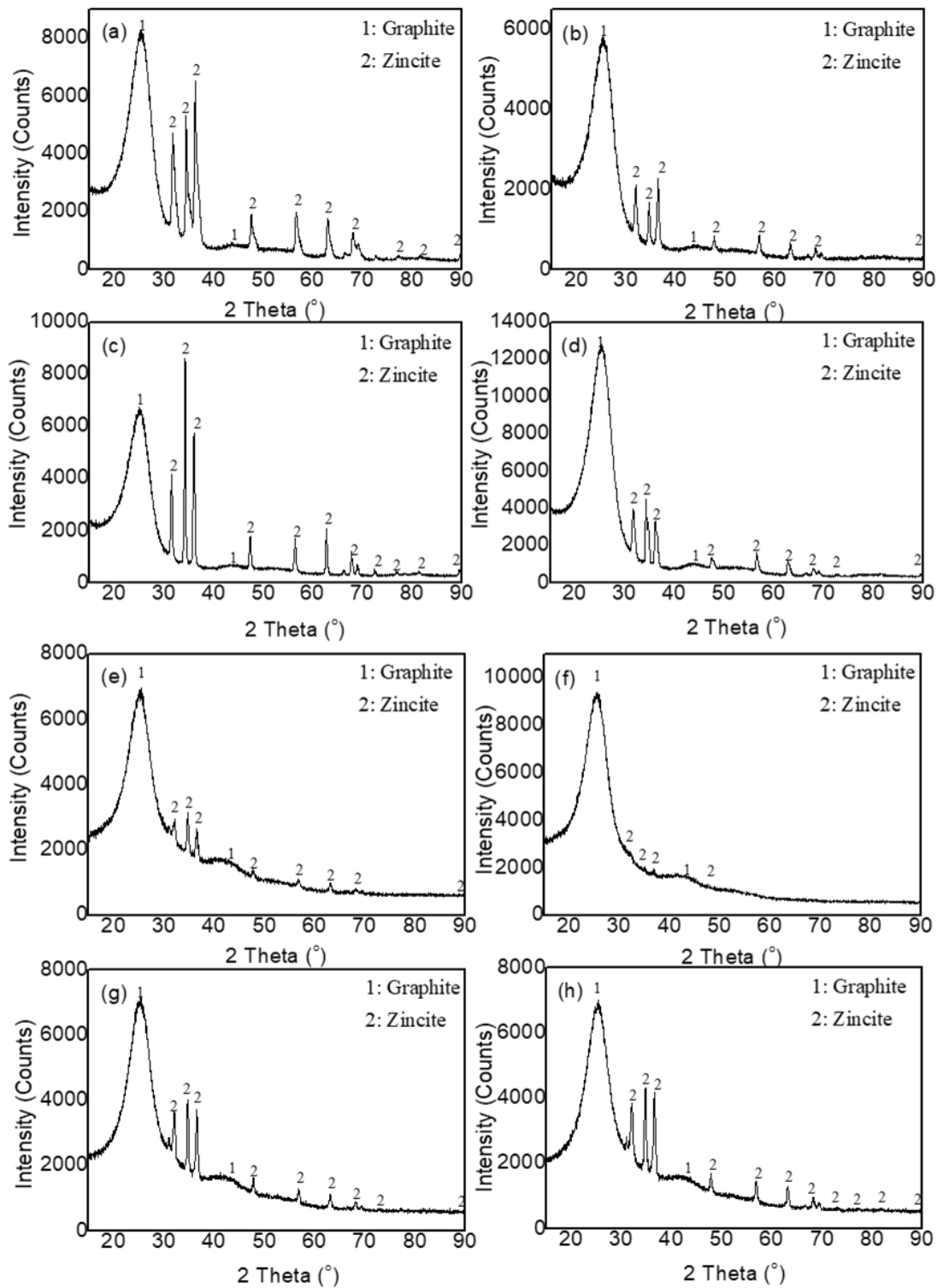
Figure 3.5 XRD patterns of corner point samples. 90 ^{o}C 10 mM 4 hour (Run 1), (a) 90 ^{o}C 10 mM 8 hour (Run 5) (b), 90 ^{o}C 30 mM 4 hour (Run 3) (c), 90 ^{o}C 30 mM 8 hour (Run7) (d), 120 ^{o}C 10 mM 4 hour (Run 2) (e), 120 ^{o}C 10 mM 8 hour (Run 6) (f), 120 ^{o}C 30 mM 4 hour (Run 4) (g), 120 ^{o}C 30 mM 8 hour (Run 8) (h).

Figure 3.6 XRD patterns of axial point samples. 80 ^{o}C (Run 18) (a), 130 ^{o}C (Run 10) (b), 3.2 mM (Run 16) (c), 37 mM (Run 17) (d), 2.6 hour (Run 1) (e) and 9.6 hour (Run 13) (f).

Figure 3.7 XRD patterns of samples produced at 105 °C, 20 mM and 6 hour (center point). C1 (Run 4) (a), C2 (Run 11) (b), C3 (Run18) (c), C4 (Run 22) (d), C5 (Run 19) (e) and C6 (Run 20) (f).

3.3.2. Photocatalytic Activity Tests

Heterogeneous photocatalytic degradation reactions, the conversion of soluble organic contaminants into CO_2 and H_2O, are mostly evaluated by monitoring the change in the concentration of the contaminates by time [59]. The changes in the concentration are mostly displayed Langmuir–Hinshelwood (L-H) kinetics model. Langmuir–Hinshelwood (L–H) is the most commonly used model to describe the kinetics of the heterogeneous catalytic systems. The L-H model was evaluated by the following Eq. 4.2:

$$ln\ (\frac{C_0}{C_t}) = k_{app} \times t \qquad\qquad (4.2)$$

where C_t is the instant dye concentration, C_0 is the initial dye concentration, k_{app} is the apparent reaction rate constant and t is time. This model demonstrates the linear relation between $Ln(C_0/C_t)$ and t having a slope of k_{app} [49]. The degradation efficiency (*DE%*) was calculated as:

$$DE\% = \frac{(C_0 - C_t)}{C_0 \times 100} \qquad\qquad (4.3)$$

Photocatalytic kinetics, degradation ratios, and percent degradation of the MB solutions are given in Figure 3.8(a), 3.8(b) and 3.8(c), respectively. The calculated k_{app} and *DE%* values are listed in Table 3.3 for the all samples. The highest degradation rate, 1.2707 h^{-1}, is seen with the sample produced at 120 ^{o}C with 30 mM $Zn(NO_3)_2.6H_2O$ solution for 4 hours. The photocatalytic kinetics pointed out that there is no significant effect of temperature and time on the degradation reactions. On the other hand, increasing $Zn(NO_3)_2.6H_2O$ concentration (10 mM to 30 mM) led to higher degradation reaction rates. Here, it is important to note that samples with lower $Zn(NO_3)_2.6H_2O$ concentrations, with higher aspect ratios (with increased catalyst surface area) exhibit lower photocatalytic performance. In contrast to SEM observations from a local point of the samples, the obtained incoherent photocatalytic results could be addressed to the discontinuity in macro level along the carbon fiber during the growth process. Similar results can be observed in a study in which ZnO was deposited by sol-gel dip coating method. According to the study, the continuous films, deposited from the solutions with higher concentration, exhibited higher degradation rates [54]. Additionally, similar behavior as shown in Figure 3.8(b) for self-degradation at dark for 24 hours, reported by Chen et al [32]. However, in the study of Zhang et al, in which the duration of self-degradation for only 60 minutes, they observed a slight change in concentration [10]. Finally, the higher percent degradation was observed with the same sample (hydrothermal process parameters: 120 ^{o}C 30 mM and 4 hours) as 99.86%. Results indicates that enlarged surface area of ZnO NWs/CFs led to an increased adsorption ability.
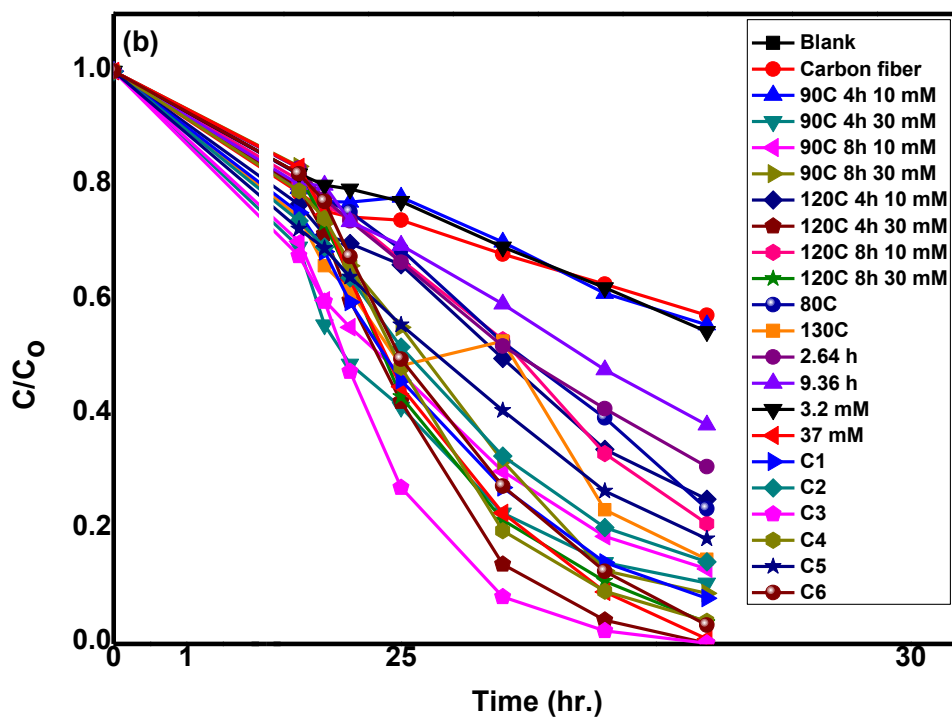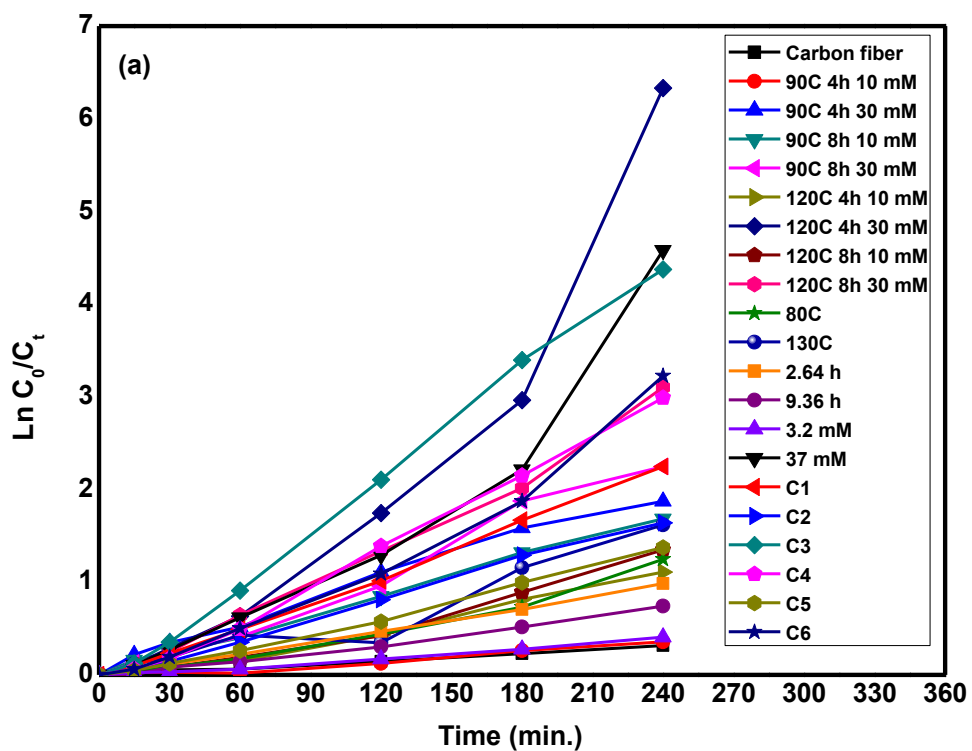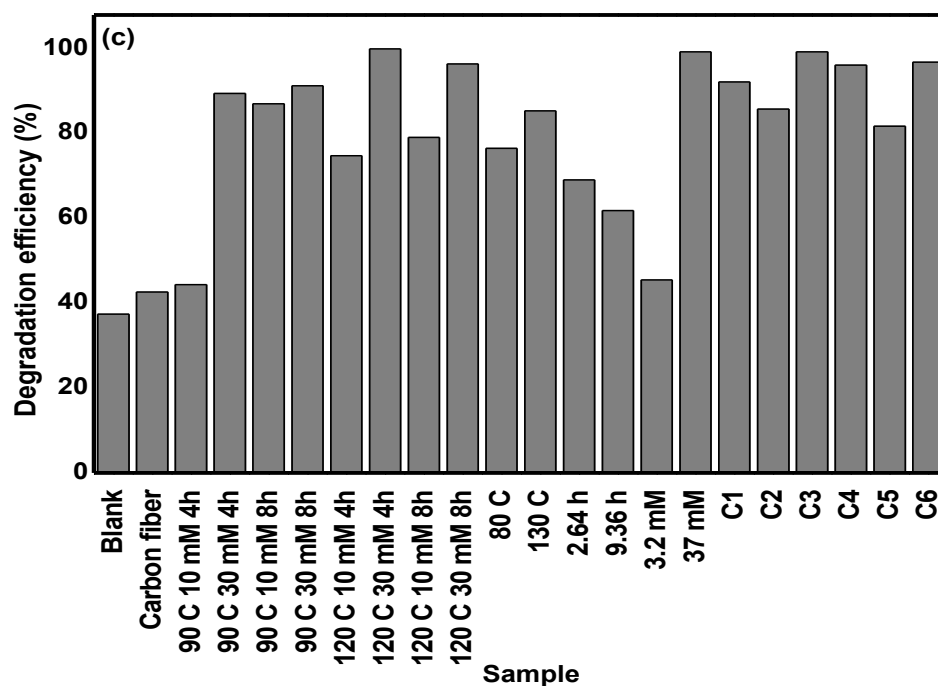
Figure 3.8 (a) Photocatalytic degradation kinetics, (b) degradation ratio and (c) bar chart illustration of percent degradation of methylene blue solutions.

Table 3.3 Photocatalytic degradation kinetic data.

Sample	Degradation efficiency (%)	$k_{app}(h^{-1})$	R^2
Blank	37.36	0.0807	0.9374
Carbon fiber	42.61	0.0775	0.9854
90 ^{o}C 10 mM 4h	44.32	0.0827	0.9436
90 ^{o}C 30 mM 4h	89.35	0.5018	0.9826
90 ^{o}C 10 mM 8h	86.93	0.4273	0.9973
90 ^{o}C 30 mM 8h	91.19	0.564	0.9818
120 ^{o}C 10 mM 4h	74.72	0.2625	0.9746
120 ^{o}C 30 mM 4h	99.86	1.2707	0.8899
120 ^{o}C 10 mM 8h	78.98	0.3019	0.9544
120 ^{o}C 30 mM 8h	96.31	0.7231	0.9871
80 ^{o}C	76.42	0.2734	0.956
130 ^{o}C	85.23	0.3692	0.9166
2.64 h	69.03	0.2408	0.9982
9.36 h	61.79	0.1751	0.9853
3.2 mM	45.45	0.0953	0.9811
37 mM	99.15	0.9346	0.9047
C1*	92.05	0.5495	0.9962
C2*	85.65	0.4121	0.9952
C3*	99.15	1.0893	0.9938
C4*	96.02	0.7185	0.9862
C5*	81.68	0.3292	0.9894
C6*	96.73	0.7029	0.9525

C: Central points

3.3.3. Response Surface Regression of Length of ZnO Nanowires

The hydrothermal synthesis parameters employed as the variables in the experimental design; $ZnNO_3 \cdot 6H_2O$ concentration, time and temperature were evaluated by response surface methodology. To find the most important effects and interactions, analysis of variance (ANOVA) was calculated using the results obtained from previous characterizations as in Table 3.4.

Table 3.4 Design matrix and experimental results at length and thickness for the central composite design.

Exp. run	Temp.* °C	Conc.** mM	Time hour	Length nm	Thickness nm	Aspect ratio	k_{app} h^{-1}
1	90	10	4	906	23	39.4	0.0827
2	120	10	4	819	42	19.5	0.2625
3	90	30	4	1429	99	14.4	0.5018
4	120	30	4	678	72	9.4	1.2707
5	90	10	8	1188	31	38.3	0.4273
6	120	10	8	699	41	17.1	0.3019
7	90	30	8	1368	111	12.3	0.564
8	120	30	8	1070	76	14.1	0.7231
9	80	20	6	774	80	9.7	0.2734
10	130	20	6	1167	77	15.2	0.3692
11	105	3.2	6	620	28	22.1	0.0953
12	105	37	6	1200	109	11.0	0.9346
13	105	20	2.64	492	50	9.8	0.2408
14	105	20	9.36	828	65	12.7	0.1751
15	105	20	6	1151	97	11.9	0.7029
16	105	20	6	785	46	17.1	0.4121
17	105	20	6	1038	74	14.0	0.3292
18	105	20	6	854	75	11.4	1.0893
19	105	20	6	662	57	11.6	0.5495
20	105	20	6	849	75	11.3	0.7185

*Temp.:Temperature, **Conc.: Concentration

The relationship between dependent parameters and independent parameters was obtained using a quadratic model fitting method as shown in following equation (Eq. 4.4).

$$Length = 3343 - 60.4\,A + 32.0\,B + 129\,C + 0.296\,A*A + 0.424\,B*B - 11.1\,C*C - 0.394\,A*B + 0.21\,A*C + 1.06\,B*C \qquad (4.4)$$

where *A*, *B* and *C* are denoting the process variables temperature, concentration and process time, respectively. This designation is used in the following tables and equations. Additionally; "variable1*variable2" (i.e. A*B) was used to show 2-way

interaction or to express combined effect of the variables. The negative sign in front of the terms indicates the antagonistic effect, whereas the positive sign shows the synergistic effect.

ANOVA shows whether the variations related to the model are significant according to the variability of the experimental results or not. The non-significant lack of fitted p-values are more than 0.05 for the response indicated bad predictability of the model [60].

Initial ANOVA results, effect of temperature, concentration and process time on the length are shown in Table 3.5. The results demonstrate that, all of the parameters are not significant and not predictable for the length of ZnO NWs since the p-values are equal to or greater than 0.05. Adjusted R squared and R-squared values as 0.00% and 45.40%, respectively indicate a bad predictability for the model. The large residuals were obtained for 80 °C (Run 9) and 90 °C 10 mM 8 h (Run 5) as given in Table 3.6. The residual plots of statistical analysis are given in Figure 3.9.

Table 3.5 ANOVA for the response quadratic model of length.

Source	DF	Adj SS	Adj MS	F-Value	P-Value
Model	9	578513	64279	0.92	0.543
Linear	3	97478	32493	0.47	0.712
A (Temperature)	1	52089	52089	0.75	0.407
B (Concentration)	1	12144	12144	0.17	0.685
C (Time)	1	7444	7444	0.11	0.750
Square	3	131767	43922	0.63	0.611
A*A	1	61998	61998	0.89	0.367
B*B	1	26261	26261	0.38	0.553
C*C	1	32493	32493	0.47	0.510
2-Way Interaction	3	31861	10620	0.15	0.926
A*B	1	27966	27966	0.40	0.540
A*C	1	325	325	0.00	0.947
B*C	1	3570	3570	0.05	0.825
Error	10	695675	69568		
Lack-of-Fit	5	539665	107933	3.46	0.100
Pure Error	5	156011	31202		
Total	19	1274189			

DF: Degree of freedom, SS: Sum of squares, MS: Mean square

Table 3.6. Fits and diagnostics for unusual observations.

Run	Response	Fit	Residual	Std Residual
5	1188	874	314	2.06 R
9	774	1190	-416	-2.49 R

R: Large residual

Pareto chart of the standardized effects shows if the factor is significant or not (Figure 3.9(a)). In good agreement with p values, pareto chart indicates the factors that are not significant. Figure 3.9(b) clarifies the normal probability plot of the residuals. The points in this plot should form a straight line which proves the normal distribution. The points on the plot departed from a straight line, the normality assumption is invalid. Residuals versus fitted values are shown in Figure 3.9(c) This plot demonstrated a random pattern of residuals on both sides of 0. Some points lay far from the majority of points, which may be an outlier. Figure 3.10 represents the three-dimensional fitted response surface plots for the ZnO nanowire length versus temperature, concentration and process time.
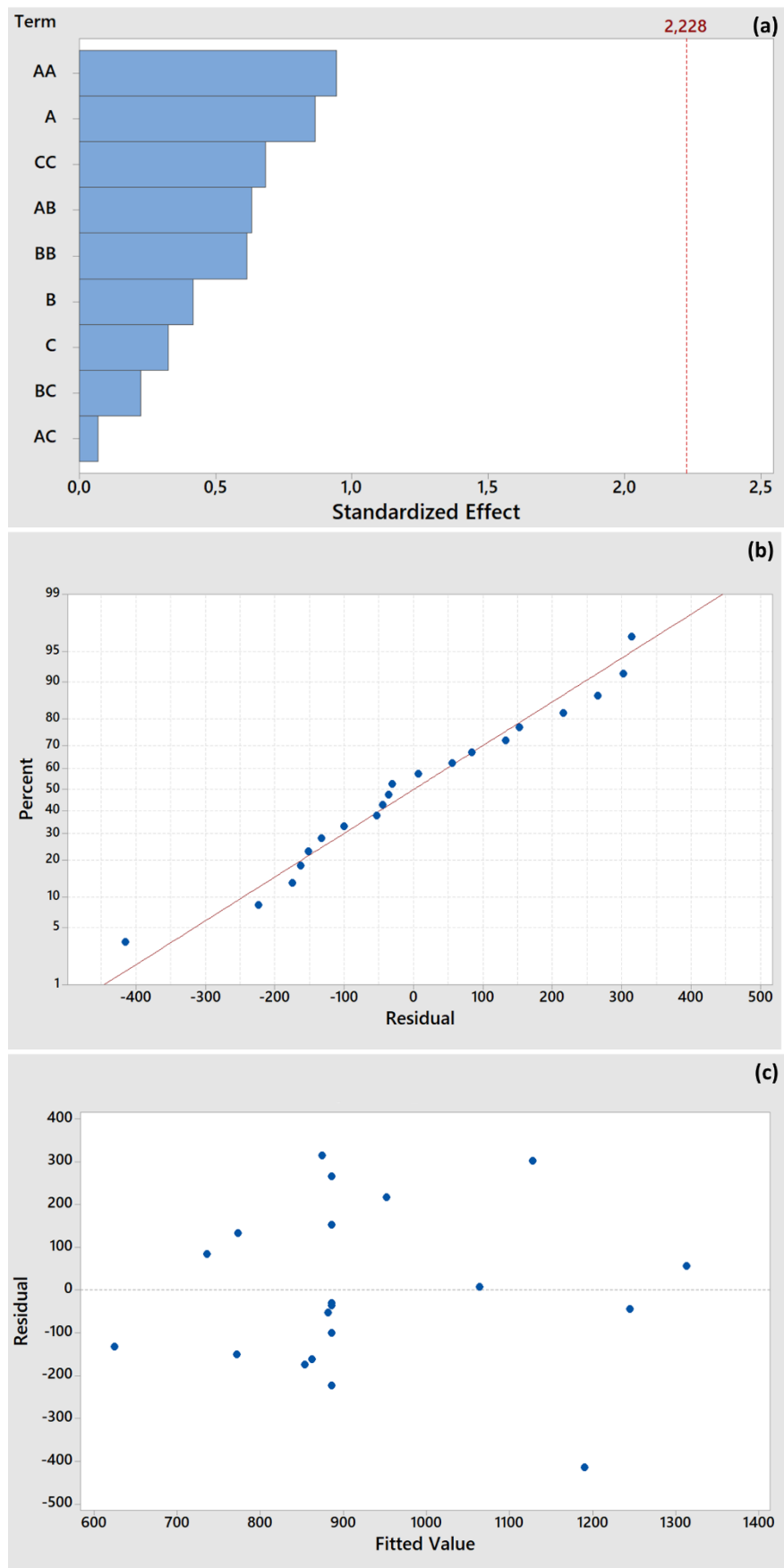
Figure 3.9 (a) Pareto chart, (b) residuals versus fitted values, (c) the normal probability plot of residuals for length.
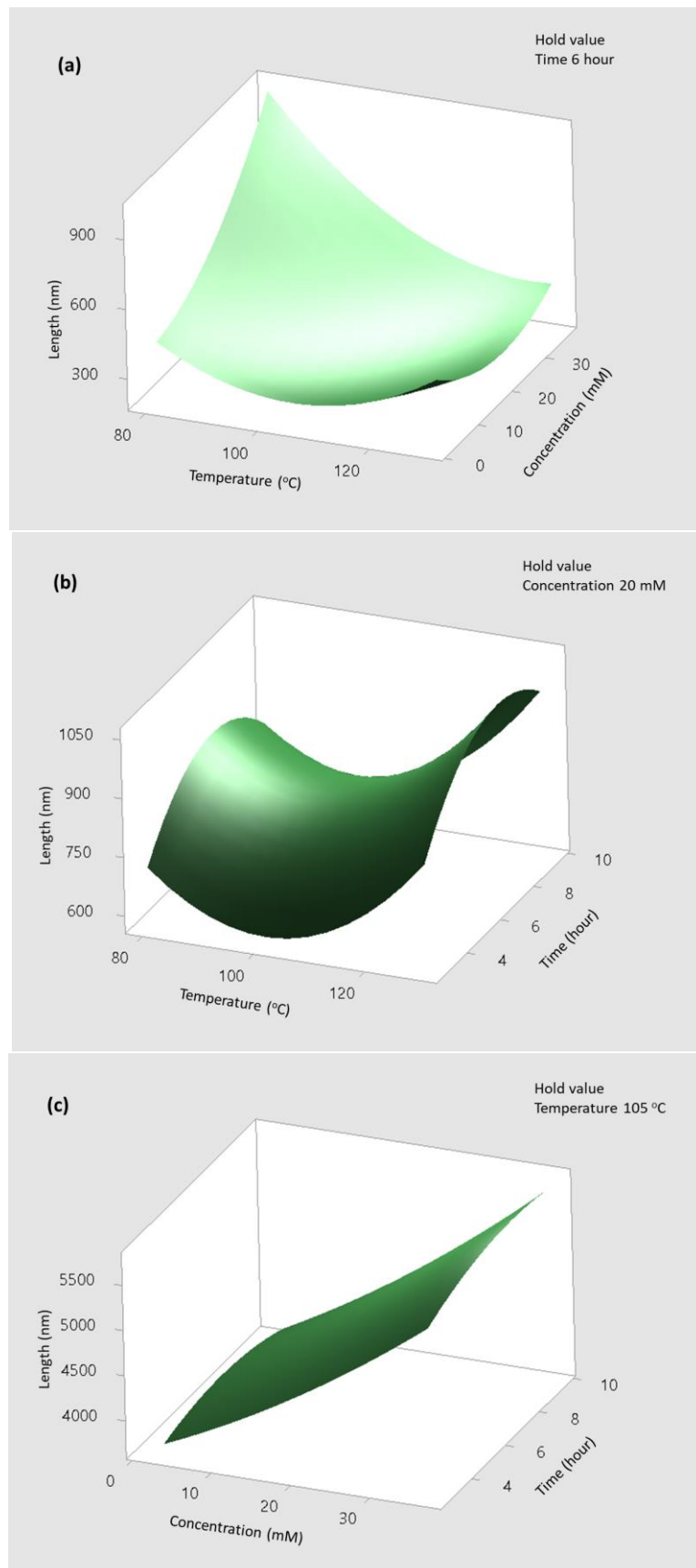
Figure 3.10 Surface plots of length versus (a) concentration, temperature, (b) temperature, time, and (c) concentration, time (A:Temperature, B:Concentration, C:Time).

3.3.4. Response Surface Regression of Thickness of ZnO Nanowires

Table 3.7 shows the effects of process variables on thickness of ZnO nanowires with a confidence level of 86.50%. According to our results, concentration is a significant factor on ZnO nanowires thickness (p<0.05). A*B 2-way interaction, which shows the combined effects of temperature and concentration, has also a significant effect on the thickness. The regression model is given by following equation:

$$Thickness = -159 + 0.43\,A + 11.12\,B + 24.6\,C + 0.0063\,A*A - 0.0220\,B*$$
$$B - 1.370\,C*C - 0.0758\,A*B - 0.071\,A*C + 0.056\,B*$$
$$C \tag{4.5}$$

Table 3.7 ANOVA for the response quadratic model of thickness.

Source	DF	Adj SS	Adj MS	F-Value	P-Value
Model	9	11293.6	1254.85	7.12	0.003
Linear	3	9592.8	3197.60	18.14	0.000
A (Temperature)	1	123.4	123.36	0.70	0.422
B (Concentration)	1	9326.3	9326.29	52.89	0.000
C (Time)	1	145.5	145.46	0.82	0.385
Square	3	597.1	199.04	1.13	0.383
A*A	1	27.9	27.92	0.16	0.699
B*B	1	70.3	70.34	0.40	0.542
C*C	1	492.9	492.86	2.80	0.125
2-Way Interaction	3	1081.4	360.46	2.04	0.172
A*B	1	1035.1	1035.13	5.87	0.036
A*C	1	36.1	36.13	0.20	0.660
B*C	1	10.1	10.12	0.06	0.815
Error	10	1763.2	176.32		
Lack-of-Fit	5	225.9	45.17	0.15	0.972
Pure Error	5	1537.3	307.47		
Total	19	13056.8			

Adjusted R squared of 74.34% and R-squared of 86.45% indicate a high predictability of the model. The residual plots of statistical analysis are given in Figure 3.11. Pareto chart of the standardized effects shows that the concentration is a significant factor on thickness of ZnO nanowires (Figure 3.11(a)). Pareto chart, also indicates that the interaction of concentration and temperature is significant and they are in good agreement with p-values. The normal probability plot of residuals is shown in Figure 3.11(b). The points in this plot formed a straight line which proves normal distribution. Residuals versus fitted values are given in Figure 3.11(c). Some

points lay far from the majority of points, which may be an outlier. In general, there's not any recognizable pattern in the residual plot. Three-dimensional fitted response surface plots for the ZnO nanowire length vs. variables are given in Figure 3.12. Surface plots of response concentration vs temperature (B;A) (Figure 3.12(a)) can be used for prediction.
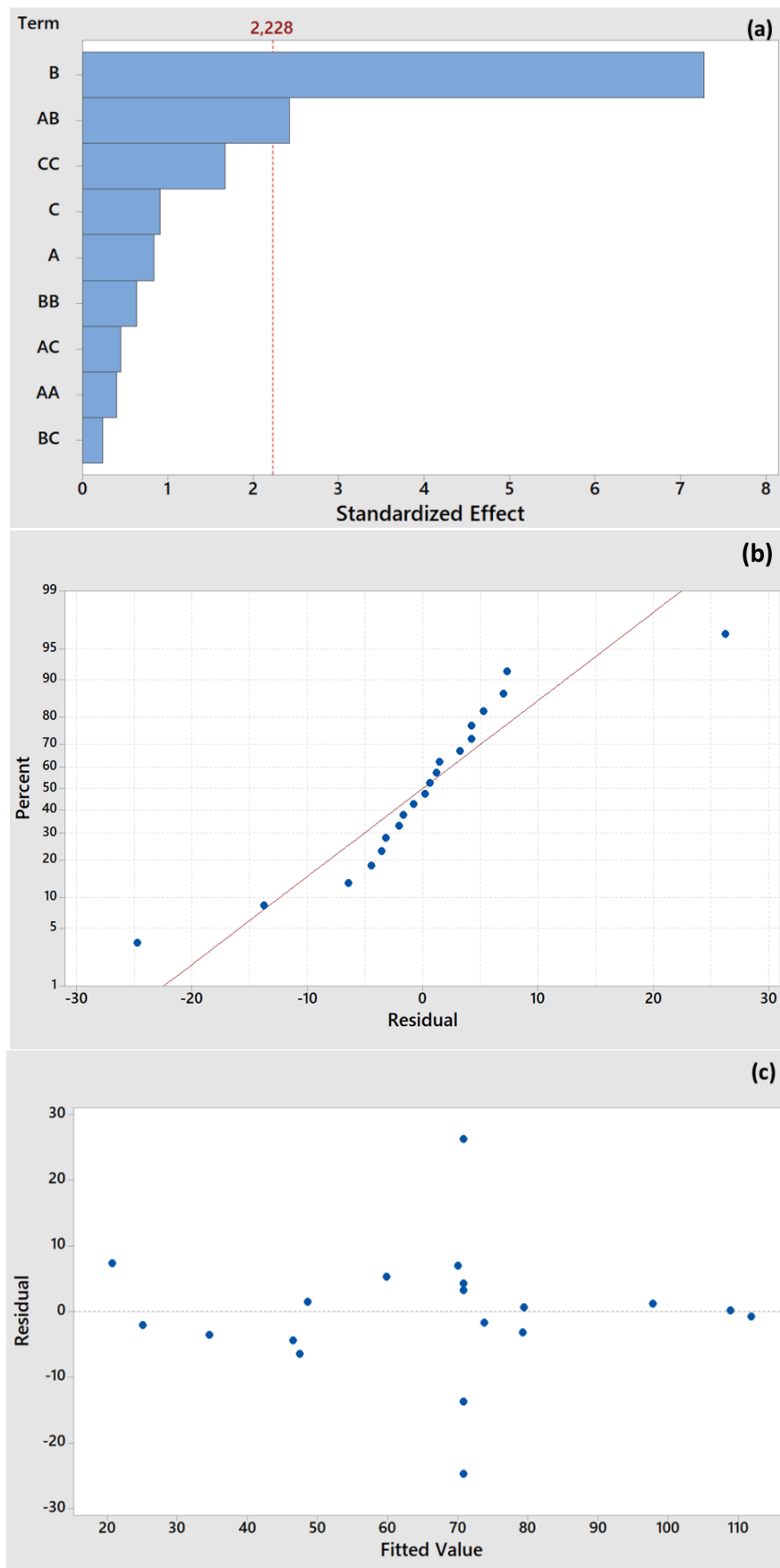
Figure 3.11 (a) Pareto chart, (b) residuals versus fitted values, (c) the normal probability plot of residuals for thickness.
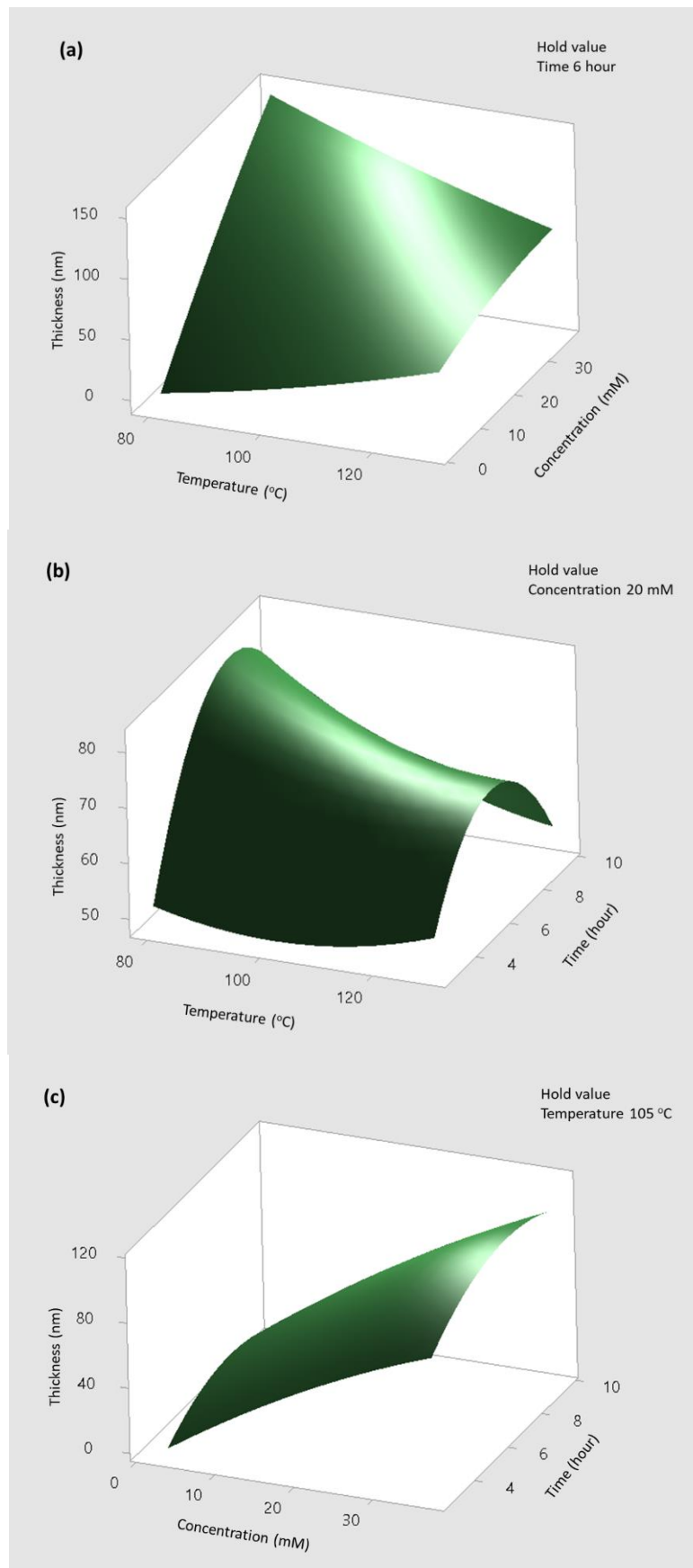
Figure 3.12 Surface plots of thickness versus (a) concentration, temperature, (b) temperature, time, and (c) concentration, time (A:Temperature, B:Concentration, C:Time).

3.3.5. Response Surface Regression of Aspect Ratio of ZnO Nanowires

The p-values and pareto chart of the study for aspect ratio are given respectively in Table 3.8 and Figure 3.13(a). It can be expressed that the concentration is a significant variable with p=0.008, as well as the combined effect of temperature and concentration (p=0.072) on aspect ratio prediction [60]. The regression model is given by the equation:

$$Aspect\ ratio = 214 - 2.25\,A - 5,27\,B - 5.35\,C + 0.00624\,A*A + 0.0280\,B*B + 0.191\,C*C + 0.0316\,A*B + 0.0229\,A*C + 0.038\,B*C \hspace{2cm} (4.6)$$

Table 3.8 ANOVA for the response quadratic model of aspect ratio.

Source	DF	Adj SS	Adj MS	F-Value	P-Value
Model	9	914.67	101.630	2.29	0.106
Linear	3	574.41	191.471	4.32	0.034
A (Temperature)	1	85.03	85.030	1.92	0.196
B (Concentration)	1	487.89	487.888	11.01	0.008
C (Time)	1	1.44	1.440	0.03	0.861
Square	3	134.09	44.695	1.01	0.429
A*A	1	27.46	27.464	0.62	0.449
B*B	1	114.46	114.462	2.58	0.139
C*C	1	9.63	9.630	0.22	0.651
2-Way Interaction	3	187.98	62.661	1.41	0.296
A*B	1	179.55	179.551	4.05	0.072
A*C	1	3.78	3.781	0.09	0.776
B*C	1	4.65	4.651	0.10	0.753
Error	10	443.29	44.329		
Lack-of-Fit	5	416.94	83.389	15.82	0.004
Pure Error	5	26.35	5.270		
Total	19	1357.97			

Adjusted R squared of 37.98% and R-squared of 67.36% indicates a bad agreement. Lack of fit is seen on the residual plots of statistical analysis (Figure 3.13(b), Figure 3.13(c)) and Table 3.9. The three-dimensional surface plots of aspect ratio are given in Figure 3.14.

Table 3.9 Fits and diagnostics for unusual observations.

Run	Response	Fit	Residual	Std Residual
8	38.30	29.86	8.44	2.19 R
16	22.10	30.81	-8.71	-2.07 R
18	9.70	20.92	-11.22	-2.66 R
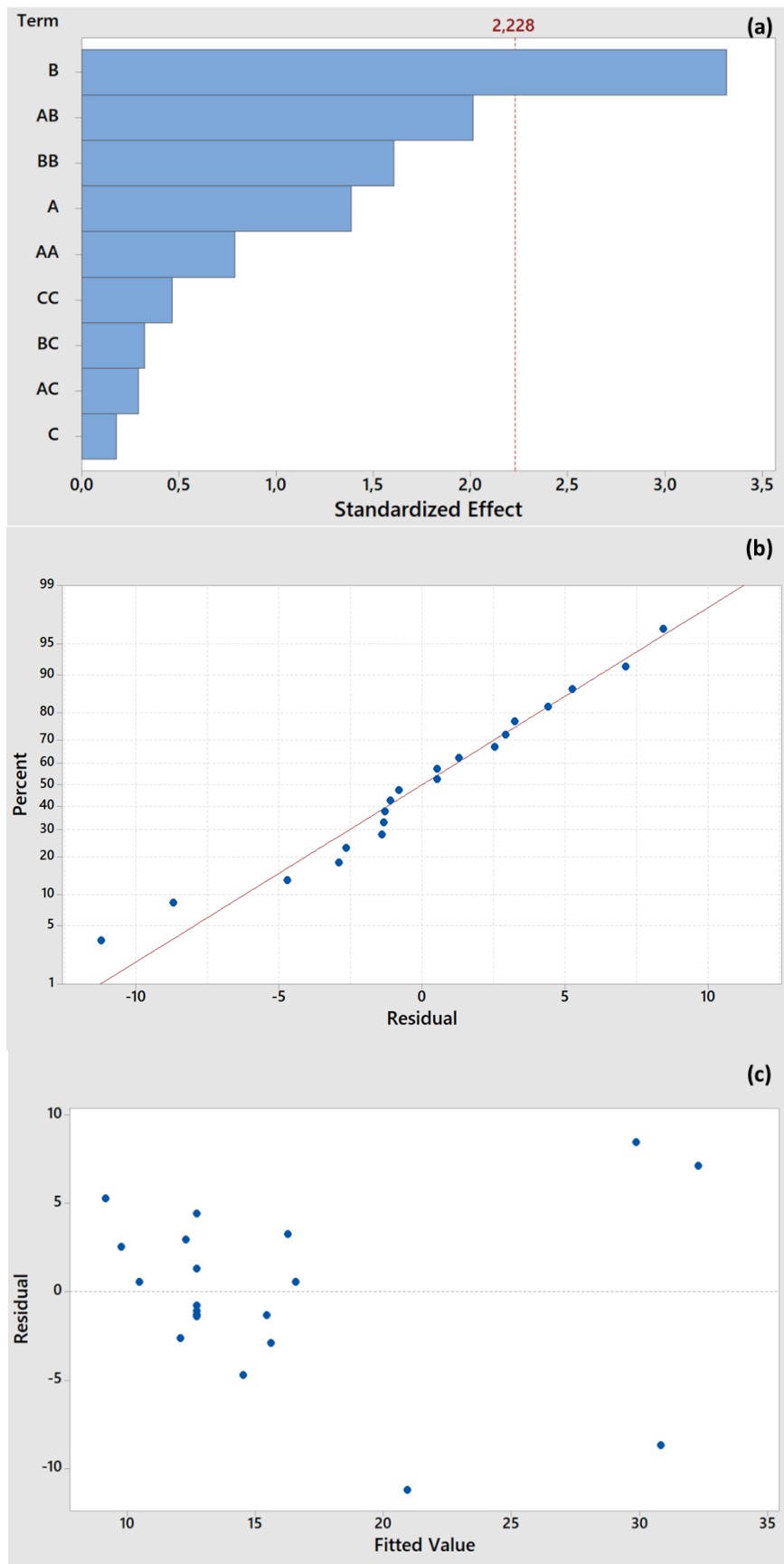
Figure 3.13 (a) Pareto chart, (b) residuals versus fitted values, (c) the normal probability plot of residuals for aspect ratio.
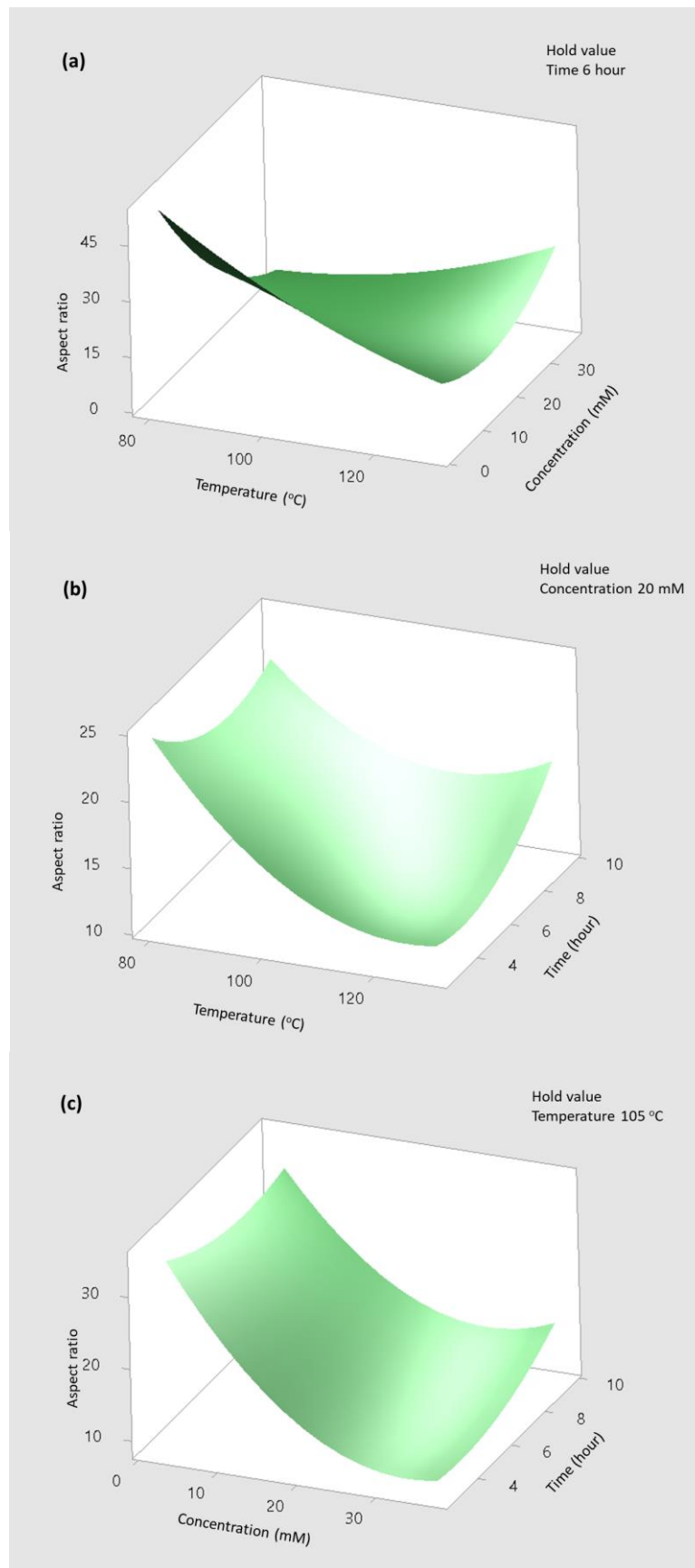
Figure 3.14 Surface plots of aspect ratio versus (a) concentration, temperature, (b) temperature, time, and (c) concentration, time (A:Temperature, B:Concentration, C:Time).

3.3.6. Response Surface Regression of Photocatalytic Activity

When it comes to photocatalytic activity, p values and pareto chart are given in Table 3.10 and Figure 3.15(a) respectively. Again, the concentration displayed a significant character with p=0.001 on the photocatalytic activity of ZnO/CFs. The regression model is given by the equation 4.7:

$$Photocatalytic\ activity\ =\ -7.24\ +\ 0.0931\ A\ -\ 0.0124\ B\ +\ 0.874\ C\ -$$
$$0.000377\ A*A\ -\ 0.000166\ B*B\ -\ 0.0311\ C*$$
$$C\ +\ 0.000728\ A*B\ -\ 0.00381\ A*C\ -$$
$$0.00543\ B*C \qquad\qquad (4.7)$$

Table 3.10 ANOVA for the response quadratic model of photochatalytic kinetic rate.

Source	DF	Adj SS	Adj MS	F-Value	P-Value
Model	9	1.53582	0.170646	2.17	0.122
Linear	3	0.89960	0.299867	3.81	0.047
A (Temperature)	1	0.08557	0.085565	1.09	0.322
B (Concentration)	1	0.80244	0.802444	10.19	0.010
C (Time)	1	0.01139	0.011393	0.14	0.712
Square	3	0.29693	0.098977	1.26	0.341
A*A	1	0.10080	0.100802	1.28	0.284
B*B	1	0.00405	0.004052	0.05	0.825
C*C	1	0.22190	0.221903	2.82	0.124
2-Way Interaction	3	0.29453	0.098177	1.25	0.344
A*B	1	0.09540	0.095397	1.21	0.297
A*C	1	0.10465	0.104653	1.33	0.276
B*C	1	0.09448	0.094482	1.20	0.299
Error	10	0.78778	0.078778		
Lack-of-Fit	5	0.15715	0.031430	0.25	0.923
Pure Error	5	0.63063	0.126126		
Total	19	2.32360			

R-squared of 66.10% and Adjusted R squared of 35.58% indicate a bad agreement on fitted and predicted values. The large residuals were obtained for C3 (Run 12) as shown in Figure 3.15(b), Figure 3.15(c) and Table 3.11. Although C3 is the sample with lack of fit, it randomly exhibits the 2nd highest photocatalytic activity.

Table 3.11 Fits and diagnostics for unusual observations.

Run	Response	Fit	Residual	Std Residual
12	1.0893	0.666	0.423	2.57 R

Finally, three-dimensional fitted response surface plots of the photocatalytic activity of ZnO NWs/CFs can be seen in Figure 3.16. Here, since the concentration was determined as the only efficient variable, the plots of binary interactions cannot be used.
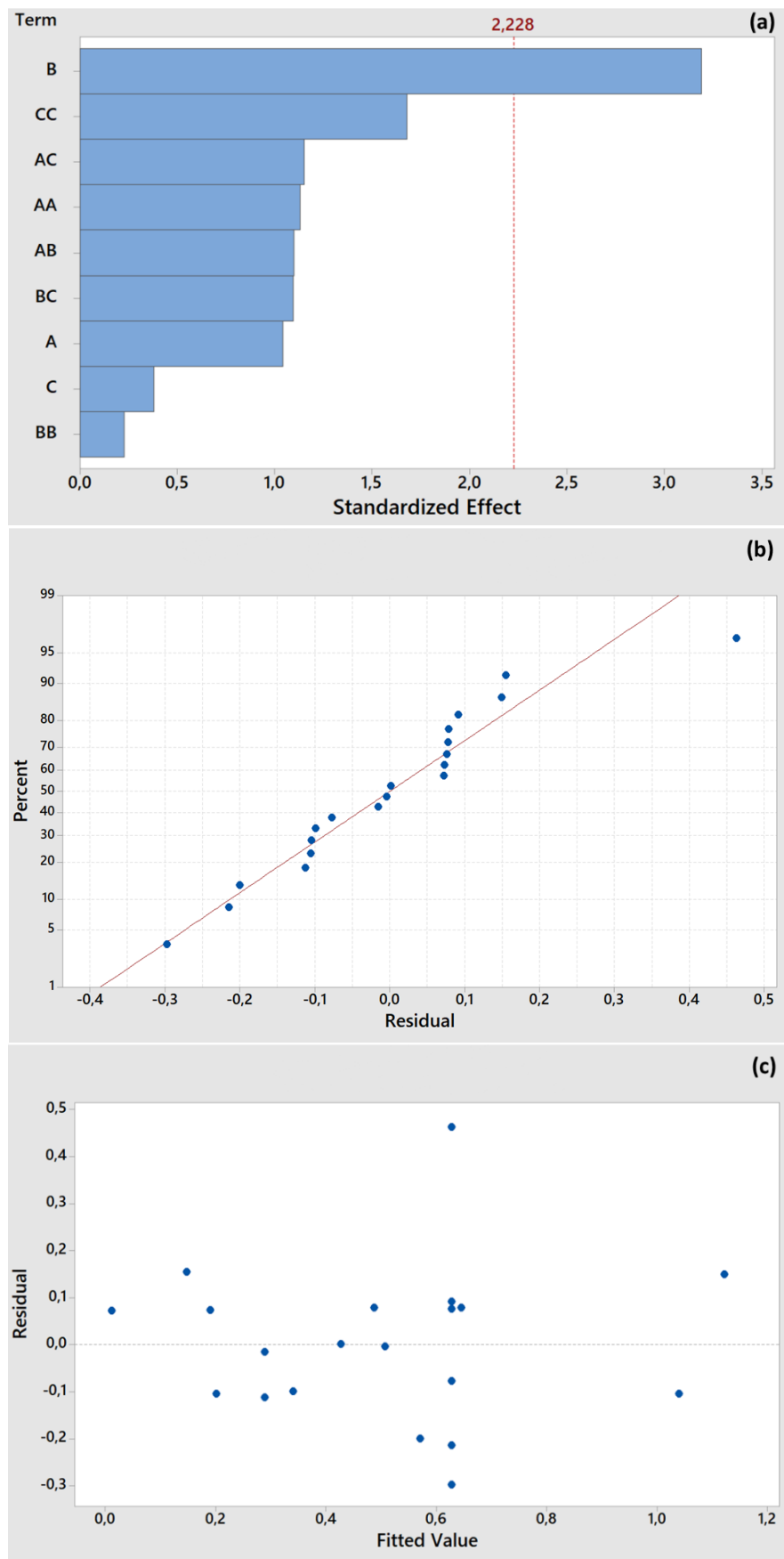
Figure 3.15 (a) Pareto chart, (b) residuals versus fitted values, (c) the normal probability plot of residuals for photocatalytic kinetic rate.

52
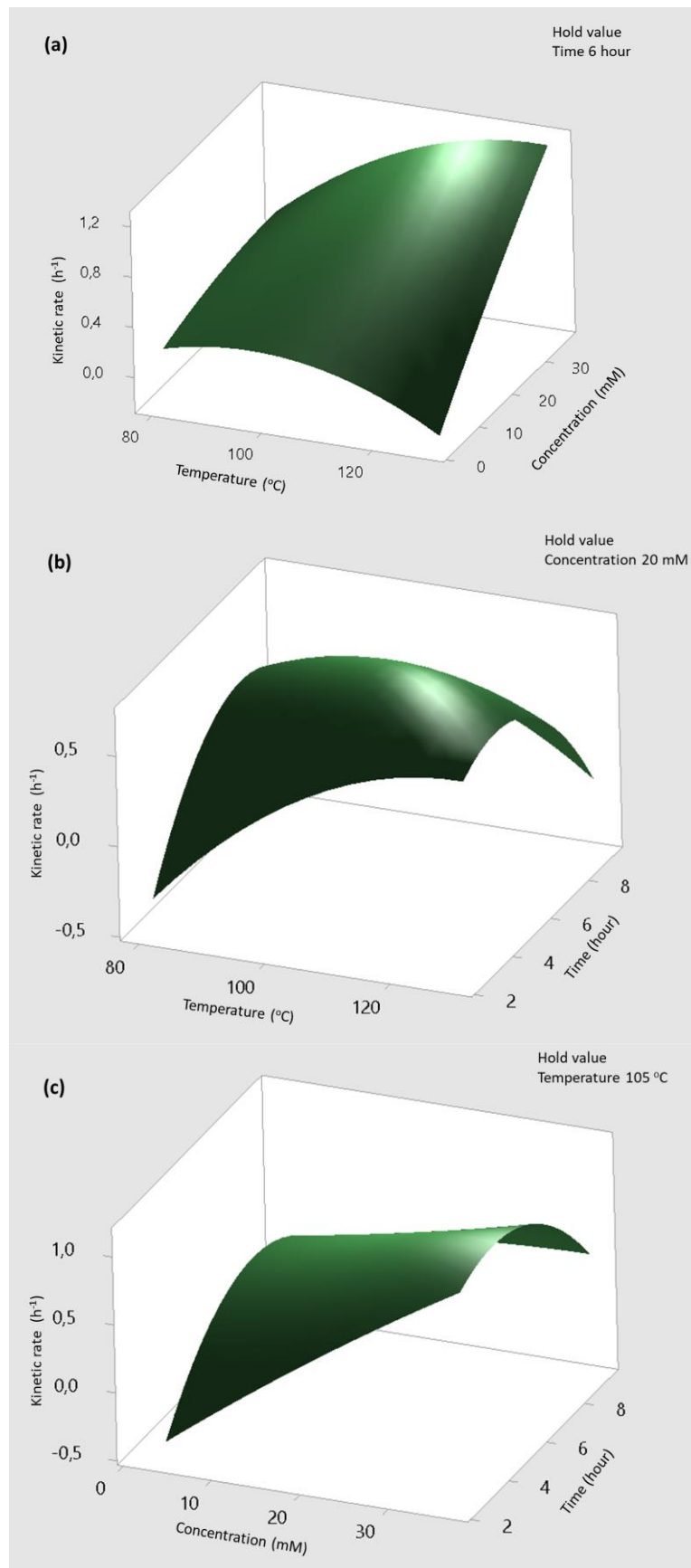
Figure 3.16 Surface plots of photocatalytic kinetic rate versus (a) concentration, temperature, (b) temperature, time and (c) concentration, time (A:Temperature, B:Concentration, C:Time).

3.4. Conclusion

In this study, well aligned and crystalline ZnO NWs/CFs structures were successfully grown via hydrothermal synthesis method as seen on SEM and XRD results. The thicknesses of 23 nm to 111 nm, and the lengths of 492 nm to 1429 nm were obtained for ZnO NWs under varying temperatures, $ZnNO_3.6H_2O$ concentrations and process time. Among the samples, highest photocatalytic degradation reaction rate and efficiency was recorded for the sample produced under the following hydrothermal process conditions as: 120 ^{o}C 30 mM and 4 hours with k_{app} and $DE\%$, 1.2707 h^{-1} and 99.86%, respectively.

In design of experiments, CCD model was applied for optimizing the hydrothermal process conditions for the growth of ZnO nanowires on carbon fibers. Temperature, concentration, and process time were the variables studied in ANOVA analysis. The results revealed that the effect of hydrothermal process variables on the length of ZnO nanowires are not significant. The concentration strongly influences the thickness and the aspect ratio of zinc oxide nanowires. Additionally, it was verified that with increase in concentration and temperature, thickness and aspect ratio of ZnO NWs are increased. Photocatalytic degradation kinetic rates were also evaluated in design of experiment in which the concentration was found to be a significant variable. All in all, in such studies employing design of experiments resulting in the evaluation of the effects of process parameters can help researchers on time consuming and laborious studies.

CHAPTER 4

The Effect of Potassium Substitution on Structural, Morphological, Optical and Photocatalytic Properties of ZnO Nanowires on Carbon Fibers

Abstract

Potassium substituted ZnO nanowires grown on carbon fibers were fabricated with improved photocatalytic activity by hydrothermal synthesis method. Potassium substitution was achieved by simple treatment with KNO_3 solution. The treatment with 0.5%, 1%, 5% and 10% concentration values of $Zn(NO_3)_2.6H_2O$ were tested. Structure and morphology of the ZnO nanowires characterized by X-ray diffraction (XRD) and scanning electron microscopy (SEM). Optical properties of structure analysed by UV-Vis diffuse reflectance spectroscopy . The resulting potassium substituted ZnO nanowires (K-ZnO NWs/CFs) exhibited photocatalytic properties superior to those of pristine ZnO. The Fermi level of zinc oxide was up-shifted, of which decreased the band gap of the structure.

Keywords: Zinc Oxide Nanowires; Carbon fiber; Hydrothermal synthesis; Photocatalysis; Potassium.

4.1.   Introduction

It is found that the incorporation of metals into ZnO structure can improve its optical properties. As a result of incorporation of metals, the fermi level of ZnO reveals below its conduction band, narrows its band gap and extends its response to the visible light range. In order to improve the photocatalytic activity of ZnO and reduce its band gap, alkali metals, rare earth metals and noble metals has been extensively studied [61]. Substitution of Na, K and Li into ZnO structure have been reported. Substitution of alkali metals improve its optical properties. It is reported that among the group-I elements, potassium is calculated to be the most appropriate element for p-type doping in wurtzite (zincite) ZnO structure [62].

There is only a few study reported on potassium substituted ZnO nanowires. Potassium was incorporated into ZnO structure to produce p-type ZnO. Sa´aedi et al.

reported the optical properties of group-I-doped ZnO nanowires [63]. Gupta et al. reported the p-type K-doped ZnO nanorods for optoelectronic applications [64]. Gosh reported vacancy-induced intrinsic d^0 ferromagnetism and photoluminescence in potassium doped ZnO nanowires [65].

ZnO can be produced by various methods such as, chemical vapour deposition [66], electrochemical deposition [31], sol-gel [33], laser deposition [44] and hydrothermal method [67]. Among these methods, hydrothermal method (HT) is one of the significant methods to produce high quality ZnO nanowires with high crystallinity.

In this study, pristine and potassium substituted ZnO nanowires were grown on carbon fibers via hydrothermal method. The effect of K substitution at different concentration ratios was investigated. Morphological, structural and optical properties were analysed. Photocatalytic activities of K substituted ZnO nanowires on carbon fiber structures were evaluated on photodegradation of methylene blue in water under solar irradiation.

4.2.   Materials and Method

The synthesis method was presented in our previous work [43] (Tunç et al 2020). At first, carbon fibers were washed with nitric acid, water, ethanol and acetone to remove residuals. Then, carbon fibers were coated with ZnO seed layer by deep coating method. Seeding layer solution was prepared with 25 mg zinc acetate dihydrate and 10 mg NaOH in 100 mL ethanol and the solution was mixed for 1.5 hours at room temperature. CFs were immersed in ZnO seed solution for 10 min. Then, CFs were annealed at 150 °C for 10 min. The process was repeated for four times. Hydrothermal synthesis of ZnO nanowires on CFs was performed in Teflon-lined stainless steel reactor. 30 mM zinc nitrate hexahydrate ($ZnO(NO_3)_2.6H_2O$) and 30 mM hexamethylenetetramine (HMTA) poured into the reactor and carbon fibers were immersed into the solution, vertically. Hydrothermal process performed at 90 °C for 4 hours. For the potassium substitution, potassium nitrate was added into zinc nitrate solution at different percent mol ratios. The ratios of 0.5 %, 1 %, 5% and 10% of 30 mM $ZnO(NO_3)_2.6H_2O$ were tested (0.5% K, 1% K, 5% K, 10% K). After hydrothermal process, obtained structures were washed with distilled water several times and dried at 60 °C in air. Thermal process was followed by this process to let the transformation of amorphous structure into crystalline zincite phase (250 °C, 120 min, in air).

The structure of ZnO was analyzed using X-ray diffractometer (Panalytical Empyrean XRD, Empreyan Package T-T). The X-ray diffraction patterns were obtained by using Cu Kα radiation (1.5406 A^o). The intensity data were recorded over a 2Θ range of 20° to 90°. The morphology of the samples were analysed with scanning electron microscope (SEM). Elemental analyses of samples were performed by energy dispersive X-ray spectroscopy (EDX) (Carl Zeiss 300VP SEM). Band gap value of structures were analysed by diffuse reflectance spectroscopy (DRS) (Perkin Elmer Lambda 950, UV/Vis/NIR Spectrometer).

The photocatalytic degradation kinetics of samples were monitored by the UV-Visible spectrophotometer (Shimadzu UV-1240). Photocatalytic activity of ZnO NWs/CFs were investigated by photodegradation of 10^{-5} M methylene blue (MB) solution in pure water under UV light source (Osram, UltraVitalux E27, 300 W). 50±5 mg ZnO NWs/CFs were placed in 20 mL MB solution. To derive photocatalytic kinetics, various irradiation time intervals were tested up to 240 min. To show photocatalyst-free degradation of MB aqueous solution, a blank sample was prepared. Additionally, bare CFs were tested to show adsorption abilities of CFs and ZnO NWs. To reveal the self-degradation of MB and adsorption characteristics, the samples in MB aqueous solutions were kept in dark for 24 hour. The distance between the light source and the MB aqueous solution was 25 cm. The characteristic absorbance decrease of MB at 664 nm was recorded between 0-240 min. time intervals to reveal the photocatalytic kinetics. The average irradiation intensity of the employed light source was 18 W/m^2 for the visible bandwidth, 3.2 W/m^2 for UV-A, 0.004 W/m^2 for UV-B and 0.004 W/m^2 for UV-C. All chemicals and solvents were purchased from Sigma Aldrich and used without any further purification.

4.3.   Results and Discussion

4.3.1. Materials Characterization

Morphological structure of pristine and K substituted ZnO NWs/CFs was analysed by SEM (Figure 4.1). Well aligned ZnO nanowires was observed on carbon fibers. The length of ZnO nanowires varies from 1.2 μm to 2.0 μm and the thickness of ZnO nanowires varies from 90 nm to 180 nm. Elemental analysis of K substituted ZnO NWs/CFs was performed by EDX (Figure 4.1(f)).
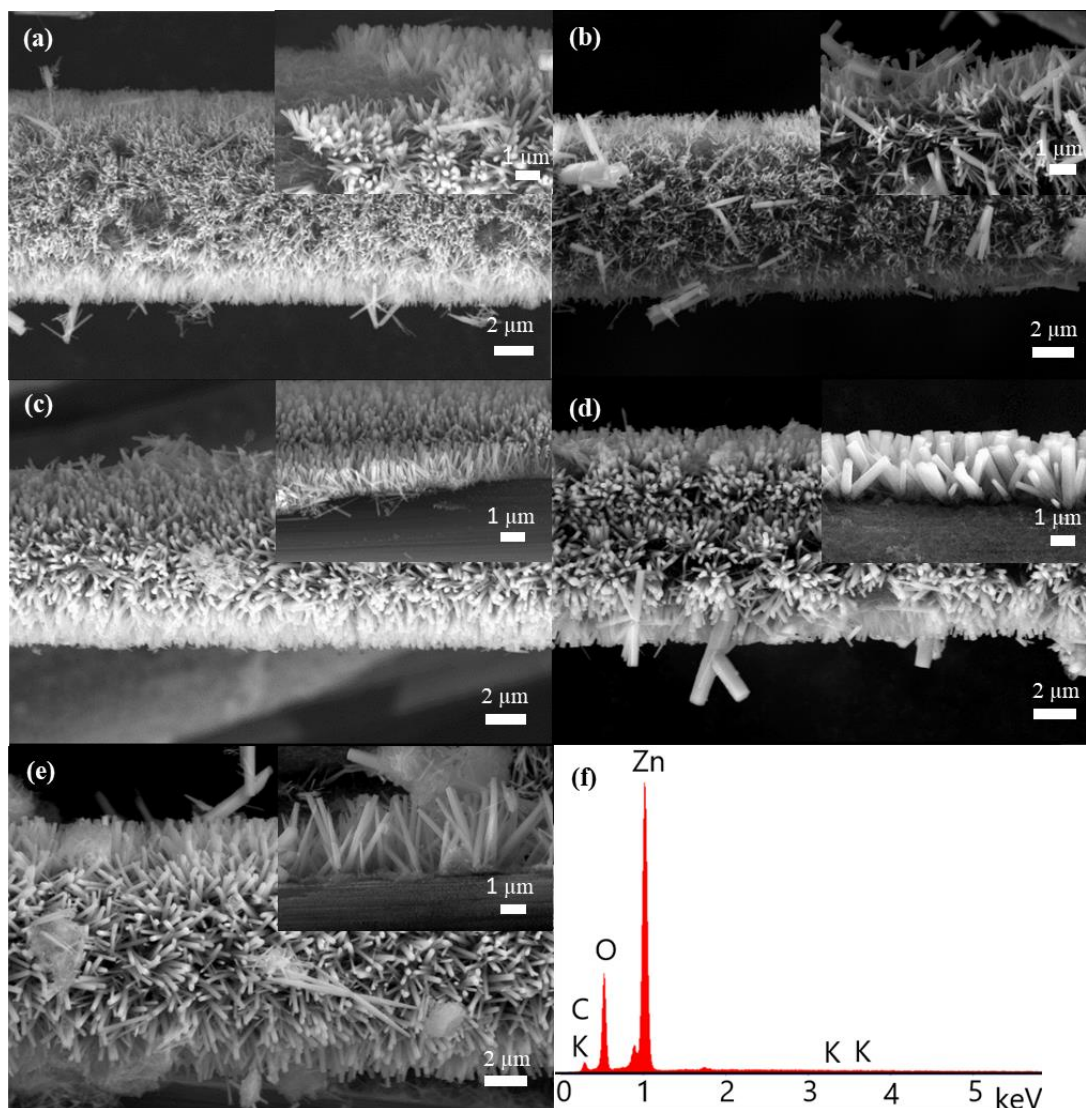
Figure 4.1 Nanostructure and morphology of pristine ZnO (a), 0.5% K (b), 1% K (c), 5% K (d), 10% K (e) and EDX results (f).

The crystal structure analysis of pristine and K substituted ZnO nanowires coated on carbon fibers was performed with X-ray diffraction method. XRD pattern of K incorporated ZnO is shown in Figure 4.2. XRD patterns of the samples indicates that all the samples has zincite crystal structure which are in very good agreement with JCPDS numbers 00-036-1451. No other phases are observed in the XRD patterns. In the XRD patterns, there are three prominent peaks of (100), (002) and (101) planes that indicates the structure has the hexagonal zincite structure. With incorporation of potassium into ZnO, its crystal structure remained same and only the peak intensities and the peak widths were changed.

The crystallite size and strain were estimated using Williamson Hall equation (Eq. 4.1):

$$\beta \cos\theta = \frac{K\lambda}{D} + 4\,\varepsilon\sin\theta \tag{4.1}$$

where β, θ, λ and ε are the peak width at half-maximum intensity, the Bragg diffraction angle in radians, X-ray wavelength and the strain, respectively. The term $\varepsilon\sin\theta$ (x-axis) is plotted against $\beta\cos\theta$ (y-axis) (Figure 4.2). The y-intercept and slope of the fitted line display crystallite size and strain, respectively. The stress values were calculated by the following equation [68]:

$$\sigma = \frac{-233 \times 10^{9}\,(c_{sample} - c_{bulk})}{c_{bulk}} \tag{4.2}$$

where c_{sample} is the lattice constant of the material and c_{bulk} (5.206 Å) is the strain free constant. Results are listed in Table 4.1.

The crystal parameters of the material were determined by Eq. 4.3 and Eq. 4.4:

$$\lambda = 2d_{hkl}\,\sin\theta_{hkl} \tag{4.3}$$

where λ is the wavelength of light, d is interplanar distance and θ is the Bragg diffraction angle in radians.

$$\frac{1}{d_{hkl}^2} = \frac{4}{3}\left(\frac{h^2 + hk + k^2}{a^2}\right) + \frac{l^2}{c^2} \tag{5.4}$$

where d_{hkl} is the interplanar distance. Results are given in Table 4.1 [69]. High K concentrations reduces the crystallinity of ZnO. Crystallite size decreased dramatically from 40.78 nm to 0.78 nm. This might be due to the occupation of some K atoms on the Zn site [70]. Other samples patterns also showed similar changes at peak positions and intensities slightly, indicating the lattice constant of the crystal increases due to the larger ionic radius of potassium (1.38 Å) with respect to zinc (0.74 Å). Athma et al. reported similar results about the change of lattice parameters [69]. The addition of potassium leds also to stress increase. Due to the different ionic radii between K^+ (0.136nm) and Zn^{2+} (0.060nm), with substitution of K^+ lattice distortion is observed, causing stress increase in the crystal. Increase in tensile stress is interpreted positive for the un-doped ZnO and negative for K substituted ZnO.
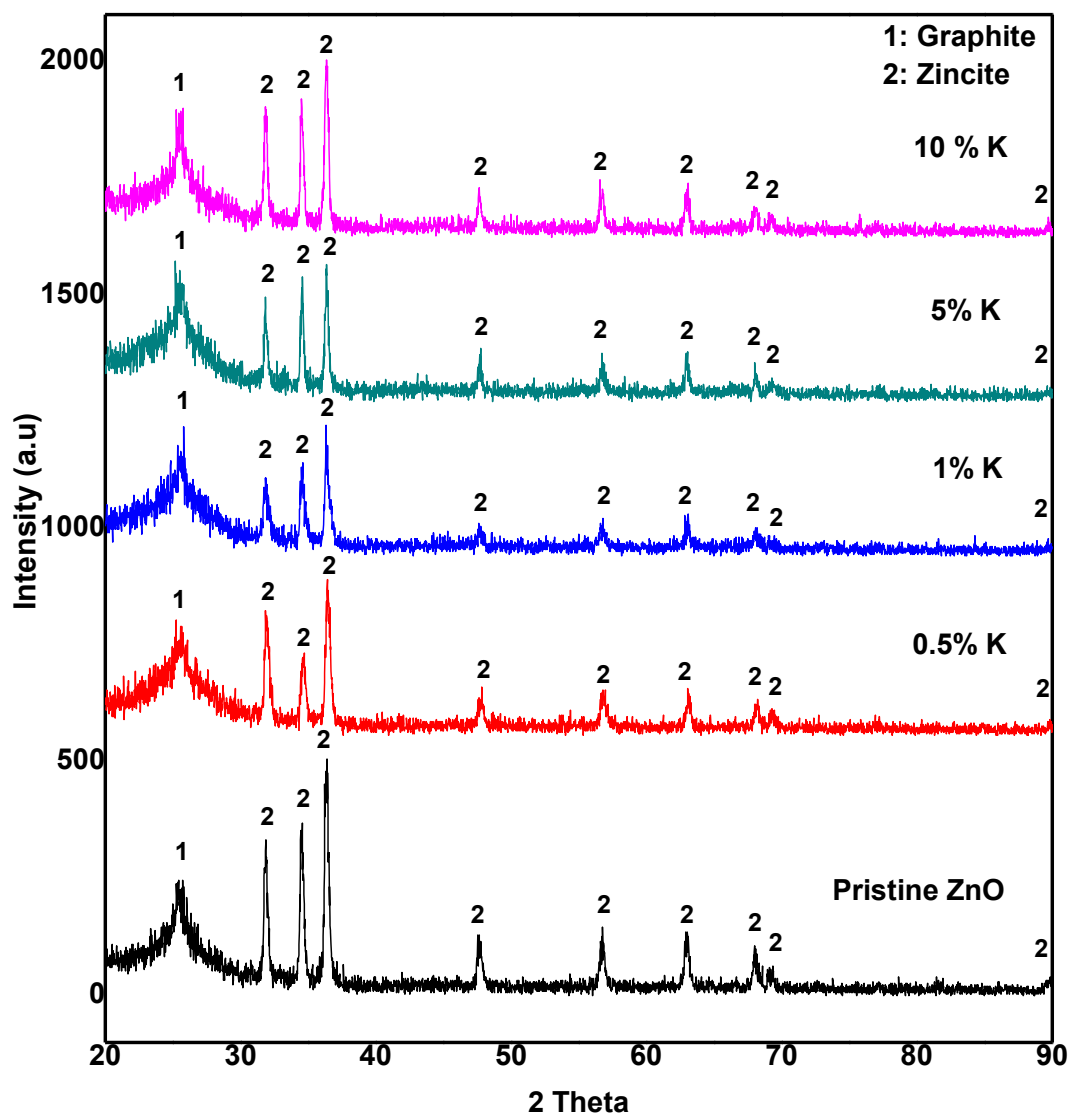
Figure 4.2 XRD plots of pristine and K substituted ZnO nanowires grown on carbon fibers.
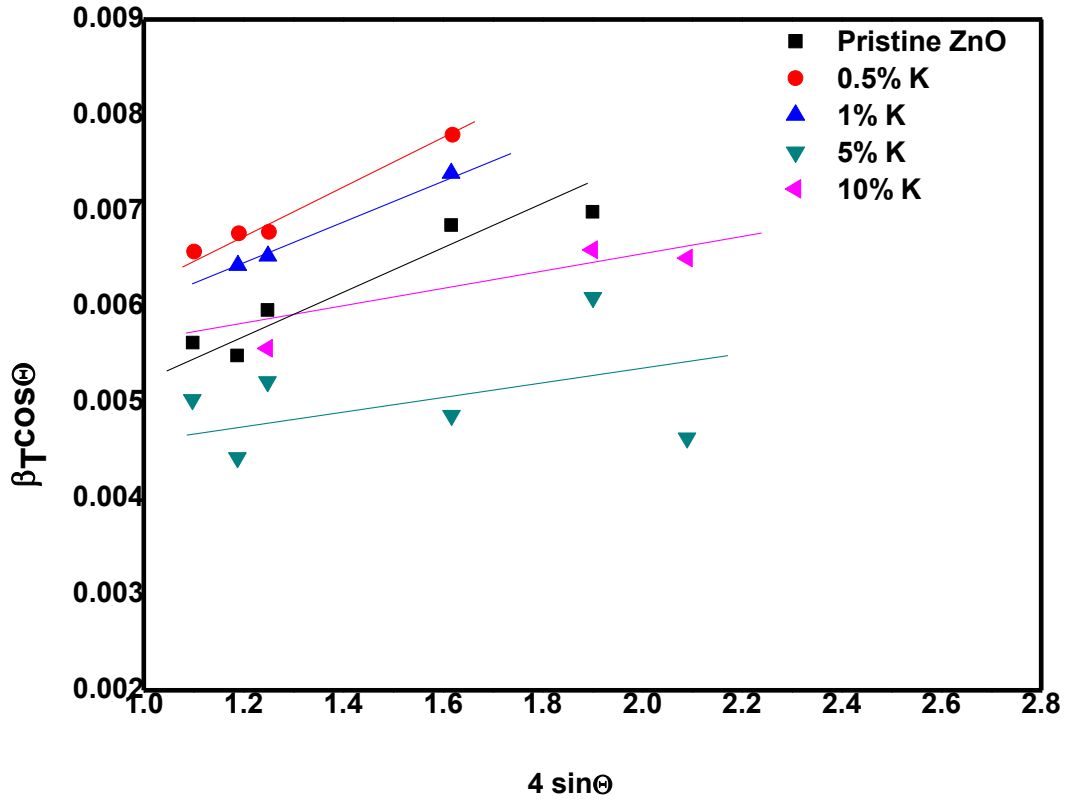
Figure 4.3 Williamson Hall plots of pristine and K substituted ZnO nanowires grown on carbon fibers.

Table 4.1 XRD peak analysis of K substituted ZnO nanowires grown on carbon fibers.

Sample	D (nm)	ε (10^{-3})	Lattice constant		σ (10^9 Pa)
			a	c	
Pristine ZnO	40.78	2.0	3.2397	5.1902	0.70
0.5% K	26.66	2.4	3.2317	5.1741	-1.43
1% K	37.47	2.3	3.2390	5.1835	-1.00
5% K	30.81	4.0	3.2410	5.1880	-0.80
10% K	33.82	12.0	3.2404	5.1892	-0.75

In order to determine optical properties of ZnO NWs/CFs structure, diffuse reflectance spectroscopy (DRS) analyses was performed. The reflectance spectra of the ZnO NWs/CFs structures were obtained in the range of 250–800 nm. The electron transitions from the valence band to the conduction band at wavelengths lower than 500 nm caused a variation in reflectance spectroscopy. The optical band gap energies (Eg) was determined by Kubelka–Munk method (Eq. 4.2) [71]:

$$F(R) = \frac{K}{S} = \frac{(1-R)^2}{2R} \tag{4.2}$$

where K is the absorption coefficient, S is the scattering coefficient, R is the reflectance and F(R) is the Kubelka–Munk function. Plots of reflectance spectrums and $(F(R)h\nu)^2$ versus photon energy were demonstrated in Figure 4.4. Obtained band gap results of K substituted ZnO/CF were summarized in Table 4.2. E_g value for pristine ZnO NWs on CFs structure was found to be 3.30 eV, lower than bulk ZnO (3.36 eV). Band gap value decreased with 0.5% K substitution, then increased again in between 0.5 and 10 %K substitutions. This change of the band gap can be explained by Burnstein-Moss effect which results from the increase of carrier concentration and filling of the conduction band (CB) of n-type semiconductor or of the valence band (VB) of p-type semiconductor [72]. Tabib reported similar results for Na substituted ZnO nanostructure [68].

Figure 4.4 Plots of reflectance spectrums and $(F(R)h\nu)^2$ versus photon energy (hν) of the pristine and K substituted ZnO nanowires grown on carbon fibers.

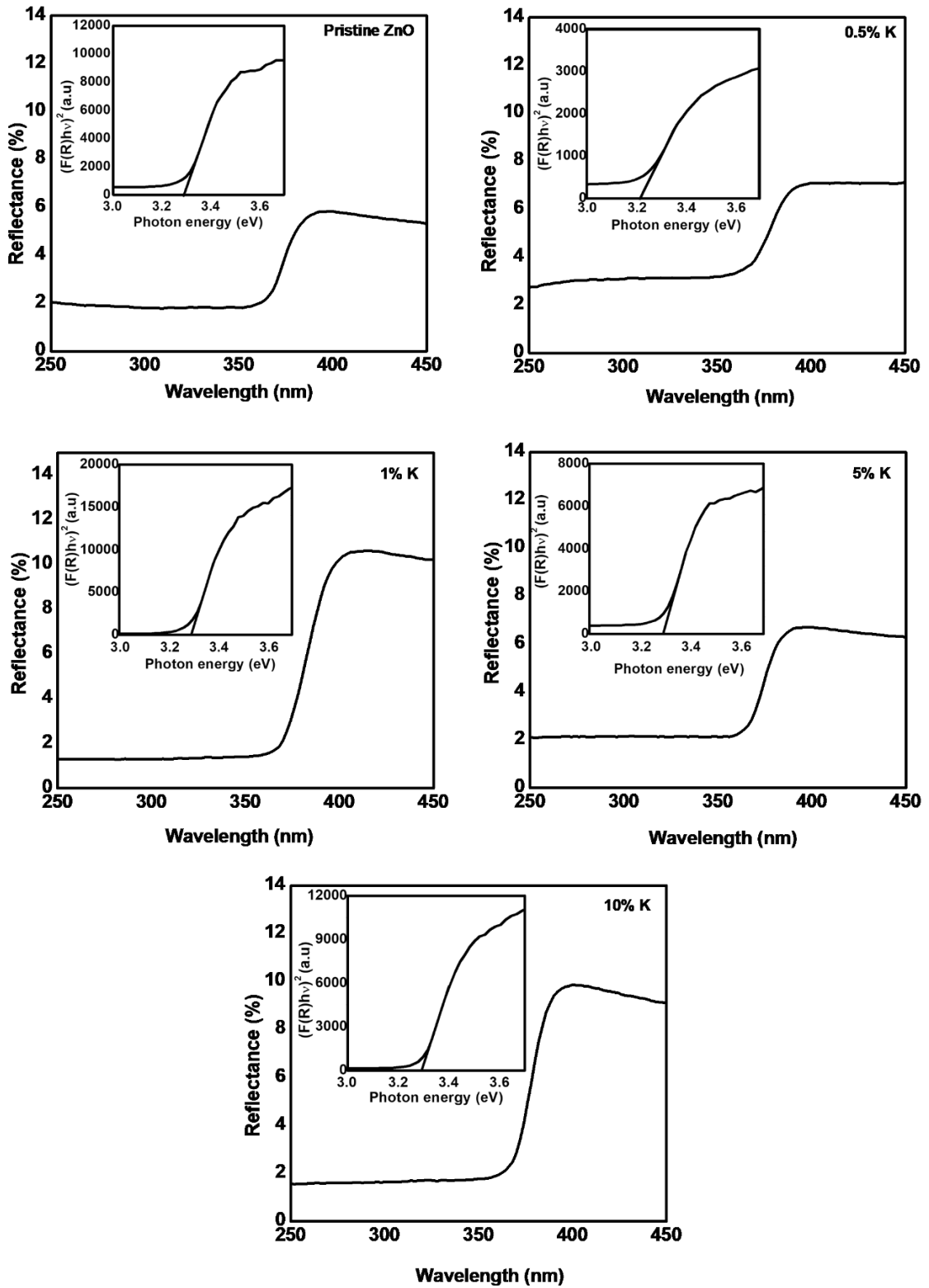**Table 4.2** Band gap values of pristine and K substituted ZnO nanowires grown on carbon fibers.

Sample name	Band gap (eV)
Pristine ZnO	3.30
0.5% K	3.20
1% K	3.30
5% K	3.26
10% K	3.29

4.3.2. Photocatalytic Activity Tests

Photocatalytic activity of K substituted ZnO NWs/CFs was analyzed. The kinetic and percent degradation plots are given in Figure 4.5 and photocatalytic degradation kinetic data are given in Table 4.3. Results indicate that samples are in consistent with Langmuir–Hinshelwood (L-H) kinetics model. Langmuir–Hinshelwood (L–H) kinetics model is used very often to describe the kinetics of the heterogeneous catalytic systems. The L-H model was evaluated by the following equation (Eq. 4.4):

$$ln\left(\frac{C_0}{C_t}\right) = k_{app} \times t \tag{4.4}$$

where C_0 is the initial dye concentration, C_t is the instant dye concentration, k_{app} is the apparent reaction rate constant and t is time. This model demonstrates the linear relation between $Ln(C_0/C)$ and t having a slope of k_{app} [49].

The degradation efficiency (*DE%*) was calculated by the given equation below (Eq. 4.5):

$$DE\% = \frac{(C_0 - C_t)}{C_0 \times 100} \tag{4.5}$$

where C_0 is the initial MB concentration, C_t is instant MB concentration and t is the irradiation time. From the dark test results, a preliminary decrease is observed due to the adsorbance of MB. It is also observed that K substitution increases the photocatalytic activity of ZnO NWs/CFs structure. With increase in K concentration photocatalytic activity increases to 99.71 %, degradation efficiency and k_{app} increases to 1.2988 h^{-1}. The reason for the increase of photocatalytic activity may be due to the abundant defect side on the surface of the K-substituted ZnO structure. Another reason can be due to that the improvement of the photocatalytic activity is increasing crystal interface area as a result of decreasing crystal size.
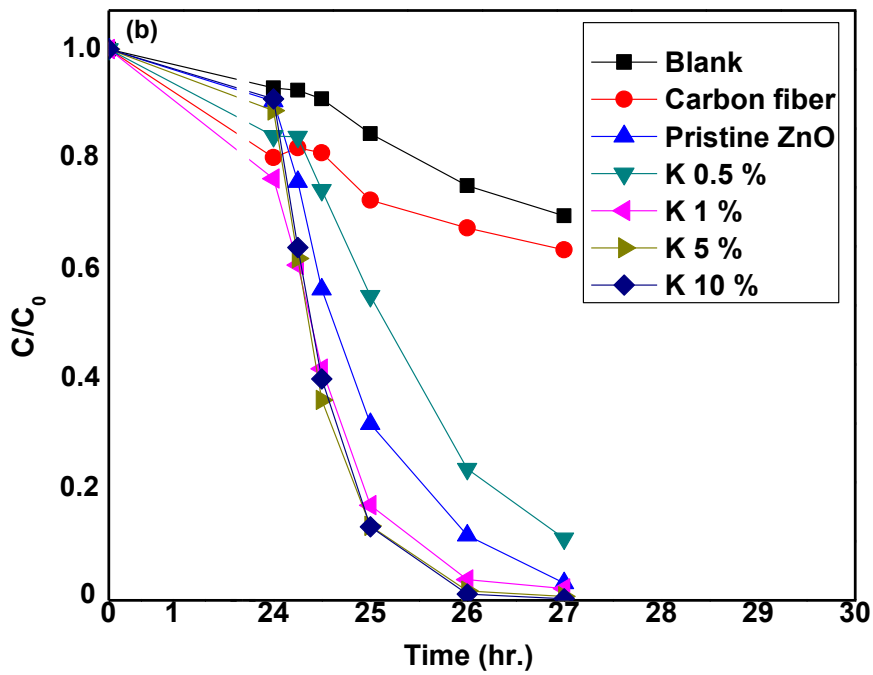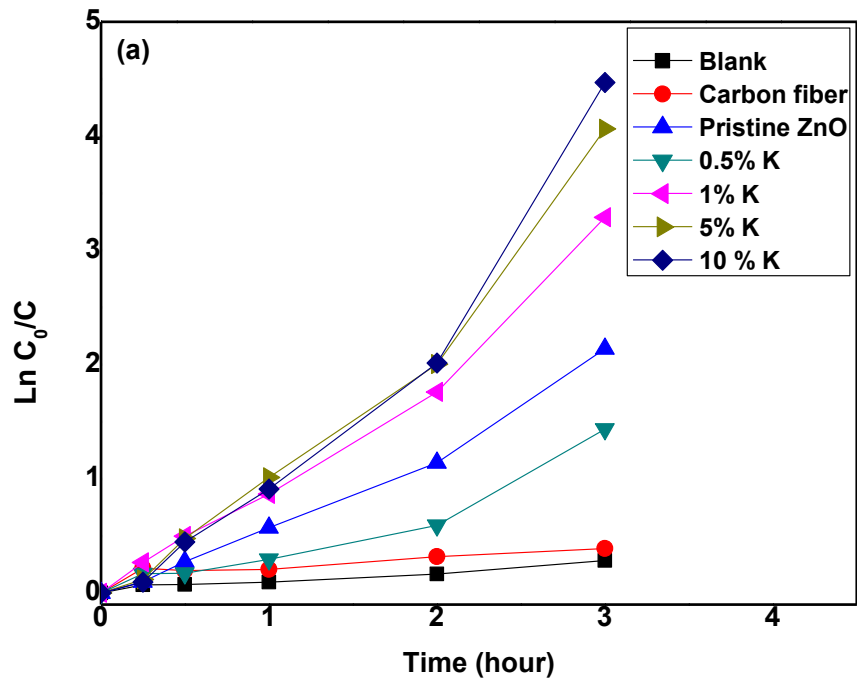
Figure 4.5 Photocatalytic activity of pristine and K incorporated ZnO nanowires grown on carbon fibers. (a) Photocatalytic degradation kinetics (b) degradation ratio.

65

Table 4.3 Photocatalytic degradation kinetic data of pristine and K incorporated ZnO NWs/CFs.

Sample	Degradation efficiency (%)	$k_{app}(h^{-1})$	R^2
Blank	30.27	0.0937	0.9208
Carbon fiber	36.44	0.1522	0.3789
Pristine ZnO	96.84	0.6592	0.978
0.5% K	88.81	0.4133	0.9182
1% K	97.85	1.0178	0.9795
5% K	99.28	1.2210	0.9627
10% K	99.71	1.2988	0.9375

4.4.   Conclusion

Pristine and K substituted ZnO NWs were hydrothermally synthesized on carbon fibers. The effect of K mole ratios on structural, morphological, optical and photocatalytic activity of ZnO nanowires grown on carbon fibers was studied. XRD analyses shows that all samples has hexagonal zincite phase. K incorporation reduces the crystallinity of ZnO. Optical properties of potassium substituted zinc oxide nanowires grown on carbon fiber were evaluated. It is observed that 0.5% K-ZnO NWs/CFs had lower band gap. Finally, photocatalytic activity tests were performed under solar irradiation. The p-type K substituted ZnO NWs/CFs sample was featured a better photocatalytic activity. It can be concluded that the K incorporation is efficient and a simple way to improve the optical and photocatalytic properties of zinc oxide nanowires.

CHAPTER 5

Production of Aluminum Substituted ZnO Nanowires on Carbon Fibers by Hydrothermal Method for Photocatalytic Degradation of Methylene Blue Aqueous Solutions

Abstract

Pristine and aluminum substituted ZnO nanowires grown on carbon fibers was successfully produced by hydrothermal synthesis method. The effect of Al concentration on morphology, structure, optical properties and photocatalytic activity on methylene blue was investigated and characterized by scanning electron microscopy, X-ray Diffraction, diffuse reflectance spectroscopy and UV-Vis diffuse reflectance spectroscopy. The concentration values of 0.5%, 1%, 5% and 10% $Zn(NO_3)_2.6H_2O$ were tested. XRD results indicates that pristine and aluminum substituted ZnO nanowires has hexagonal zincite crystal structure. Optical band gap of structures was analysed. Al substitution reduces the band gap of ZnO. Photocatalytic activity of pristine and aluminum substituted ZnO nanowires on carbon fibers structures were tested on degradation of methylene blue (MB). Al substitution enhances the photocatalytic activity of ZnO nanowires coated on carbon fibers.

Keywords: Zinc Oxide; Nanowire; Carbon fiber; Hydrothermal synthesis; Photocatalysis; Aluminum.

5.1. Introduction

As mentioned in previous sections, incorporation of metals into ZnO structure is good strategy to improve zinc oxides optical and electrical properties. The effect of alkali metals, rare earth metals and noble metals has been extensively studied. In consequence of incorporation of metals into semiconductor materials, Fermi level reveals below the conduction band of semiconductor material that narrows its band gap and extends its response to the visible range [61]. Al^{3+} is a suitable element for

substitution into zinc oxide owing to its high valance that can alter its electrical properties [73]. Due to its smaller ionic radius, Al^{3+} can be substituted into zinc oxides crystal lattice effectively (rAl^{3+} = 0.054 nm and rZn^{2+} =0.074 nm) [74]. There are several studies reported on the aluminum substituted ZnO with different morphologies. Xing et al. reported the macro-/nanoporous Al-doped ZnO via self-sustained decomposition of metal-organic complexes for the degradation of Congo Red [73]. Mitra et al. reported the facile synthesis of aluminum doped zinc oxide-polyaniline hybrids for photoluminescence and enhanced visible-light assisted photo-degradation of organic contaminants [75]. Aydın et al. produced Al-doped ZnO as a multifunctional nanomaterial and investigated its structural, morphological, optical and low-temperature gas sensing properties [76]. Khayatian et al. synthesized Al doped ZnO NPs on graphene nanocomposites by solvothermal method [77]. Zhang et al. reported Al-doped ZnO nanoparticles with high photocatalytic performance [78]. Ganesh et al. investigated the influence of Al doping on the structural, morphological, optical and gas sensing properties of ZnO nanorods [74].

In this work, pristine and Al substituted ZnO nanowires (NWs) grown on carbon fibers (CFs) prepared by the hydrothermal method (HT). The effect of Al concentrations on morphology, structure, optical properties and photocatalytic activity of ZnO NWs on CFs were investigated. The crystal structure, morphology, elemental composition and band gap of pristine and Al substituted ZnO nanowires were characterized by XRD, SEM, EDX, and DRS. Photocatalytic properties of the samples were also analyzed by using UV-Visible spectrophotometer.

5.2.   Materials and Method

The sample preparation and synthesis method was presented in a previous work [43] (Tunç et al 2020). To remove residuals, carbon fibers were washed with sequentially with nitric acid, water, ethanol and acetone. After that, to provide growth of ZnO NWs on carbon fibers surface, carbon fibers were coated with ZnO seed layer by dip coating method. 25 mg zinc acetate dihydrate and 10 mg NaOH dissolved in 100 mL ethanol and this solution was mixed for 1.5 hour at room temperature. Afterwards, carbon fibers immersed in ZnO seed solution for 10 min. and then, annealed at 150 °C for 10 min. This process was repeated four times. Afterwards NWs were grown on seed layer coated CFs via hydrothermal synthesis. Hydrothermal growth solution prepared   by   dissolving   30   mM $ZnO(NO_3)_2.6H_2O$ and   30   mM

hexamethylenetetramine (HMTA) in pure water. This solution was then poured into Teflon-lined stainless steel reactor and carbon fibers immersed into solution vertically. Hydrothermal synthesis was carried out at 90 °C for 4 hour. For aluminum substitution into ZnO structure, aluminum nitrate is added to HT growth solution at different percent mol ratios of zinc nitrate. 0.5 %, 1 %, 5% and 10% aluminum of 30 mM $ZnO(NO_3)_2.6H_2O$ were tested (0.5% Al, 1% Al, 5% Al, 10% Al). After hydrothermal synthesis process, ZnO NWs coated on carbon fibers were washed with distilled water several times and dried at 60 °C in air. Finally, to let the transformation of amorphous structure into crystalline zincite (wurtzite) phase, thermal process was carried out at 250 °C for 120 min in air.

The crystallographic structure of ZnO NWs was analyzed using X-ray Diffractometer (Panalytical Empyrean XRD, Empreyan Package T-T). The X-ray diffraction patterns were analysed by using Cu Kα radiation (1.5406 A^o). The intensity data were recorded in a 2Θ from 20° to 90°. The morphology of the ZnO were analyzed with scanning electron microscope (SEM). Elemental analyses were performed by energy dispersive X-ray spectroscopy (EDX) (Carl Zeiss 300VP SEM). Band gap value of samples were analysed by diffuse reflectance spectroscopy (DRS) (Perkin Elmer Lambda 950, UV/Vis/NIR Spectrometer). Photocatalytic activity of ZnO NWs/CFs were analyzed by the UV-Visible spectrophotometer (Shimadzu UV-1240). The photocatalytic degradation kinetics of samples were investigated by photodegradation of 10^{-5} M methylene blue (MB) solution in pure water under UV light source (Osram, UltraVitalux E27, 300 W). 50±5 mg ZnO NWs/CFs were placed in a beaker with 20 mL methylene blue solution. The characteristic absorbance decrease of methylene blue at 664 nm was recorded over 0-240 min time intervals to derive the photocatalytic kinetics of ZnO NWs/CFs. To derive the self-degradation of MB and adsorption characteristics of ZnO NWs and CFs, the samples in MB aqueous solutions were kept in dark for 24 hour. MB solution were analyzed as blank sample, to demonstrate photocatalyst-free degradation of MB. Additionally, bare carbon fibers were tested to reveal adsorption abilities of ZnO NWs and CFs. The distance between the MB aqueous solution and the light source was 25 cm. The average irradiation intensity of the employed light source was 18 W/m^2 for the visible bandwidth, 3.2 W/m^2 for UV-A, 0.004 W/m^2 for UV-B and 0.004 W/m^2 for UV-C. All chemicals and solvents were purchased from Sigma Aldrich and used without any further purification.

5.3. Results and Discussion

5.3.1. Material Characterization

Morphology of the pristine and Al substituted ZnO NWs grown on CFs was analysed by SEM. It is clear from SEM images that ZnO nanowires have been grown on carbon fibers, successfully (Figure 5.1). Aluminum content of ZnO nanowire structure was determined by EDX.
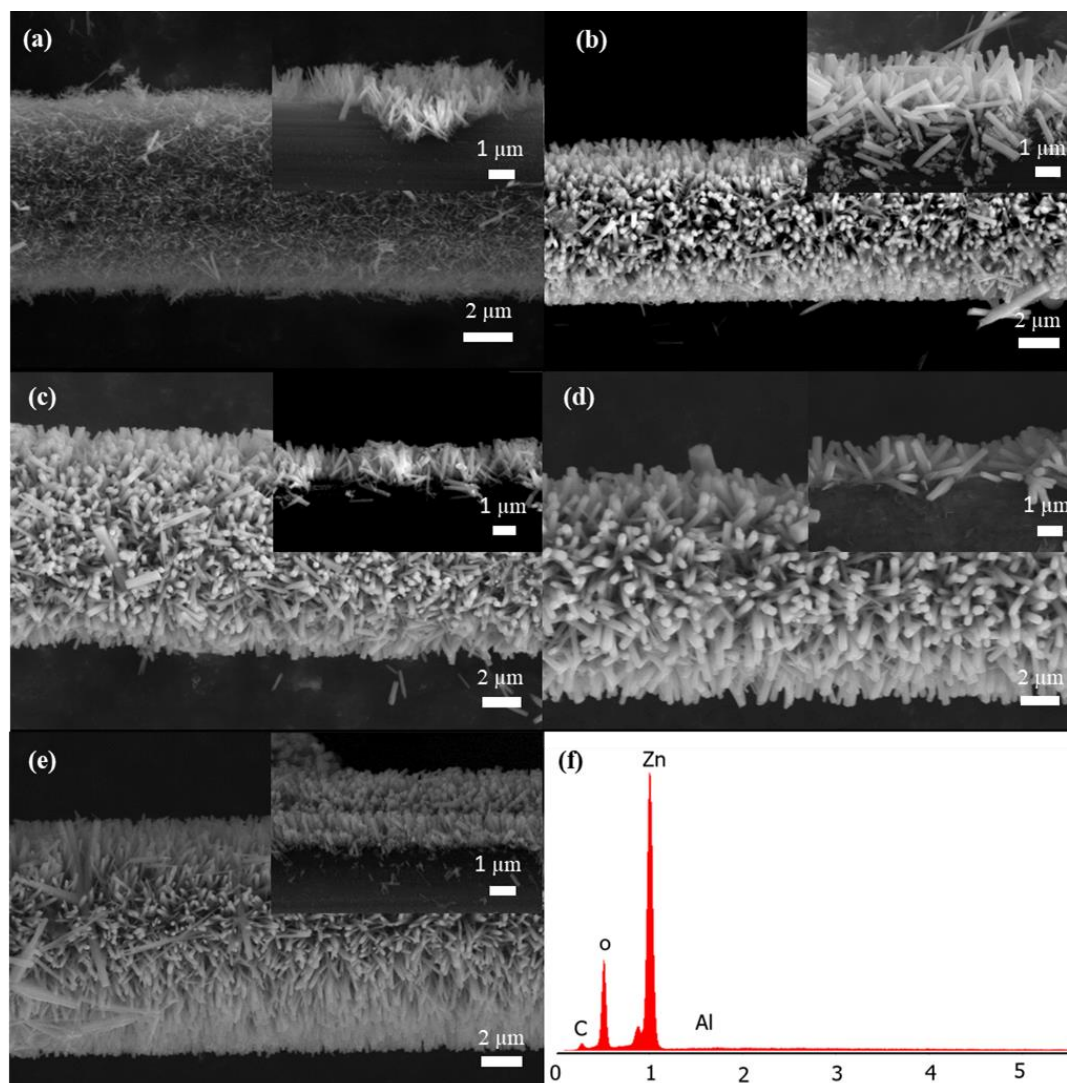
Figure 5.1 Nanostructure and morphology of Al substituted ZnO nanowires grown on carbon fibers. Pristine ZnO (a), 0.5% Al (b), 1% Al (c), 5% Al (d), 10% Al (e) and EDX results (f).

The crystal structure analyses of unsubstituted and Al substituted ZnO nanowire coated carbon fibers produced with hydrothermal method at different molar concentrations of Al were performed with X-ray diffraction method (Figure 5.3).

Characteristic reflections from (100), (002) and (101) planes of ZnO can be clearly observed on diffractogram which is in well agreement with JCPDS file 36-1451 indicating the hexagonal zincite (wurtzite) crystal structure. XRD patterns shows no peak for aluminum oxide or other possible impurities indicating that the samples were fabricated in high purity.

Crystallite sizes and strains of the samples were calculated with the help of the following equation which is also known as Williamson Hall equation (Eq. 5.1):

$$\beta cos\,\theta = \frac{K\lambda}{D} + 4\,\varepsilon\,sin\,\theta \qquad (5.1)$$

where β is the peak width at half-maximum intensity, θ is the Bragg diffraction angle in radians, λ is the X-ray wavelength and ε is the strain. The term $\beta cos\theta$ (y-axis) is plotted against $\varepsilon\,sin\theta$ (x-axis) (Figure 5.2). The y-intercept and slope of the fitted line shows crystallite size and strain values, respectively. The stress values of the crystals were determined by the following equation (Eq. 5.2) [68]:

$$\sigma = \frac{-233\,x\,10^9\,(c_{sample}-c_{bulk})}{c_{bulk}} \qquad (5.2)$$

where c_{sample} is the lattice constant of the material and c_{bulk} (5.206 Å) is the strain free constant. Estimated crystallite sizes, strains and stress values are listed in Table 5.1.

The crystal parameters of the structures were calculated by Eq. 5.3 and Eq. 5.4:

$$\lambda = 2d_{hkl}\,sin\theta_{hkl} \qquad (5.3)$$

where λ, d, θ are the wavelength of light, interplanar distance and the Bragg diffraction angle in radians, respectively.

$$\frac{1}{d_{hkl}^2} = \frac{4}{3}\left(\frac{h^2+hk+k^2}{a^2}\right) + \frac{l^2}{c^2} \qquad (5.4)$$

where d_{hkl} is the interplanar distance. The crystallite size of the samples decreases with increasing Al ratio. The observed decrease in crystal size is attributed to the substitution of Al^{3+} ions having lower atomic radius (rAl^{3+} = 0.054 nm) in the Zn^{2+} crystal plane (rZn^{2+} =0.074 nm). Additionally, the covalent bond length of Al-O is shorter than that of Zn-O, which was associated with the reduction of the crystal size due to the decreased unit cell length. The obtained crystal size values are compatible with the values reported in the previous studies on aluminum incorporated ZnO

nanoparticles in the literature. Aydın et al. reported similar results about the change of lattice parameters with incorporation of Al into ZnO structure [76]. Stress increases with incorporation of potassium because of the different ionic radii between Al^{3+} and Zn^{2+}. As a result of Al substitution, lattice distortion is clear causing a stress increase in the structure. The tensile stress of the specimen is interpreted as positive.
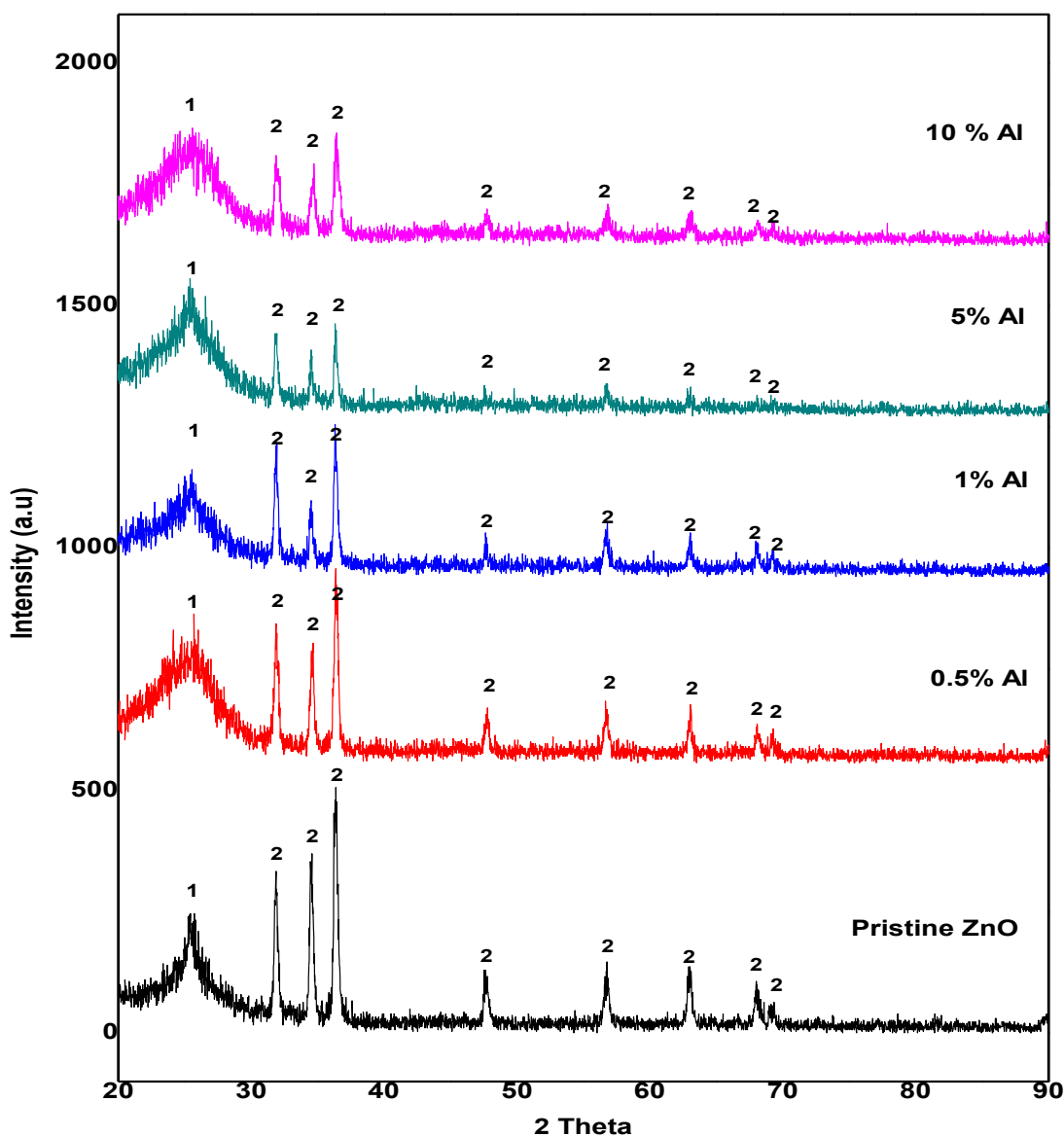
Figure 5.2 XRD plots of pristine and Al substituted ZnO nanowires grown on carbon fibers.
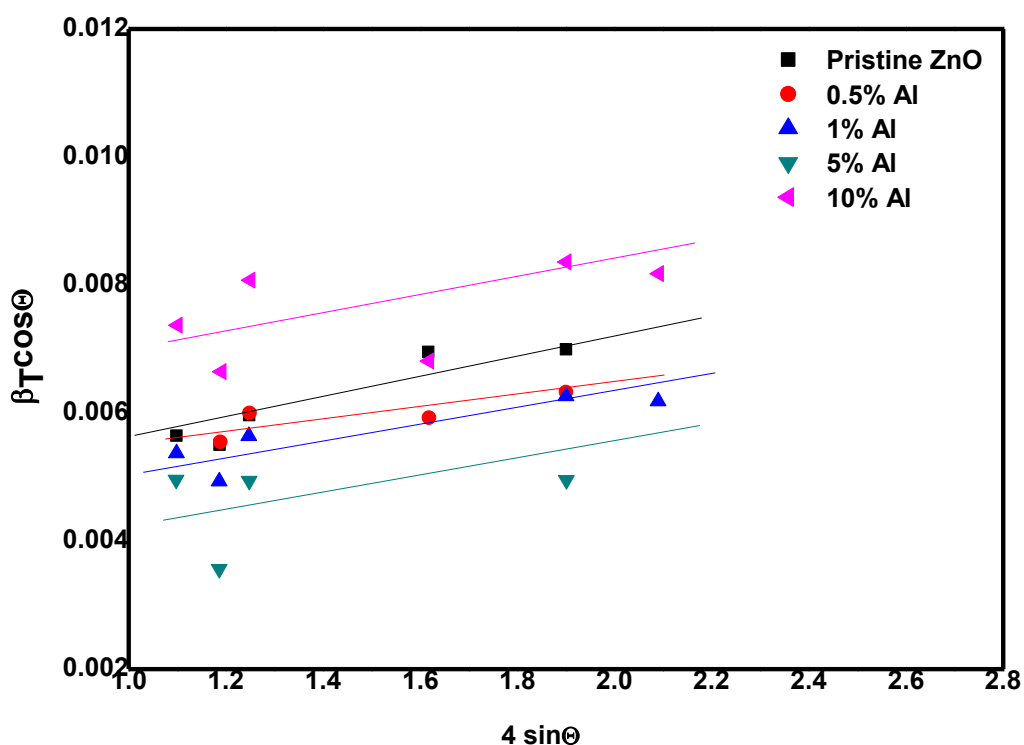
Figure 5.3 Williamson Hall plots of pristine and Al substituted ZnO nanowires grown on carbon fibers.

Table 5.1 XRD peak analysis of Al substituted ZnO nanowires grown on carbon fibers.

Sample name	D (nm)	ε (10^{-3})	Lattice constant		σ (10^9 Pa)
			a	C	
Pristine ZnO	40.78	2.0	3.2397	5.1902	0.70
0.5% Al	28.89	0.8	3.2377	5.1826	1.04
1% Al	33.82	1.1	3.2393	5.1923	0.61
5% Al	36.49	0.6	3.2403	5.1928	0.59
10% Al	22.73	10.0	3.2327	5.1751	1.38

The optical properties of samples were analysed by diffuse reflectance spectroscopy (DRS). The reflectance spectrum were recorded in the range of 250-800 nm. The electron transitions occurs at wavelength lower than 500 nm from the valence band to the conduction band cause a variation in reflectance spectroscopy. The optical band gap values of samples (Eg) were evaluated by Kubelka–Munk function (Eq. 5.5) [71]:

$$F(R) = \frac{K}{S} = \frac{(1-R)^2}{2R} \qquad (5.5)$$

where S is the scattering coefficient, K is the absorption coefficient, R is the reflectance and F(R) is the Kubelka–Munk function. The plot of $(F(R)hv)^2$ versus photon energy is given in Figure 5.4. The band gap values of aluminum substituted ZnO NWs/CFs were given in Table 5.2. The sample with the lowest band gap is 0.5% Al-ZnO with 3.25 eV. With the increase in Al concentration, the band gap value of the samples were generally increased because the Al substitution causes an increase in the carrier concentration. Increasing the carrier charge concentration led to an increase in forbidden energy range of metal-oxide semiconductors based on the Burstein-Moss effect [72]. Replacement of Al^{3+} with Zn^{2+} ions led to an extra free electron to be released with the reaction of Al^{3+} —>Al^{2+} + e-. These extra electrons occupy the low energy levels beneath the conduction band and push Fermi level towards to the conduction band. This causes an increase in the band gap of Al substituted ZnO nanowires. The obtained forbidden energy range values are compatible with the theoretical values in the literature. Aydın el al reported similar results for Al substituted ZnO [76].

Figure 5.4 Plots of reflectance spectrums and $(F(R)h\nu)^2$ versus photon energy (hν) of the pristine and Al substituted ZnO nanowires grown on carbon fibers.

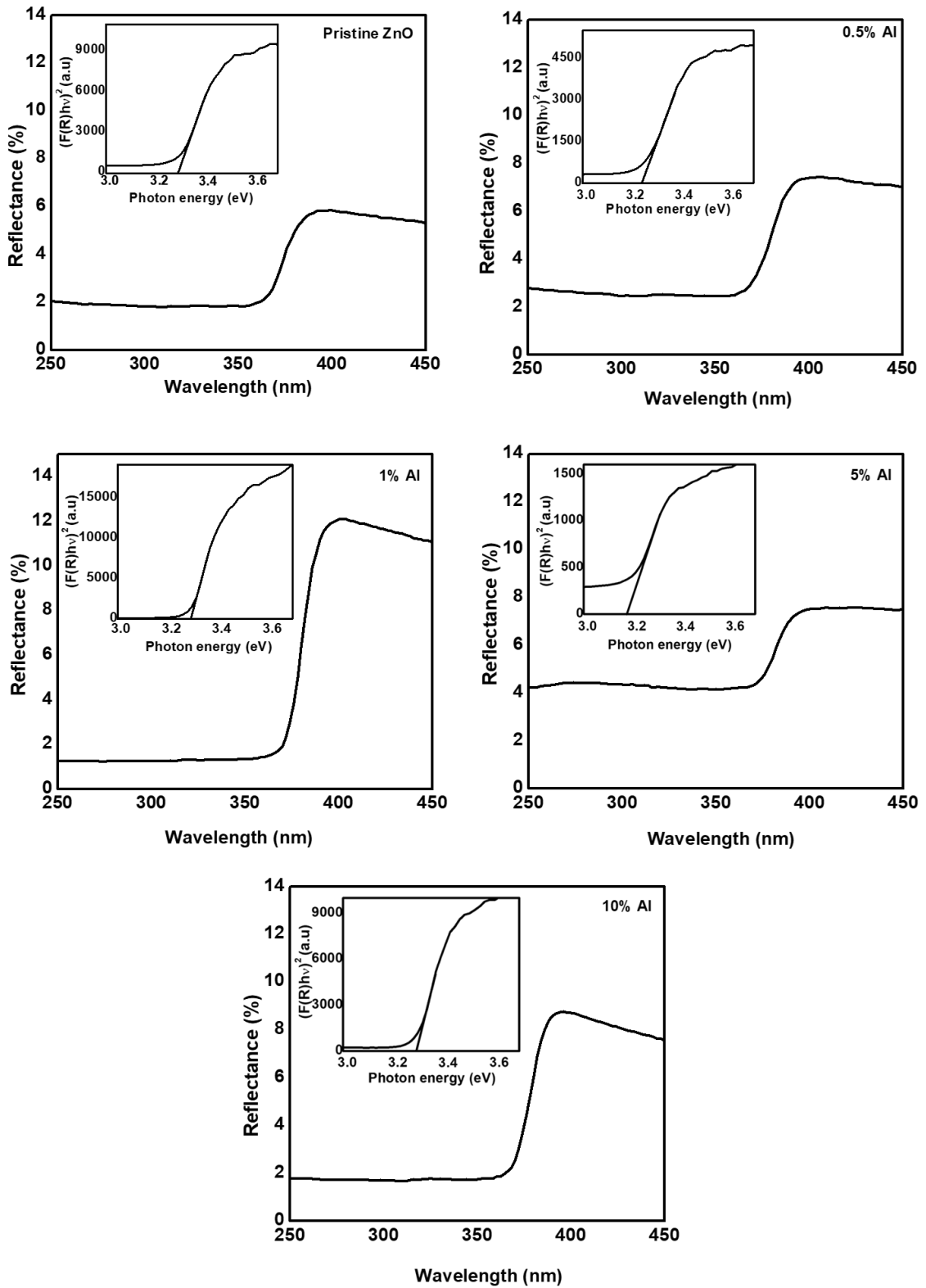**Table 5.2** Band gap values of Al substituted ZnO nanowires grown on carbon fibers.

Sample name	Bandgap (eV)
Pristine ZnO	3.30
0.5% Al	3.25
1% Al	3.29
5% Al	3.19
10% Al	3.29

5.3.2. Photocatalytic Activity Test

Photocatalytic activity of Al substituted ZnO NWs grown on CFs on degradation of methylene blue was analysed under visible light irradiation. It is observed that the samples are in consistent with the Langmuir–Hinshelwood (L-H) kinetics model, of which is successfully utilized in this work to describe the kinetics of the heterogeneous catalytic processes. The Langmuir–Hinshelwood model was evaluated by the given Eq. 5.4:

$$ln \left(\frac{C_0}{C_t} \right) = k_{app} \times t \tag{5.4}$$

where C_0 is the initial dye concentration, C_t is the instant dye concentration, k_{app} is the apparent reaction rate constant and t is time. In this model, linear relation is seen between $Ln(C_0/C)$ and t having a slope of k_{app} [49].

The degradation efficiency (*DE%*) was calculated by the given equation below (Eq. 5.5):

$$DE\% = \frac{(C_0 - C_t)}{C_0 \times 100} \tag{5.5}$$

where C_0 is the initial reactant concentration, C_t is instant reactant concentration and t is the irradiation time.

The photocatalytic degradation kinetic and the percent degradation plots are given in Figure 5.5 and the degradation kinetic data are given in Table 5.4. Degradation ratio plot demonstrates that after dark test a preliminary decrease is observed on methylene blue concentration due to the adsorbtion of methylene blue. In dark test, the amount of adsorption into pristine carbon fibers is higher than that of the carbon fibers with ZnO NWs. Highest degradation efficiency is obtained with 1% Al substituted ZnO NWs on CFs with 0.9879 h⁻¹ kinetic rate. The reason for the increase of photocatalytic activity might be due to the reduction of band gap of zinc oxide as a result of Al substitution. Another reason for improving the photocatalytic activity

could be increasing crystal interface area as a result of decreasing crystal size and increasing defect sides of the ZnO structure with Al substitution.
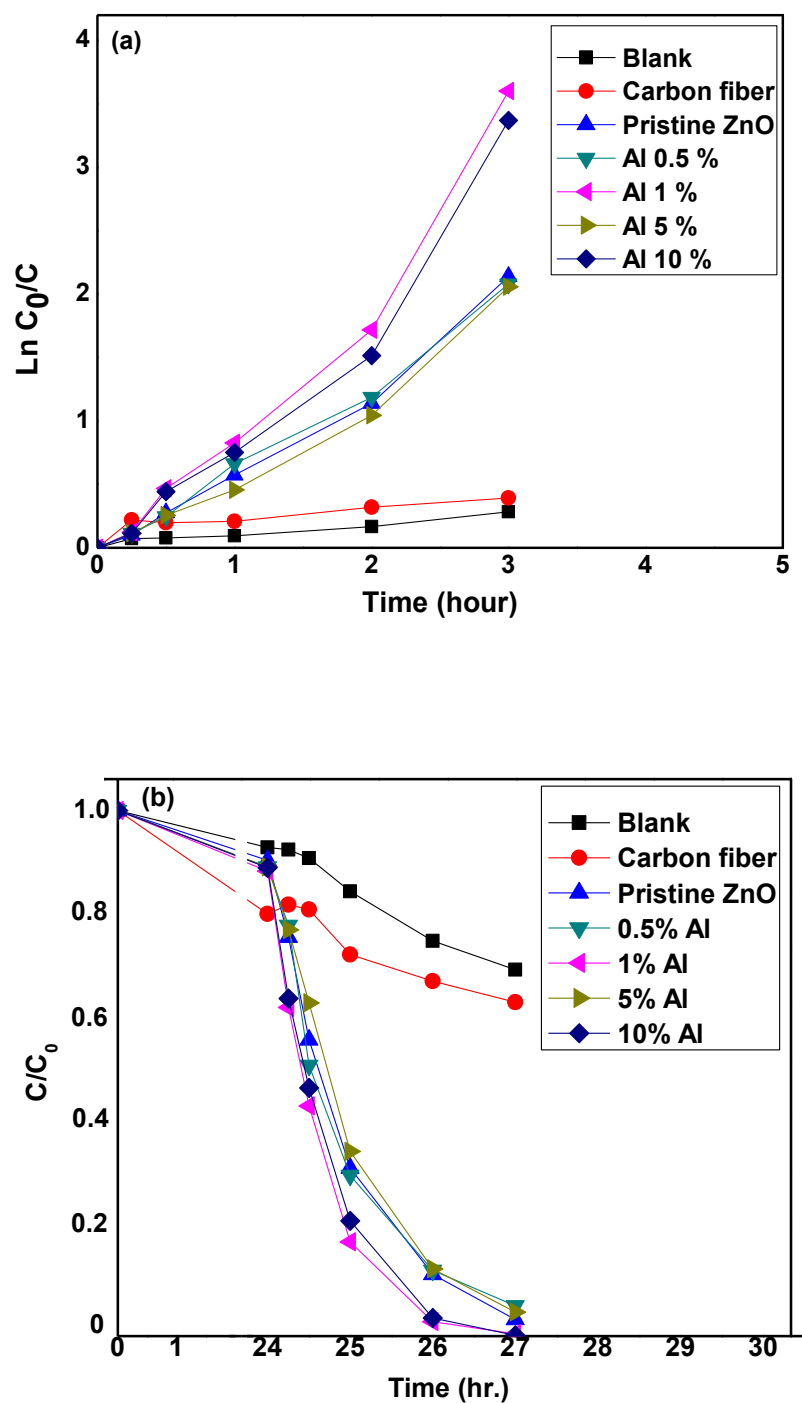
Figure 5.5 Photocatalytic activity of Al incorporated ZnO nanowires grown on carbon fibers. (a) Photocatalytic degradation kinetics, (b) degradation ratio.

Table 5.4 Photocatalytic degradation kinetic data of Al incorporated ZnO nanowires grown on carbon fibers.

Sample	Degradation efficiency (%)	$k_{app}(h^{-1})$	R^2
Blank	30.27	0.0937	0.9208
Carbon fiber	36.44	0.1522	0.3789
Pristine ZnO	96.84	0.6592	0.978
0.5% Al	94.26	0.6588	0.9881
1% Al	99.57	1.0715	0.9551
5% Al	95.41	0.6203	0.9643
10% Al	99.86	0.9879	0.9438

5.4. Conclusions

In this study, pristine and aluminum substituted ZnO nanowires on carbon fibers were successfully synthesized by hydrothermal method. Structural, morphological, optical and photocatalytic properties of the bare and aluminum substituted ZnO nanowires on carbon fibers were investigated. XRD results indicates that the bare and aluminum substituted ZnO NWs have been grown on the carbon fibers with zincite hexagonal phase. DRS results shows that Al incorporation led to a 0.05 eV decrease in the bandgap of ZnO NWs/CFs structure. Photocatalytic activity test results shows that Al substitution increased the photocatalytic activity of the structure. It can be concluded that the produced ZnO NWs on CFs can be a good candidate for photocatalytic degradation of organic pollution.

CONCLUSION

As a summary, ZnO NWs were deposited on CFs by hydrothermal method, successfully. SEM and XRD analyses were performed in order to get information on the morphology and crystal structure of the samples, respectively. SEM images showed clearly that ZnO NWs were grown successfully and well aligned on carbon fibers. XRD patterns showed that ZnO nanowires were grown on carbon fiber with hexagonal crystal structure. The effects of temperature, concentration and time of hydrothermal process on the formation of ZnO nanowires have been evaluated.

The effect of concentration on the dimensions of zinc oxide nanowires was investigated. It was observed that with the increase in concentration from 10 to 50 mM $Zn(NO_3)_2$. $6H_2O$, both, length and thickness were increased, yet aspect ratios were decreased.

CCD model was applied for optimizing the hydrothermal process conditions. Temperature, concentration and process time were evaluated. ANOVA results revealed that the effect of hydrothermal process variables on the length of ZnO nanowires was not significant. Concentration has a strong influence on the thickness and the aspect ratio of zinc oxide nanowires. Additionally, it was verified that with increase in the concentration and temperature, the thickness and aspect ratio of ZnO NWs were increased. The thicknesseses of ZnO nanowires varied from 23 nm to 111 nm, and the lengths of ZnO nanowires varied from 492 nm to 1429 nm. Aspect ratio values differed from 39.4 to 9.4 for the samples produced at 10 mM and 30 mM hydrothermal process concentration, repectively. Photocatalytic degradation kinetic rates on degradation of methylene blue aquous solution were evaluated by design of experiment. ANOVA results showed that concentration is a significant variable on thickness, aspect ratio and photocatalytic activity of ZnO nanowires grown on carbon fibers. ZnO nanowires with lower aspect ratio produced at 30 mM showed higher photocatalytic activity. This can be due to the discontunity of ZnO nanowires along carbon fiber in macro level produced at lower hydrothermal process concentration. Highest photocatalytic degradation reaction rate and efficiency were seen at the sample produced at 120 ^{o}C 30 mM concentration and for 4 hours process time with

k_{app} and *DE%*, 1.2707 h^{-1} and 99.86%, respectively. As result, by employing design of experiments the effects of process parameters were evaluated in detail with a few number of experiments.

Potassium and aluminum incorporated ZnO nanowires were also grown on carbon fibers. Morphologies of potassium and aluminum substituted ZnO Nws/CFs were analysed by SEM, of which well aligned ZnO nanowires were clearly observable on carbon fibers. The XRD patterns of potassium and aluminum incorporated ZnO nanowires exhibit hexagonal zincite phase. The changes of crystal size, crystal parameters, strain and stress with potassium and aluminum substitution were investigated. Increasing concentration of potassium and aluminum reduced the crystallinity of ZnO. A dramatic change was seen in crystallite size from 40.78 nm to 0.78 nm. Distortion is seen on crystal structure of substituted ZnO causing stress due to different ionic radii between Zn^{2+} and substituent ions. Tensile stress for potassium and aluminum substituted ZnO nanowires chages from 0.70 Pa to -0.75 Pa and 1.38 Pa, respectively. Larger ionic radii of potassium causes negative tensile stress and smaller ionic radii of aluminum causes positive tensile stress.

Optical properties of substituted ZnO nanowires grown on carbon fibers were evaluated by DRS. Band gap values were decreased to 0.1 eV and 0.05 eV with 0.5% potassium and aluminum substitution concentration of zinc concentration of, respectively. Kinetic rate and percent degradation of methylene blue at presence of substituted ZnO nanowires grown on carbon fiber were estimated. In general, increasing substituent concentration in ZnO nanowires causes higher photocatalytic activity.

In adition to the performed analyzes, Raman spectroscopy and Photoluminesence spectroscopy analyzes can be performed for further investigation on optical properties of substituted ZnO nanowires grown on carbon fiber. As well as, elemental composition of substituted ZnO nanowires can be determined by x-ray photoelectron spectroscopy spectroscopy. Also, different elements can be utilized for the substitution into zinc oxide nanowires in future. Moreover, different materials and carbon based substrates can be utilized for the comparison. Production procedure can be developed to increase the number and the concentration of zinc oxide nanowires on carbon fibers. Furthermore, obtained hybrid structure, can be tested on industrial pollutions and it can be applied in different areas such as biosensors, dye sensitised solar cells, antibacterial materials, and gas sensors.

REFERENCES

1.Zhang Y. Chapter 1 Overview. ZnO Nanostructures: Fabrication and Applications: The Royal Society of Chemistry; 2017;1-7.

2.Kim YK, Seo HJ, Kim S, Hwang SH, Park H, Lim SK. Effect of ZnO Electrodeposited on Carbon Film and Decorated with Metal Nanoparticles for Solar Hydrogen Production. Journal of Materials Science & Technology. 2016;32(10):1059-65.

3.Liu L. Controllable ZnO nanorod arrays@carbon fibers composites: Towards advanced CO_2 photocatalytic reduction catalysts. Ceramics International. 2016;42(10):12516-20.

4.Manivannan K, Sivakumar M, Cheng C-C, Lu C-H, Chen J-K. An effective electrochemical detection of chlorogenic acid in real samples: Flower-like ZnO surface covered on PEDOT:PSS composites modified glassy carbon electrode. Sensors and Actuators B: Chemical. 2019;301:1-8.

5.Dang VT, Nguyen TTO, Truong TH, Le AT, Nguyen TD. Facile synthesis of different ZnO nanostructures for detecting sub-ppm NO_2 gas. Materials Today Communications. 2020;22:1-7.

6.Erol M. Karbon Fiber/ZnO Fotokatalizörlerin Üretimi ve Karakterizasyonu. Deu Muhendislik Fakultesi Fen ve Muhendislik. 2018;20:924-9.

7.Huang C, Xu C, Lu J, Li Z, Tian Z. 3D Ag/ZnO hybrids for sensitive surface-enhanced Raman scattering detection. Applied Surface Science. 2016;365:291-5.

8.Pant B, Pant HR, Barakat NAM, Park M, Jeon K, Choi Y, et al. Carbon nanofibers decorated with binary semiconductor (TiO_2/ZnO) nanocomposites for the effective removal of organic pollutants and the enhancement of antibacterial activities. Ceramics International. 2013;39(6):7029-35.

9.Pant B, Park M, Kim H-Y, Park S-J. Ag-ZnO photocatalyst anchored on carbon nanofibers: Synthesis, characterization, and photocatalytic activities. Synthetic Metals. 2016;220:533-7.

10.Zhang WL, Sun YG, Xiao ZY, Li WY, Li B, Huang XJ, et al. Heterostructures of CuS nanoparticle/ZnO nanorod arrays on carbon fibers with improved visible and solar light photocatalytic properties. Journal of Materials Chemistry A. 2015;3(14):7304-13.

11.Chen HN, Zhu LQ, Liu HC, Li WP. Growth of ZnO nanowires on fibers for one-dimensional flexible quantum dot-sensitized solar cells. Nanotechnology. 2012;23(7):7.

12.Rasouli S. Radial growth of zinc oxide nanowire for piezoelectric nanogenerator application. Applied Physics A. 2017;123:1-7.

13.Du Y, Fu C, Gao Y, Liu L, Liu Y, Xing L, et al. Carbon fibers/ZnO nanowires hybrid nanogenerator based on an insulating interface barrier. RSC Advances. 2017;7(35):21452-8.

14. Liu L. Controllable ZnO nanorod arrays@carbon fibers composites: Towards advanced CO_2 photocatalytic reduction catalysts. Ceramics International. 2016;42:12516-12520.

15. Shakir I, Shahid M, Rana U, Alnashef I, Hussain R. Nickel–Cobalt Layered Double Hydroxide Anchored Zinc Oxide Nanowires grown on Carbon Fiber Cloth for High-Performance Flexible Pseudocapacitive Energy Storage Devices. Electrochimica Acta. 2014;129:28–32.

16. Malakooti MH, Patterson BA, Hwang H-S, Sodano HA. ZnO nanowire interfaces for high strength multifunctional composites with embedded energy harvesting. Energy & Environmental Science. 2016;9(2):634-43.

17. Qiu Y, Yang D, Yin B, Lei J, Zhang H, Zhang Z, et al. Branched ZnO nanotrees on flexible fiber-paper substrates for self-powered energy-harvesting systems. RSC Adv. 2015;5:5941-5.

18. Gu B, Liu Z, Wang X, Dong X-X. RF magnetron sputtering synthesis of carbon fibers/ZnO coaxial nanocable microelectrode for electrochemical sensing of ascorbic acid. Materials Letters. 2016;181:265-7.

19. Brince Paul K, Kumar S, Tripathy S, Vanjari SRK, Singh V, Singh SG. A highly sensitive self assembled monolayer modified copper doped zinc oxide nanofiber interface for detection of Plasmodium falciparum histidine-rich protein-2: Targeted towards rapid, early diagnosis of malaria. Biosensors and Bioelectronics. 2016;80:39-46.

20. Liu H, Gu C, Hou C, Yin Z, Fan K, Zhang M. Plasma-assisted synthesis of carbon fibers/ZnO core–shell hybrids on carbon fiber templates for detection of ascorbic acid and uric acid. Sensors and Actuators B: Chemical. 2016;224:857-62.

21. Yang C, Gu B, Zhang D, Ge C, Tao H. Coaxial carbon fiber/ZnO nanorods as electrodes for the electrochemical determination of dopamine. Analytical Methods. 2016;8(3):650-5.

22. Usha S, Shrivastav A, Gupta B. Silver nanoparticle noduled ZnO nanowedge fetched novel FO-LMR based H_2O_2 biosensor: A twin regime sensor for in-vivo applications and H_2O_2 generation analysis from polyphenolic daily devouring beverages. Sensors and Actuators B: Chemical. 2017;241:129-45.

23. Liao Q, Mohr M, Zhang X, Zhang Z, Zhang Y, Fecht HJ. Carbon fiber–ZnO nanowire hybrid structures for flexible and adaptable strain sensors. Nanoscale. 2013;5.

24. Calestani D, Villani M, Culiolo M, Delmonte D, Coppedè N, Zappettini A. Smart composites materials: A new idea to add gas-sensing properties to commercial carbon-fibers by functionalization with ZnO nanowires. Sensors and Actuators B: Chemical. 2017;245:166-170.

25. Zhang F, Niu S, Guo W, Zhu G, Liu Y, Zhang X, et al. Piezo-Phototronic Effect Enhanced Visible/UV Photodetector of a Carbon-Fiber/ZnO-CdS Double-Shell Microwire. ACS nano. 2013;7:4537-4544.

26. Wang Z, Meng G, Huang Z, Li Z, Zhou Q. Ag-nanoparticle-decorated porous ZnO-nanosheets grafted on a carbon fiber cloth as effective SERS substrates. Nanoscale. 2014;6(24):15280-5.

27. Du P, Song L, Xiong J, Li N, Xi Z, Wang L, et al. Coaxial electrospun TiO_2/ZnO core–sheath nanofibers film: Novel structure for photoanode of dye-sensitized solar cells. Electrochimica Acta. 2012;78:392-7.

28. Krämer A, Engel S, Sangiorgi N, Sanson A, Bartolomé J, Gräf S, et al. ZnO thin films on single carbon fibres fabricated by Pulsed Laser Deposition (PLD). Applied Surface Science. 2016;399.

29. Wang L, Xu S, Li H, Yue Q, Gu X, Zhang S, et al. Study for the electrochemical deposition on single carbon fiber and electrochemiluminescence of ZnO nanostructures. CrystEngComm. 2013;15(42):8444-8449.

30. Wei RH, Du K, Gong XY, Chen QD, Yang HB. Preparation and Optical Properties of Carbon Fiber/ZnO Core-Shell Structure by a Simple Method. Advanced Materials Research. 2012;557-559:236-9.

31. Kim YK, Seo H-J, Kim S, Hwang S-H, Park H, Lim SK. Effect of ZnO Electrodeposited on Carbon Film and Decorated with Metal Nanoparticles for Solar Hydrogen Production. Journal of Materials Science & Technology. 2016;32(10):1059-65.

32. Chen GH, Wang Y, Shen QH, Song YJ, Chen GL, Yang H. Synthesis and enhanced photocatalytic activity of 3D flowerlike ZnO microstructures on activated carbon fiber. Mater Lett. 2014;123:145-8.

33. Hung M-C, Yuan s-y, Hung C-C, Cheng C-L, Ho H-C, Ko T-H. Effectiveness of ZnO/carbon-based material as a catalyst for photodegradation of acrolein. Carbon. 2014;66:93-104.

34. Sun JC, Fan H, Wang N, Ai SY. Controlled synthesis of Sn doped ZnO microspheres stringed on carbon fibers with enhanced visible-light photocatalytic activities. Sep Purif Technol. 2016;160:67-72.

35. Liu LJ. Controllable ZnO nanorod arrays@carbon fibers composites: Towards advanced CO_2 photocatalytic reduction catalysts. Ceramics International. 2016;42(10):12516-20.

36. Yue HY, Huang S, Chang J, Heo C, Yao F, Adhikari S, et al. ZnO Nanowire Arrays on 3D Hierachical Graphene Foam: Biomarker Detection of Parkinson's Disease. ACS Nano. 2014;8(2):1639-46.

37. Pant B, Park M, Ojha GP, Park J, Kuk Y-S, Lee E-J, et al. Carbon nanofibers wrapped with zinc oxide nano-flakes as promising electrode material for supercapacitors. Journal of Colloid and Interface Science. 2018;522:40-7.

38. Hsieh C-T, Tzou D-Y, Huang Z-S, Hsu J-P, Lee C-Y. Decoration of zinc oxide nanoparticles onto carbon fibers as composite filaments for infrared heaters. Surfaces and Interfaces. 2017;6:98-102.

39. Wei N, Cui H-Z, Wang X, Xie X, Wang M, Zhang L, et al. Hierarchical Assembly of In_2O_3 Nanoparticles on ZnO Hollow nanotubes Using Carbon Fibers as

Templates: Enhanced Photocatalytic and Gas-sensing Properties. Journal of Colloid and Interface Science. 2017;498:263-270.

40.Xie F, Hu W, Ning D, Zhuo L, Deng J, Lu Z. ZnO nanowires decoration on carbon fiber via hydrothermal synthesis for paper-based friction materials with improved friction and wear properties. Ceramics International. 2017;44:4204-4210.

41.Tran Thi VH, Lee B-K. Great improvement on tetracycline removal using ZnO rod-activated carbon fiber composite prepared with a facile microwave method. Journal of Hazardous Materials. 2016;324:329-339.

42.Akir S, Hamdi A, Addad A, Coffinier Y, Boukherroub R, Dakhlaoui Omrani A. Facile synthesis of carbon-ZnO nanocomposite with enhanced visible light photocatalytic performance. Applied Surface Science. 2017;400:461-70.

43.Tunç ID, Erol M, Güneş F, Sütçü M. Growth of ZnO nanowires on carbon fibers for photocatalytic degradation of methylene blue aqueous solutions: An investigation on the optimization of processing parameters through response surface methodology/central composite design. Ceramics International. 2019;46(6): 7459-7474.

44.Krämer A, Engel S, Sangiorgi N, Sanson A, Bartolomé JF, Gräf S, et al. ZnO thin films on single carbon fibres fabricated by Pulsed Laser Deposition (PLD). Applied Surface Science. 2017;399:282-7.

45.Jang G, Jeong Lee S, Lee D, Lee D, Lee W, Myoung J-M. Flexible UV detector based on carbon fibers, ZnO nanorods, and Ag nanowires. Journal of Materials Chemistry C. 2017;5(18):4537-42.

46.Mondal K, Sharma A. Recent advances in electrospun metal-oxide nanofiber based interfaces for electrochemical biosensing. RSC Advances. 2016;6(97):94595-616.

47.Erol M, Bilgin K. Boron doped titaniumdioxide nanotube arrays: production, characterization and photocatalytic properties. Journal of Porous Materials. 2017;24(5):1295-302.

48.Liu HY, Gu CC, Hou C, Yin ZZ, Fan K, Zhang MZ. Plasma-assisted synthesis of carbon fibers/ZnO core-shell hybrids on carbon fiber templates for detection of ascorbic acid and uric acid. Sensors and Actuators B-Chemical. 2016;224:857-62.

49.Erol M, Ertugrul O. HIPed TiO_2 dense pellets with improved photocatalytic performance. Ceramics International. 2018;44(3):2991-9.

50.Zheng N, Huang YD, Sun WF, Du XS, Liu HY, Moody S, et al. In-situ pull-off of ZnO nanowire from carbon fiber and improvement of interlaminar toughness of hierarchical ZnO nanowire/carbon fiber hydrid composite laminates. Carbon. 2016;110:69-78.

51.Zhang X, Qin J, Xue Y, Yu P, Zhang B, Wang L, et al. Effect of aspect ratio and surface defects on the photocatalytic activity of ZnO nanorods. Scientific Reports. 2014;4:4596.

52.Yun HJ, Lee H, Joo JB, Kim W, Yi J. Influence of Aspect Ratio of TiO_2 Nanorods on the Photocatalytic Decomposition of Formic Acid. J Phys Chem C. 2009;113(8):3050-5.

53. Kim DS, Han SJ, Kwak S-Y. Synthesis and photocatalytic activity of mesoporous TiO_2 with the surface area, crystallite size, and pore size. Journal of Colloid and Interface Science. 2007;316(1):85-91.

54. Wang JX, Li H, Sun Y, Bai B, Zhang YH, Fan YB. Anodization of Highly Ordered TiO_2 Nanotube Arrays Using Orthogonal Design and Its Wettability. International Journal of Electrochemical Science. 2016;11(1):710-23.

55. Virk RS. Study of voltage, acid concentration, andtemperature on nanopore structures. Master's Theses. 2008;3512.

56. Sharifi H, Zabihzadeh SM, Ghorbani M. The application of response surface methodology on the synthesis of conductive polyaniline/cellulosic fiber nanocomposites. Carbohydrate Polymers. 2018;194:384-94.

57. Heckert NA, Filliben JJ, Croarkin CM, Hembree B, Guthrie WF, Tobias P, Prinz J. Handbook 151: NIST/SEMATECH e-Handbook of Statistical Methods. 2002.

58. Khajelakzay M, Bakhshi SR. Optimization of spark plasma sintering parameters of Si_3N_4-SiC composite using response surface methodology (RSM). Ceramics International. 2017;43(9):6815-21.

59. Pala A, Politi R, Kursun G, Erol M, Bakal F, Öner G, Çelik E. Photocatalytic Degradation of Cyanide in Wastewater Using New Generated Nano-Thin Film Photocatalyst. Surface and Coatings Technology. 2014;271:207-216.

60. Kola AK. Experimental design data for the biosynthesis of citric acid using Central Composite Design method. Data inBrief. 2017;12:234-41.

61. Qi K, Cheng B, Yu J, Ho W. Review on the improvement of the photocatalytic and antibacterial activities of ZnO. Journal of Alloys and Compounds. 2017;727:792-820.

62. Li D, Huang J-F, Cao L-Y, OuYang H-B, Li J-Y, Yao C-Y. Microwave hydrothermal synthesis of K^+ doped ZnO nanoparticles with enhanced photocatalytic properties under visible-light. Materials Letters. 2014;118:17-20.

63. Sa´aedi A, Yousefi R, Jamali-Sheini F, Cheraghizade M, Zak AK, Huang NM. Optical properties of group-I-doped ZnO nanowires. Ceramics International. 2014;40(3):4327-32.

64. Gupta M, Sinha N, Kumar B. P-type K-doped ZnO nanorods for optoelectronic applications. Journal of Applied Physics. 2011;109:083532-5.

65. Ghosh S, Khan G, Das B, Mandal K. Vacancy-Induced Intrinsic d0 Ferromagnetism and Photoluminescence in Potassium Doped ZnO Nanowires. Journal of Applied Physics. 2011;109:123927-6.

66. Babu ES, Hong SK. Effect of indium concentration on morphology of ZnO nanostructures grown by using CVD method and their application for H_2 gas sensing. Superlattices and Microstructures. 2015;82:349-56.

67. Zhang F, Niu S, Guo W, Zhu G, Liu Y, Zhang X, et al. Piezo-phototronic Effect Enhanced Visible/UV Photodetector of a Carbon-Fiber/ZnO-CdS Double-Shell Microwire. ACS Nano. 2013;7(5):4537-44.

68.Tabib A, Bouslama W, Sieber B, Addad A, Elhouichet H, Férid M, et al. Structural and optical properties of Na doped ZnO nanocrystals: Application to solar photocatalysis. Applied Surface Science. 2017;396:1528-38.

69.Athma PV, Johns N, Anila EI, Safeera TA. Structural and optical characterization of potassium doped zinc oxide nanosheets. Optical Materials. 2014;38:223-7.

70.Shanmuganathan G, Banu IBS, Krishnan S, Ranganathan B. Influence of K-doping on the optical properties of ZnO thin films grown by chemical bath deposition method. Journal of Alloys and Compounds. 2013;562:187–93.

71.Yurddaskal M. Formation of Micro- and Nanostructured TiO_2 Films by Anodic Oxidation for Enhanced Photocatalytic Activities. Journal of Inorganic and Organometallic Polymers and Materials. 2019;29(6):2214-25.

72.Moss TS. The Interpretation of the Properties of Indium Antimonide. Proceedings of the Physical Society Section B. 1954;67(10):775-82.

73.Xing X, Deng D, Li Y, Chen N, Liu X, Wang Y. Macro-/nanoporous Al-doped ZnO via self-sustained decomposition of metal-organic complexes for application in degradation of Congo red. Ceramics International. 2016;42(16):18914-24.

74.Sankar ganesh R, Navaneethan M, Mani GK, Ponnusamy S, Tsuchiya K, Muthamizhchelvan C, et al. Influence of Al doping on the structural, morphological, optical, and gas sensing properties of ZnO nanorods. Journal of Alloys and Compounds. 2017;698:555-64.

75.Mitra M, Ghosh A, Mondal A, Kargupta K, Ganguly S, Banerjee D. Facile synthesis of aluminium doped zinc oxide-polyaniline hybrids for photoluminescence and enhanced visible-light assisted photo-degradation of organic contaminants. Applied Surface Science. 2017;402:418-28.

76.Aydın H, Yakuphanoglu F, Aydın C. Al-doped ZnO as a multifunctional nanomaterial: Structural, morphological, optical and low-temperature gas sensing properties. Journal of Alloys and Compounds. 2019;773:802-11.

77.Khayatian SA, Kompany A, Shahtahmassebi N, Zak AK. Preparation and characterization of Al doped ZnO NPs/graphene nanocomposites synthesized by a facile one-step solvothermal method. Ceramics International. 2016;42(1):110-5.

78.Zhang X, Chen Y, Zhang S, Qiu C. High photocatalytic performance of high concentration Al-doped ZnO nanoparticles. Separation and Purification Technology. 2017;172:236-41.

CURRICULUM VITAE

Irmak DOĞAN TUNÇ
1985 Gürün

Education:

- B.Sc: (2011) Department of Chemistry, Ege University, Turkey.
- M.Sc: (2014) Department of Chemistry, Izmir Institute of Technology, Turkey (in English).
- PhD: (2020) Department of Materials Science and Engineering, İzmir Katip Çelebi University, Turkey (in English).

List of Publications:

- Tunç I, Erol M, Güneş F, Sütçü M, Growth of ZnO nanowires on carbon fibers for photocatalytic degradation of methylene blue aqueous solutions: An investigation on the optimization of processing parameters through response surface methodology/central composite design. Ceramics International. 2020; 46(6): 7459-7474. Doi: 10.1016/j.ceramint.2019.11.244, (Publication no: 5905136)

Conference Papers:

- Tunç I, Erol M, Güneş F, Growth of Zinc Oxide Nanowires on Carbon Fiber through Hydrothermal Method: The effect of concentration and time. 3rd International Students Science Congress. 2019. (Abstract/Oral presentation).
- Tunç I, Erol M, Growth of Zinc Oxide Nanowires on Carbon Fiber through Hydrothermal Method. 2nd International Students Science Congress. 2018. (Full text /Oral presentation).
- Tunç I, Yalçin E, Erol M, Aykaç A, Can M, Production of Nanostructured Zinc Oxide Films on ITO/Glass Substrates through Hydrothermal Method. 2nd International Students Science Congress. 2018. (Full text/ Oral presentation).
- Tunç I, Aykaç A, Erol M, Güneş F, Synthesis of ZnO Nanowires on 3D Graphene Foam via Hydrothermal Method. The Internatinonal Conference on Materials Science Mechanical and Automation Engineerings and Technology. 2018. (Full text /Oral presentation).

Book Chapter:

- Tunç I, Baba, A, Demir, MM, Scaling problem of the geothermal system in Turkey. Geothermal Systems and Energy Resources Turkey and Greece. CRC Press, 2014. ISBN:13:978-1-315-77502-9.

Projects:

- Tuzcul bitkilerin önemi ve kullanılabilirliği için kimyasal ve biyolojik araştırmalar, Project manager: Doğan Irmak, 01/09/2010 - 01/06/2011 (National)

- Çinko oksit nanoyapıların karbon fiber üzerinde büyütülmesi: üretimi, karakterizasyonu ve fotokatalitik özellikleri, Project manager: Güneş Fethullah, Researcher: Erol Mustafa, Researcher: Tunç Irmak, 01/01/2020 - (Ongoing project) (National)